Article:
Taylor, S., Isobe, S., Cao, A. et al. (27 more authors) (2022) Endogenous retroviral elements generate pathologic neutrophils in pulmonary arterial hypertension. American Journal of Respiratory and Critical Care Medicine, 206 (8). pp. 1019-1034. ISSN 1073-449X

https://doi.org/10.1164/rccm.202102-0446oc

Endogenous Retroviral Elements Generate Pathologic Neutrophils in Pulmonary Arterial Hypertension

Shalina Taylor[1,2,3*], Sarasa Isobe[1,2,3*], Aiqin Cao[1,2,3], Kévin Contrepois[2,4], Bérénice A. Benayoun[5], Lihua Jiang[2,4], Lingli Wang[1,2,3], Stavros Melemenidis[6], Mehmet O. Ozen[7], Shoichiro Otsuki[1,2,3], Tsutomu Shinohara[1,2,3], Andrew J. Sweatt[1,8], Jordan Kaplan[1,2,3], Jan-Renier Moonen[1,2,3], David P. Marciano[2,4], Mingxia Gu[1,2,3,9], Kazuya Miyagawa[1,2,3,10], Brandon Hayes[11], Raymond G. Sierra[11], Christopher J. Kupitz[11], Patricia A. Del Rosario[1,8], Andrew Hsi[1], A. A. Roger Thompson[1,2,3,12], Maria E. Ariza[13], Utkan Demirci[7], Roham T. Zamanian[1,8], Francois Haddad[2,14], Mark R. Nicolls[8], Michael P. Snyder[2,4], Marlene Rabinovitch[1,2,3]‡

[1]Vera Moulton Wall Center for Pulmonary Vascular Diseases, Stanford University, Stanford, CA, USA

[2]Stanford Cardiovascular Institute, Stanford University School of Medicine, Stanford, CA, USA

[3] Department of Pediatrics - Cardiology, Stanford University School of Medicine, Stanford, CA, USA

[4] Department of Genetics, Stanford University School of Medicine, Stanford, CA, USA

[5]USC Leonard Davis School of Gerontology and Department of Molecular and Computational Biology at USC Dornsife College of Letters, Arts and Sciences, University of Southern California, Los Angeles, CA, USA

[6]Department of Radiation Oncology, Stanford University School of Medicine, Stanford, CA, USA

AJRCCM Articles in Press. Published June 13, 2022 as 10.1164/rccm.202102-0446OC

[7]Department of Radiology Canary Center for Cancer Early Detection, Stanford University, Stanford, CA, USA

[8]Department of Medicine - Pulmonary and Critical Care Medicine, Stanford University School of Medicine, Stanford, CA, USA

[9]Current address: Perinatal Institute, Division of Pulmonary Biology and USA Center for Stem Cell and Organoid Medicine, CuSTOM, Division of Developmental Biology, Cincinnati Children's Hospital Medical Center, Cincinnati, OH, USA

[10]Current address: Department of General Internal Medicine Nishi-Kobe Medical Center, Kobe, Japan

[11]Linac Coherent Light Source, SLAC National Accelerator Laboratory, Menlo Park, CA, USA

[12]Department of Infection, Immunity and Cardiovascular Disease, University of Sheffield, Western Bank, Sheffield, UK

[13]Department of Cancer Biology and Genetics, and Institute for Behavioral Medicine Research, The Ohio State University Wexner Medical Center, Columbus, OH, USA

[14]Department of Medicine - Cardiovascular Medicine, Stanford University School of Medicine, Stanford, CA, USA

**These authors contributed equally to this work

‡Corresponding Author: marlener@stanford.edu

AUTHOR CONTRIBUTIONS

ST and MR conceptualized the project. ST performed experiments, analyzed data, edited the figures, and wrote the manuscript. SI performed experiments and analyzed

AJRCCM Articles in Press. Published June 13, 2022 as 10.1164/rccm.202102-0446OC

data. KC, BB, and ST performed omics data processing and analysis. LJ performed omics data acquisition. ST, LW, SI, SO, TS, and JK assessed mouse cardiac hemodynamics. FH, RTZ, DH, PDR, and AJS provided human cardiac hemodynamics and samples. UD supervised extracellular vesicle (EV) isolation, MO performed EV isolation, and MO, DM, BH, RGS, and CK performed EV Nanosight analysis. SM and ST performed tail vein injections for animal experiments. MG, JM, AC, AART, KM assisted in experiments regarding cell adhesion (MG), confocal imaging (JM), neutrophil isolation (AC), co-cultures (KM), and transfections (AART). MEA provided purified HERV-K dUTPase protein and anti-HERV-K dUTPase antibodies. MPS and MRN assisted in the supervision of the project. MR supervised the project and helped prepare the manuscript. All authors discussed the results and commented on the manuscript.

SOURCES OF SUPPORT

NIH-NHLBI grants P01 HL108797 (MR), R01 HL122887 (MR, MRN and MPS) R01 HL074186 (MR), NIH-NIAID grant R01 A1084898 (MEA), NIH-NHLBI grant R01 HL 138473 (MR and MRN). ST was supported by T32 Fellowship in Pulmonary Medicine T32 HL129970-02 (PI: MRN) and an NIH/NHLBI Research Diversity Supplement P01 HL108797-04W1. SI was supported by AHA award 20POST35080009; SO was supported by a grant from Mie University Graduate School of Medicine; JRM by the California TRDRP of the University of California award 27FT-0039, and by the Netherlands Heart Foundation award 2013T116; DPM is supported by NIH-NHLBI grant K99 HL 1450970; MG by NIH/NHLBI grant K99/R00 HL135258; KM by fellowships from Japan Heart Foundation/Bayer Yakuhin Research Grant Abroad and The Uehara

AJRCCM Articles in Press. Published June 13, 2022 as 10.1164/rccm.202102-0446OC

Memorial Foundation. BH, RGS, and CK are supported by the Linac Coherent Light Source (LCLS), SLAC National Accelerator Laboratory, funded by the US Department of Energy, Office of Science, Office of Basic Energy Sciences Contract No. DE-AC02-76SF00515. AART was supported by a British Heart Foundation-Fulbright scholar award and Intermediate Clinical Fellowship (FS/18/13/33281). BAB was supported by NIA R00 AG049934. AJS was supported by NIH/NHLBI grant K23 HL151892. MR is also supported in part by the Dunlevie Chair in Pediatric Cardiology at Stanford University.

Running head: *Neutrophils, retrovirus, and pulmonary hypertension*

Subject Category: 9.35 Pulmonary Hypertension: Clinical-Diagnosis, Pathogenesis/Outcome

Total word count (manuscript body): 4,752

This article has an online data supplement, which is accessible from this issue's table of content online at www.atsjournals.org.

Some of the results of these studies have been previously reported in the form of a preprint (bioRxiv, [09 January 2021] https://doi.org/10.1101/2021.01.08.426001).

At a Glance

What is the current scientific knowledge on this subject?

Pulmonary arterial hypertension (PAH) is a disease characterized by occlusion of distal pulmonary arteries resulting in increased resistance to flow and culminating in heart failure. The appearance of fragmented elastic laminae in pulmonary arteries from patients with PAH suggested the presence of heightened elastase activity in the vessel wall, that was identified as neutrophil elastase (NE) in human cells and in experimental animals with pulmonary hypertension.

What does this study add to the field?

We describe a novel phenotype of neutrophils related to an increase in (i) production and release of elastase, (ii) generation of neutrophil extracellular traps, and (iii) adhesion mediated by vinculin, that directly contribute to the pathogenesis of PAH. This phenotype results from a cell autonomous and non-cell autonomous increase in two HERV-K family retroviral elements.

AJRCCM Articles in Press. Published June 13, 2022 as 10.1164/rccm.202102-0446OC

ABSTRACT

Rationale: The role of neutrophils and their extracellular vesicles (EVs) in the pathogenesis of pulmonary arterial hypertension is unclear.

Objectives: Relate functional abnormalities in pulmonary arterial hypertension neutrophils and their EVs to mechanisms uncovered by proteomic and transcriptomic profiling.

Methods: Production of elastase, release of extracellular traps, adhesion and migration were assessed in neutrophils from pulmonary arterial hypertension patients and control subjects. Proteomic analyses were applied to explain functional perturbations, and transcriptomic data were used to find underlying mechanisms. CD66b-specific neutrophil EVs were isolated from plasma of patients with pulmonary arterial hypertension and we determined whether they produce pulmonary hypertension in mice.

Measurements and Main Results: Neutrophils from pulmonary arterial hypertension patients produce and release increased neutrophil elastase, associated with enhanced extracellular traps. They exhibit reduced migration and increased adhesion attributed to elevated β1integrin and vinculin identified on proteomic analysis and previously linked to an antiviral response. This was substantiated by a transcriptomic interferon signature that we related to an increase in human endogenous retrovirus k envelope protein. Transfection of human endogenous retrovirus k envelope in a neutrophil cell line (HL-60) increases neutrophil elastase and interferon genes, whereas vinculin is increased by human endogenous retrovirus k dUTPase that is elevated in patient plasma.

AJRCCM Articles in Press. Published June 13, 2022 as 10.1164/rccm.202102-0446OC

Neutrophil EVs from patient plasma contain increased neutrophil elastase and human endogenous retrovirus k envelope and induce pulmonary hypertension in mice, mitigated by elafin, an elastase inhibitor.

Conclusions: Elevated human endogenous retroviral elements and elastase link a neutrophil innate immune response to pulmonary arterial hypertension.

Abstract word count: 248

Key words: extracellular vesicles (EVs), elafin, vinculin, leukocyte elastase, antiviral agents

Take home message: Abnormalities present in neutrophils and their extracellular vesicles (EVs) from patients with pulmonary arterial hypertension contribute to disease pathogenesis. Increased production and release of elastase, neutrophil extracellular traps, and vinculin mediated increased adhesion were attributed to an increased in endogenous retroviral elements, HERV-K envelope and dUTPase. Neutrophil EVs isolated from plasma of patients with pulmonary arterial hypertension contain increased elastase and HERV-K envelope and can induce pulmonary hypertension in mice, that is mitigated by the elastase inhibitor, elafin.

AJRCCM Articles in Press. Published June 13, 2022 as 10.1164/rccm.202102-0446OC

INTRODUCTION

Pulmonary arterial hypertension (PAH) is a disease characterized by occlusion of distal pulmonary arteries resulting in increased resistance to flow and culminating in heart failure. Current treatments improve quality of life and survival primarily by dilating pulmonary arteries, but these agents do not address the mechanism underlying the progressive pulmonary vascular pathology [reviewed in (1)]. The appearance of fragmented elastic laminae in pulmonary arteries from patients with PAH suggested the presence of heightened elastase activity in the vessel wall (2). Increased pulmonary arterial smooth muscle cell (SMC) elastase activity was identified as neutrophil elastase (NE) in human cells and in experimental animals with pulmonary hypertension (3). A consequence of heightened NE activity is degradation of elastin, leading to increased vascular stiffness (4), generation of elastin peptides which are highly chemotactic to monocytes (5), and release of growth factors from the extracellular matrix (6) that activate growth factor receptors (7), resulting in SMC proliferation (8). Inhibition of NE with synthetic inhibitors (9) or with the recombinant human elastase inhibitor elafin (10) is effective in preventing and reversing pulmonary hypertension in animal models, and regression of pulmonary arterial pathology in human organ cultures (10).

Neutrophils are major sources of NE; increased release of NE is observed in PAH neutrophils (11), and circulating NE levels are elevated in plasma from patients across all PAH subtypes (12, 13) and associated with worsening clinical severity and deficiency in the elastase inhibitor elafin (13). Morevoer, the neutrophil to lymphocyte ratio is increased in PAH and also correlates with clinical deterioration judged by New York Heart Association (NYHA) functional class, and event free survival (14). Other

AJRCCM Articles in Press. Published June 13, 2022 as 10.1164/rccm.202102-0446OC

alterations in neutrophil functions in response to injury, include propensity to extracellular trap (NET) formation (15), and alterations in adhesion and migration (16).

NE is critical for NET formation, and the enzyme remains proteolytically active when bound to NETs, thus contributing to tissue damage (17). Elevated markers of NET formation are observed in end-stage plexiform lesions in patients with PAH (12). In addition to local effects, NE exerts remote consequences by being packaged and transpoprted in EVs. Bronchial lavage from COPD patients contains EVs enriched with NE that caused alveolar destruction when injected intratracheally in mice (18).

To understand their contribution to the pathogenesis of PAH, we isolated circulating neutrophils from PAH patients vs. healthy controls and first assessed NE production and release, NET formation and adhesion and migration including transendothelial migration. We performed proteomic and transcriptomic profiling to identify the mechanism underlying the abnormalities observed. Our results indicated a novel antiviral response in PAH neutrophils that explained the PAH neutrophil phenotype. The mechanism accounting for increased elastase was related to an elevation in the human endogenous retrovirus HERV-K envelope in neutrophils, and the mechanism explaining increased vinculin mediated adhesion could be attributed to elevated circulating levels of HERV-K dUTPase. We showed that PAH neutrophil EVs contain elevated NE as well as HERV-K envelope, and induce pulmonary hypertension in mice, except when pretreated with elafin (19). Taken together, our studies can explain how neutrophil dysfunction contributes to PAH and can be targeted therapeutically. Some of the results of these studies have been previously reported in the form of abstracts (20-22).

AJRCCM Articles in Press. Published June 13, 2022 as 10.1164/rccm.202102-0446OC

METHODS

An Expanded Methods section is available in the Online Data Supplement.

PAH patient and control samples. Whole blood from PAH patients was obtained from the Stanford PAH biobank, and blood from healthy volunteers was obtained from the Stanford Biobank and the Stanford Blood Center. PAEC were obtained through the Pulmonary Hypertension Breakthrough Initiative **(See Tables E1-E4 in the Online Data Supplement).**

Reagents. See **Table E6** in the Online Data Supplement.

Neutrophil isolation. Human neutrophils were purified from peripheral blood using Miltenyi Biotec Macsxpress Neutrophil isolation kit.

HL-60 and dHL-60 cell culture. HL-60 cells were cultured in RPMI 1640 complete media and treated with 1.3% DMSO for 6-7 days for differentiation to dHL-60 cells.

HERV-K dUTPase protein purification. Recombinant HERV-K dUTPase protein was provided by Dr. Ariza. See online methods for additional information.

PAEC cell culture. PAEC were harvested from explanted lungs of PAH patients following lung transplantation, or from unused donor lungs (controls), and cultured in EC complete medium.

NE activity. NE activity was measured using EnzChek Elastase Assay Kit (Thermofisher Scientific).

AJRCCM Articles in Press. Published June 13, 2022 as 10.1164/rccm.202102-0446OC

Neutrophil extracellular trap (NET) formation. Neutrophils adherent to poly-d-lysine coated coverslips were treated with Phorbol Myristate Acetate with vehicle (PBS) or elafin for 60 min. Cells were washed with PBS, and then stained with cell impermeable SYTOX green, and for H3 citrullinated and neutrophil elastase as described in Expanded Methods.

Migration (Chemokinesis). Neutrophils adherent to fibronectin were treated with 100 ng/mL of IL-8 and cell migration was observed in real time using a confocal microscope.

Transmigration and Trans-endothelial Migration. Transmigration and trans-endothelial migration assays were performed in a modified Boyden chamber using the Corning FluoroBlok 24-well.

Adhesion. Neutrophils were incubated on fibronectin coated slides or on a monolayer of PAEC at 37°C for 5 min, washed with PBS, then imaged under light microscopy.

Flow cytometry. Neutrophils were stained for Alexa Fluor® 700 conjugated ITGB2, data acquired using a Beckton Dickenson LSR II flow cytometer, and analyzed using FlowJo.

Immunofluorescence staining. Adherent neutrophils were fixed with 4% paraformaldehyde and treated with HERV-K envelope antibody, followed by Alexa Fluor 488–conjugated secondary antibody, and DAPI staining.

Transmission Electron Microscopy. Pooled EV samples were visualized using a JEOL JEM-1400 120kV electron microscope.

AJRCCM Articles in Press. Published June 13, 2022 as 10.1164/rccm.202102-0446OC

Western Immunoblot. See Expanded Methods in the Online Data Supplement.

Reverse-Transcriptase qPCR (RT-qPCR). qPCR was performed using Powerup SYBR green PCR Master Mix (Applied Biosystems).

Primers. Primer sequences are listed in **Table E7** in the Online Data Supplement.

Plasmid transfection. HL-60 cells were transfected with HERV-K envelope vector or EGFP control vector (VectorBuilder) using HL-60 Cell Avalanche™ Transfection Reagent (EZ biosystems).

EV isolation from plasma and CD66b pulldown. EVs were isolated from plasma using the EV Total Isolation Chip (ExoTIC). ExoTIC-harvested EVs were further purified using Dynabeads conjugated to CD66b/CEACAM 8.

Untargeted Proteomics by LC-MS. Proteomic analysis used the LC system directly coupled in-line with an Orbitrap Fusion Lumos Mass Spectrometer.

RNA-seq analysis. Total RNA was prepared using the Takara Bio SMARTer: SMARTer Stranded Total RNA-Seq Kit v2 - Pico Input Mammalian kit and sequenced using the HiSeq 2500 sequencer.

Mouse model for the induction of pulmonary hypertension by neutrophil EVs. Adult male mice (8 weeks of age) were given tail-vein injections twice weekly for five weeks, of (i) PBS-Vehicle, (ii) pooled EVs of healthy donor controls, (iii) pooled PAH EVs, or (iv) pooled elafin treated PAH EVs. Cardiac function, right ventricular systolic pressure, and right ventricular hypertrophy and pulmonary vascular modphometry were

AJRCCM Articles in Press. Published June 13, 2022 as 10.1164/rccm.202102-0446OC

assessed. The first cohort consisted of the first three groups with n=3, and the second cohort added the fourth group, with n=6 in each group.

Statistical Analysis. Bars represent mean ± standard error of the mean (SEM) and n=number of control subject or patient cells studied. Statistical significance was determined by one-way ANOVA followed by Dunnett's multiple comparison test, or by two-sided unpaired t-test. Data with a sample size n<8 was analyzed using the Mann-Whitney non-parametric test. Samples with n of 3 are confirmatory of other assays or represent technical replicates from cell lines or pooled samples. Pathway enrichment analysis was conducted using the webtool IMPaLA.

RESULTS

Increased NE protein and NE-mediated NETosis in PAH neutrophils. Neutrophils isolated from the blood of PAH patients and control subjects were confirmed to be >95% pure, both by morphology and FACS analysis of CD66b and CD16 as shown in **Figure E1A** in the Online Data Supplement and described in the Expanded Methods section. Demographics and other data related to the cohorts used in each of the experiments are found in **Tables E1-E4** in the Online Data Supplement. While we requested samples from patients with idiopathic PAH, a small proportion (3/68) were later reclassified as having drug and toxin related Group 1 PAH (23), and 5/68 had some cardiopulmonary co-morbidities not thought to be causing the PAH. We observed an almost two-fold increase in levels of NE protein in PAH neutrophils when compared to those of control subjects as assessed by western immunoblot (**Figure 1A)**. A comparable increase in NE activity was established using a fluorescent labeled (DQ)

AJRCCM Articles in Press. Published June 13, 2022 as 10.1164/rccm.202102-0446OC

elastin substrate (**Figure 1B**) and the release of NE activity observed in response to interleukin-8 (IL-8) stimulation (**Figure 1C** and time course in **Figure E1B** in the Online Datra Supplement) is consistent with these observations. More than 2/3 of elastase activity measured by DQ elastin could be attributed to NE, assessed using a selective inhibitor, N-methoxysuccinyl-Ala-Ala-Pro-Val-chloromethyl ketone. There also appeared to be an elevation in non-NE elastolytic activity in PAH neutrophils (**Figures E1C and E1D** in the Online Data Supplement); however, this did not reflect an overall increase in proteolytic activity as levels of myeloperoxidase were similar in control and PAH neutrophils (**Figure E1E**).

Elevated NE activity was normalized to neutrophil counts. These were also increased in this cohort of PAH patients compared to control subjects (**Figure 1D**), resulting in higher NE activity per milliliter of blood (**Figure 1E**). NE contributes to the release of neutrophil extracellular traps (NETs), by translocating from granules to the nucleus to cleave histones, causing chromatin decondensation and release (15). NETosis incurs tissue damage, including endothelial cell (EC) injury (17), through the exteriorization of chromatin accompanied by NE. Using SYTOX green and citrullinated histone 3 staining of the spread area of exteriorized DNA, we showed heightened release of NETs upon PMA stimulation of PAH vs. control neutrophils, that was inhibited by the NE inhibitor elafin (10) (**Figure 1F**). We also showed increased NE exteriorized on NETs from PAH patients (**Figure E1E**). It is interesting that the low levels of NET formation in the control cells are not completely abolished by elafin. This could reflect the low sensitivity of the assay at those levels of NET formation or that a mechanism for

AJRCCM Articles in Press. Published June 13, 2022 as 10.1164/rccm.202102-0446OC

NET formation is unrelated to elastase in the control cells (24) or that elafin does not penetrate control cells.

PAH neutrophils exhibit increased adhesion and reduced migration. Increased NE production and NETosis suggested that other neutrophil functions could be altered or exaggerated in response to inflammatory stimuli. The functions considered were adhesion, migration and transendothelial migration. We observed heightened adhesion to a fibronectin substrate in PAH vs. control neutrophils (**Figure 2A**), that we related to an increase in β1 integrin (ITGB1, **Figure 2B**). This was consistent with reduced chemokinesis of PAH vs. control neutrophils was reduced, as assessed by confocal microscopic live cell imaging of total distance moved in response to IL-8 stimulation (**Figure 2C, Video E1** in the Online Data Supplement) and longitudinal distance migrated across the fibronectin substrate (**Figure 2D**) and with fMLP stimulation (**Figure E2A** in the Online Data Supplement), suggesting that impaired migration appeared independent of a specific receptor activated pathway. IL-8 stimulation of neutrophil migration across a monolayer of PAH or control pulmonary arterial endothelial cells (PAEC) was next assessed. While control neutrophils exhibited increased migration across PAH vs. control PAEC, PAH neutrophils displayed impaired migration across both control and PAH PAEC (**Figure 2E**), suggesting the the impaired neutrophil migration was not compensated by the PAH PAEC. This also suggests that while neutrophils may be attracted to the vessel wall, their increased adhesion to the endothelium, shown in **Figure E2B** in the Online Data Supplement, may lead to NET formation and to failed emigration from the tissue.

AJRCCM Articles in Press. Published June 13, 2022 as 10.1164/rccm.202102-0446OC

Proteomic analysis links increased vinculin to PAH neutrophil dysfunction. To investigate a mechanism that could explain the increase in NE activity and neutrophil adhesion and the decrease in migration, we carried out protein expression profiling by high-resolution mass spectrometry non-targeted proteomics on unstimulated cells. Principal component analysis (PCA) of the proteome revealed some overlap between PAH and control neutrophils (**Figure E3A** in the Online Data Supplement), but 483 differentially regulated proteins were identified with a false discovery rate (FDR) of 10% (**Figure 3B**). Pathway Enrichment Analysis from IMPaLA, revealed proteins related to neutrophil degranulation, host interactions with HIV factors, adhesion, and transendothelial migration (**Figure 3B** and **Figure E3B** in the Online Data Supplement). While we documented an increase in elastase protein by western immunoblot and activity by substrate assay, the increase in NE evident by proteomic analysis gave a p-value of 0.04, but an FDR of 11% (**Figure 3C**) and would have been missed with the 10% FDR. This result reinforces the limitations of high throughput analyses. Cathepsin G (CTSG), another serine protease present in azurophillic granules, was increased with a p-value of 0.006 and an FDR of 6% (**Figure 3C**). No significant differences were evident in other azurophilic proteases such as myeloperoxidase and azurocidin (**Figure E3C** in the Online Data Supplement).

Proteomic analysis also revealed reduced Ras-related Rho GTPase (RAC2) (p=0.03, FDR, 9%) and C-X-C Motif Chemokine Receptor 2 (CXCR2) (p=0.04, FDR 11%, **Figure 3C**) in PAH vs. control samples. RAC2 is an important mediator of neutrophil chemotaxis (25), and IL-8 induces a migratory response through CXCR2 as reviewed in (26). The reduction in RAC2 and CXCR2 could therefore contribute to

AJRCCM Articles in Press. Published June 13, 2022 as 10.1164/rccm.202102-0446OC

decreased PAH neutrophil migration. CXCR1 is involved in neutrophil degranulation (27) but was unchanged in the PAH vs. control samples. STRING analysis was applied to find central protein nodes that could reveal key regulators in the adhesion and transendothelial migration pathways. Vinculin (VCL) was identified as a central node in PAH samples that was linked to a reduction in integrin beta 2 (ITGB2), also known to play an integral role in adhesion and migration (28) (**Figure 3D**). We confirmed the increase in VCL in PAH vs. control neutrophils by western immunoblot (**Figure 3E**) and the decrease in ITGB2 by Fluorescence Activated Cell Sorting (FACS) (**Figure 3F**). The increase in adhesion could be explained by heightened VCL, since VCL knockout neutrophils show reduced adhesion (29). Moreover, fibronectin was used as the substrate for adhesion, and a strong VCL-fibronectin complex was previously reported (30) that could be explained by the increase in ITGB1 shown in Figure 2B. The reduction in ITGB2, like that of RAC2 and CXCR2 could explain reduced migration (31).

Transcriptomic analysis reveals an antiviral signature in PAH neutrophils. To elucidate mechanisms that could explain why NE and VCL are increased in PAH vs. control neutrophils we conducted transcriptomic analyses using RNA-seq**.** The PCA analysis of the transcriptome revealed better separation of unstimulated PAH and control neutrophils when compared with the proteomic analysis (**Figure E4A** in the Online Data Supplement). Using an FDR below 5%, we identified 1,483 differentially expressed genes as displayed in the heat map (**Figure 4A**). By utilizing Pathway Enrichment Analysis from IMPaLA, the top enriched pathway was related to neutrophil degranulation, consistent with the proteomic analysis. Other pathways were related to the immune system, innate immune system, and interferon signaling, suggesting an

AJRCCM Articles in Press. Published June 13, 2022 as 10.1164/rccm.202102-0446OC

antiviral response (**Figure 4B and Figure E4B** in the Online Data Supplement). As has been observed (32), only a small subset of 34 genes and proteins were similarly up or down regulated on the proteomic and transciptomic analyses (**Table E5** in the Online Data Supplement).

There were 15 differentially expressed genes in the interferon signaling pathway as displayed in the heatmap (**Figure 4C**). STRING analysis was applied and the interferon-induced double-stranded RNA-dependent protein kinase *(PKR)* was determined to be a central node (**Figure 4D**). When activated, PKR limits viral replication during viral infection. An increase in *PKR*, retinoic acid-inducible gene I (*RIG-I)*, type I IFN receptor (*IFNAR1),* and Interferon Gamma Receptor 2 (*IFNGR2)*, and a decrease in Ariadne RBR E3 Ubiquitin Protein Ligase 1 (*ARIH1)* are critical in mounting an effective antiviral immune response in neutrophils (33, 34). We chose five interferon related genes for validation by qPCR and confirmed a PAH neutrophil vs. control increase in *PKR, RIG-I*, and *IFNAR1*, and a decrease in *ARIH1* (**Figure 4E**). Consistent with the antiviral signature in the transcriptome, VCL and ITGB2 are also implicated in an anti-viral response. The upregulation of VCL inhibits retrovirus infection in human cells (35), and a reduction in ITGB2 in monocyte-derived macrophages results in impaired integrity of the human immunodeficiency virus (HIV) (36).

An increase in HERV-K envelope protein in PAH neutrophils is related to the antiviral signature and heightened NE. The anti-viral signature, evident from both the transcriptome and the proteome led us to investigate whether an increase in endogenous retroviral elements might be present in PAH vs. controls neutrophils. We previously reported upregulation of HERV-K dUTPase in circulating monocytes of PAH

AJRCCM Articles in Press. Published June 13, 2022 as 10.1164/rccm.202102-0446OC

patients and an increase in both the HERV-K dUTPase and the envelope protein in perivascular macrophages in PAH lung tissue sections (37). We assessed HERV-K proteins in PAH vs. control neutrophils and found an increase in the HERV-K envelope protein, but not in HERV-K dUTPase (**Figure 5A and Figure E5A** in the Online Data Supplement**)** by western immunoblot and a consistent increase by confocal microscopic analysis (**Figure 5B**). HERV-K peptides were not included in the proteomics database and HERV-K mRNA may not have been expressed in mature neutrophils accounting for its absence from the transcriptomic analyses.

To determine whether the increase in HERV-K envelope was responsible for heighted NE and VCL as well as interferon signaling, HL-60 (a neutrophil promyelocytic cell line) was transfected with a HERV-K envelope vector or a control GFP vector, and gene expression was analyzed by qPCR (**Figure 5C**). Overexpression of *HERV-K envelope* resulted in a reproducible increase in interferon genes *RIG-I* and *PKR* as well NE mRNA (**Figure 5C**) and protein (**Figure 5D**). There was, however, no significant elevation in VCL levels (**Figure E5B** in the Online Data Supplement).

Although we did not observe a difference in PAH neutrophil HERV-K dUTPase **(Figure E5E** in the Online Data Supplement**)**, monocytes can release HERV-K dUTPase and circulating levels of this retroviral protein were increased in PAH versus control plasma samples (**Figure 5E**). We added the recombinant form of HERV-K dUTPase to differentiated HL-60 cells and observed a reproducible increase in VCL (**Figure 5F and Figure E5B** in the Online Data Supplement). HERV-K dUTPase did not induce an elevation in *PKR or RIG-1 mRNA* or in NE protein (**Figure E5C and E5D** in the Online Data Supplement). The dose of dUTPase chosen was based upon

AJRCCM Articles in Press. Published June 13, 2022 as 10.1164/rccm.202102-0446OC

previous studies by our group showing the impact of dUTPase on cytokine release (37) and EndMT (38). We then determined whether the increase in vinculin could explain the increase in adhesion and the reduction in migration. Indeed, reducing vinculin by siRNA (**Figure E6A**) completely suppressed the increase in adhesion of dHL-60 cells in response to HERV-K dUTPase **(Figure E6B).** Migration of dHL-60 cells was neither increased by HERV-K dUTPase nor suppressed by vinculin siRNA **(Figure E6C).**

CD66b PAH EVs display increased NE and elevated HERV-K envelope. Transport of increased NE via neutrophil EVs was observed in bronchial secretions from patients with chronic obstructive pulmonary disease (COPD) and these EVs caused COPD-like changes in mice (18). A CD66b antibody was used to purify neutrophil specific EVs from PAH and control plasma after total EV isolation using a nanofiltration-based EV isolation tool, EV Total Isolation Chip (39)**.** EV size was confirmed by NanoSight (**Figure 6A**) and by transmission electron microscopy (**Figure 6B).** However, the neutrophil supernatant following depletion of CD66b EVs also expressed about 50% of the elastase activity seen in the EVs with a relative increase in PAH vs. control **(Figure E7A** in the Online Data Supplement), suggesting that only about half of the elastase released is in neutrophil EVs. Approximately 50% of total EVs in the plasma were CD66b but neither total EVs, CD66b EVs, or non CD66b EVs were increased in PAH vs. control plasma **(Figure E7B** in the online Data Supplement**).** On the other hand, pooled PAH EVs exhibited an approximately 2-fold increase in NE protein, assessed by western immunoblot (**Figure 6C**) and by activity (**Figure 6D**) as well as a 4-fold increase in HERV-K envelope (**Figure 6C**). Moreover, EV elastase and HERV-K

AJRCCM Articles in Press. Published June 13, 2022 as 10.1164/rccm.202102-0446OC

envelope were primarily in the neutrophil (CD66b) vs. non-neutrophil (non-CD66b) EVs (**Figure E7C** in the Online Data Supplement).

CD66b PAH EVs cause pulmonary hypertension in a mouse model. Neutrophil EVs isolated from pooled PAH and control plasma were given by tail vein injection, twice a week for five weeks to adult male mice (**Figure 7A)** following a protocol similar to that used by other investigators to induce COPD in mice (18). The use of pooled plasma minimized the variability form patient to patient but allowed for variability in the response of the mice. One mouse in the PAH cohort died prior to assessment. Experimental pulmonary hypertension was evident following injection of PAH but not control neutrophil EVs, judged by decreased pulmonary artery acceleration time (PAAT) (**Figure 7B**), and increased right ventricular systolic pressure (RVSP), right ventricular hypertrophy (RVH), and peripheral pulmonary arterial muscularizaton (**Figure 7B-E**). Pre-treatment of the EVs with the NE inhibitor and antiviral agent elafin prevented the increase in RVSP and RVH (**Figure 7C and 7D**) as well as the increased muscularization of the pulmonary arteries (**Figure 7E**). Cardiac output, left ventricular ejection fraction **(Figure E8A)** and the relative proportions of neutrophils, monocytes, lymphocytes, and eosinophils **(Figure E8B)** were not affected by the EV treatment.

DISCUSSION

Despite many advances in our understanding of the sequelae of chronic inflammation related to PAH pathology, the role of neutrophils has remained elusive. Here, we provide evidence of neutrophil dysfunction in PAH that we link to an antiviral response that results in adverse remodeling of the pulmonary vasculature. PAH

AJRCCM Articles in Press. Published June 13, 2022 as 10.1164/rccm.202102-0446OC

neutrophils produce an increase in NE leading to a propensity to form NETs and are characterized by increased adhesion and reduced transendothelial migration attributed to elevated levels of VCL (35, 36). Augmentation of HERV-K envelope in PAH neutrophils can explain the increase in elastase and in interferon genes, whereas a heightened level of circulating HERV-K dUTPase can induce VCL. EVs released from PAH neutrophils contain increased NE and HERV-K envelope and cause pulmonary hypertension in mice, mitigated by the elastase inhibitor elafin (summary schema, **Figure 8**).

Our previous studies attributed the increase of NE in PAH to its production by pulmonary arterial SMC in patients and experimental models (40). Here we demonstrate that PAH neutrophils also have heightened NE, which markedly increases the propensity for elastase mediated tissue damage, in part as a result of heightened predisposition to NET formation previously described in PAH tissues (12, 17, 41), and in part related to NE released in EVs (18). While NET markers (DNA, myeloperoxidase, and citrullinated histone H3) were previously identified in PAH lung tissue (42), and NE on NETs is shielded from natural circulating large molecule inhibitors such as alpha-1 antitrypsin (41), our studies now provide evidence that small protein inhibitors such as elafin can block NE activity and NET formation. They also raise the question as to whether the success of elafin in previous studies in the Sugen/hypoxia rat model (10) is related to its ability to block neutrophil derived NE in EVs.

PAH neutrophils are further characterized by increased adhesion and reduced migration that we relate to an increase in neutrophil VCL previously shown to be

AJRCCM Articles in Press. Published June 13, 2022 as 10.1164/rccm.202102-0446OC

responsible for these abnormalities (29). Furthermore, vinclulin suppresses ITGB2 (43), consistent with reduced neutrophil emigration in ITGB2 null mice (31).

A PAH neutrophil anti-viral signature consistent with an interferon innate immune response (44) is related to increased NE and VCL. PAH neutrophils express high levels of endogenous retrovirus HERV-K, consistent with our previous observation in PAH monocytes and macrophages (37). HERVs are non-infectious remnants of ancient viral infections incorporated in our genome. They are highly expressed in embryonic stem cells as part of an innate immune response but undergo silencing in differentiated cells in response to extensive methylation of regulatory elements (45). Expansion of retroviral RNA sequences with production of double stranded RNA and proteins can occur as part of an innate defense mechanism (46) in response to systemic and environmental cues such as exogenous viruses, including human herpesviruses and HIV (47). Although an increase in HERVs has been described in cancer (48) and in autoimmunity, and associated with an antiviral interferon response (44), HERV expansion in neutrophils has not been described and, the mechanism for HERV upregulation in disease has been largely elusive . KAP1 is a methylase implicated in HERV methylation (49) that is controlled by a BMP responsive lnc RNA, BORG (50). So, it is possible that with reduced BMPR2 function, as occurs in PAH, BORG and KAP1 are reduced, resulting in demethylation and increased expression of HERVs (50).

Overexpression of HERV-K envelope in a neutrophil cell line was sufficient to induce the production of NE. While the increase in NE likely represents the activation of an innate immune response, future studies will be of interest in delineating the molecular mechanism involved. HERVs can also mediate a chronic interferon response

AJRCCM Articles in Press. Published June 13, 2022 as 10.1164/rccm.202102-0446OC

in association with the production of double stranded RNA (46, 51), and interferon treatment is associated with the development of PAH (52) but interferons have not previously been linked to elastase production. Our studies showing that HL60 cells transfected with HERV-K plasmid induce elastase mRNA suggests that the increase in elastase may take place when mRNA synthesis of elastase is evident, i,e., at the promyelocyte stage. Whether this occurs in response a specific transcription factor or to a reduction in a microRNA would be of interest ot pursue in future studies.

Infection of monocyte-derived macrophages with HIV led to the upregulation of VCL, and as a consequence, VCL negatively affected the propagation of the virus (53). Similar to HIV, recombinant HERV-K dUTPase also resulted in an increase in VCL, presumably by a similar mechanism.

Pathologic EVs are recognized in many diseases, including autoimmunity (54), cancer (48), and COPD (18). It is interesting that inhibition of EV formation prevented chronic hypoxia-induced PAH in mice (55), Recent studies support HERV-K delivery in tumor EVs as a mechanism contributing to cancer (48), and NE on EVs as directly related to degradation of airway structure in mice, phenocopying COPD (18, 56). In that model, NE on EVs was susceptible to inhibition by small molecules but evaded large protease inhibitors such as alpha-1 anti-trypsin (18). Here we identify an increase in both NE and HERV-K envelope in PAH neutrophil EVs, and demonstrate that recombinant elafin, a small 6 kDa protein, successfully blocked pulmonary hypertension induced by PAH EVs. Elafin is a potent, naturally occurring NE inhibitor (10), with anti-inflammatory and antiviral properties that could explain its effect in preventing the adverse impact of HERV-K transferred in neutrophil PAH EVs, but only if the mice

AJRCCM Articles in Press. Published June 13, 2022 as 10.1164/rccm.202102-0446OC

recognize HERV-K envelope as a molecule similar to their own retroviral element, as they did with HERV-K dUTPase. Elafin is an NFκB inhibitor, and NFκB activation is associated with the interferon antiviral response (57). Elafin also suppresses viral attachment and transcytosis (19). Taken together, our studies reveal a mechanistic relationship between PAH and an increase in HERV-K mRNA and proteins that reprograms neutrophils by inducing an antiviral response. The production of large amounts of NE released in NETs and in EVs can have local and long-range adverse impact on vascular cells. These features can be targeted therapeutically by elafin.

ACKNOWLEDGMENTS

We thank Drs. Angela Rogers and David Cornfield at Stanford University for their critical input to our work; Devon Kelley, Matthew A. Bill, Jordan Burgess, Audrey Inglis, Alex A. Yacob, and Divya Rajmohan for collecting PAH patient blood samples, and Kalyani A. Boralkar and Shadi P. Bagherzadeh for the collection of healthy donor control blood samples. We greatly appreciate Dr. Michal B. Roof for her input, editorial, and technical assistance and Ms. Michelle Ameri for her administrative help. We thank Dr. Oliver Wiedow and Proteo-Biotech-AG in Kiel, Germany, for the kind gift of Elafin. We thank Ms. Ruiqi Jian for proteomic sample preparation, Dr. Tushar Desai for the use of the Leica confocal microscope, Dr. Dan Bernstein for the use of his cardiac phenotyping equipment. This work used the Genome Sequencing Service Center of the Stanford Center for Genomics and Personalized Medicine Sequencing Center, supported by NIH grants S10 OD025212 and P30 DK116074 (MPS). Proteomic peptide isolation was performed under the guidance of Anna Okuma, Ryan Leib, Christopher M. Adams, and Roasa Mehmood at the Vincent Coates Foundation Mass Spectrometry Laboratory,

AJRCCM Articles in Press. Published June 13, 2022 as 10.1164/rccm.202102-0446OC

Stanford University. Mouse histology sectioning was performed by the Stanford Department of Comparative Medicine Animal Histology Services (AHS). Transmission electron microscopy imaging was performed by the Stanford Cell Sciences Imaging Facility (CSIF), which is partly supported by ARRA/NCRR grant S10 RR026780. Flow samples were run at the Stanford Shared FACS Facility. The Pulmonary Hypertension Breakthrough Initiative (PHBI), funded by NIH/NHLBI R24 HL123767 and the Cardiovascular Medical Research and Education Fund (CMREF) UL1RR024986, provided PAEC from PAH patients and unused donor lungs.

COMPETING INTERESTS

None

DATA AVAILABILITY

RNAseq data is deposited in the NCBI Sequence Read Archive (SRA) with accession number PRJNA822411.

Proteomic Data are available via ProteomeXchange with identifier PXD023134.

Code availability: Code related to RNA-seq data analysis is available on the Benayoun lab github.

AJRCCM Articles in Press. Published June 13, 2022 as 10.1164/rccm.202102-0446OC

REFERENCES

1. Rabinovitch M. Molecular pathogenesis of pulmonary arterial hypertension. *J Clin Invest* 2012; 122: 4306-4313.

2. Rabinovitch M, Bothwell T, Hayakawa BN, Williams WG, Trusler GA, Rowe RD, Olley PM, Cutz E. Pulmonary artery endothelial abnormalities in patients with congenital heart defects and pulmonary hypertension. A correlation of light with scanning electron microscopy and transmission electron microscopy. *Lab Invest* 1986; 55: 632-653.

3. Kim YM, Haghighat L, Spiekerkoetter E, Sawada H, Alvira CM, Wang L, Acharya S, Rodriguez-Colon G, Orton A, Zhao M, Rabinovitch M. Neutrophil elastase is produced by pulmonary artery smooth muscle cells and is linked to neointimal lesions. *Am J Pathol* 2011; 179: 1560-1572.

4. Dodson RB, Morgan MR, Galambos C, Hunter KS, Abman SH. Chronic intrauterine pulmonary hypertension increases main pulmonary artery stiffness and adventitial remodeling in fetal sheep. *Am J Physiol Lung Cell Mol Physiol* 2014; 307: L822-828.

5. Senior RM, Griffin GL, Mecham RP, Wrenn DS, Prasad KU, Urry DW. Val-Gly-Val-Ala-Pro-Gly, a repeating peptide in elastin, is chemotactic for fibroblasts and monocytes. *J Cell Biol* 1984; 99: 870-874.

6. Thompson K, Rabinovitch M. Exogenous leukocyte and endogenous elastases can mediate mitogenic activity in pulmonary artery smooth muscle cells by release of

AJRCCM Articles in Press. Published June 13, 2022 as 10.1164/rccm.202102-0446OC

extracellular-matrix bound basic fibroblast growth factor. *J Cell Physiol* 1996; 166: 495-505.

7. Jones PL, Crack J, Rabinovitch M. Regulation of tenascin-C, a vascular smooth muscle cell survival factor that interacts with the alpha v beta 3 integrin to promote epidermal growth factor receptor phosphorylation and growth. *J Cell Biol* 1997; 139: 279-293.

8. Li DY, Brooke B, Davis EC, Mecham RP, Sorensen LK, Boak BB, Eichwald E, Keating MT. Elastin is an essential determinant of arterial morphogenesis. *Nature* 1998; 393: 276-280.

9. Cowan KN, Heilbut A, Humpl T, Lam C, Ito S, Rabinovitch M. Complete reversal of fatal pulmonary hypertension in rats by a serine elastase inhibitor. *Nat Med* 2000; 6: 698-702.

10. Nickel NP, Spiekerkoetter E, Gu M, Li CG, Li H, Kaschwich M, Diebold I, Hennigs JK, Kim KY, Miyagawa K, Wang L, Cao A, Sa S, Jiang X, Stockstill RW, Nicolls MR, Zamanian RT, Bland RD, Rabinovitch M. Elafin Reverses Pulmonary Hypertension via Caveolin-1-Dependent Bone Morphogenetic Protein Signaling. *Am J Respir Crit Care Med* 2015; 191: 1273-1286.

11. Rose F, Hattar K, Gakisch S, Grimminger F, Olschewski H, Seeger W, Tschuschner A, Schermuly RT, Weissmann N, Hanze J, Sibelius U, Ghofrani HA. Increased neutrophil mediator release in patients with pulmonary hypertension--suppression by inhaled iloprost. *Thromb Haemost* 2003; 90: 1141-1149.

AJRCCM Articles in Press. Published June 13, 2022 as 10.1164/rccm.202102-0446OC

12. Aldabbous L, Abdul-Salam V, McKinnon T, Duluc L, Pepke-Zaba J, Southwood M, Ainscough AJ, Hadinnapola C, Wilkins MR, Toshner M, Wojciak-Stothard B. Neutrophil Extracellular Traps Promote Angiogenesis: Evidence From Vascular Pathology in Pulmonary Hypertension. *Arterioscler Thromb Vasc Biol* 2016; 36: 2078-2087.

13. Sweatt AJ, Miyagawa K, Rhodes CJ, Taylor S, Del Rosario PA, Hsi A, Haddad F, Spiekerkoetter E, Bental-Roof M, Bland RD, Swietlik EM, Gräf S, Wilkins MR, Morrell NW, Nicolls MR, Rabinovitch M, Zamanian RT. Severe Pulmonary Arterial Hypertension Is Characterized by Increased Neutrophil Elastase and Relative Elafin Deficiency. *Chest* 2021; 160: 1442-1458.

14. Ozpelit E, Akdeniz B, Ozpelit ME, Tas S, Bozkurt S, Tertemiz KC, Sevinc C, Badak O. Prognostic value of neutrophil-to-lymphocyte ratio in pulmonary arterial hypertension. *J Int Med Res* 2015; 43: 661-671.

15. Papayannopoulos V, Metzler KD, Hakkim A, Zychlinsky A. Neutrophil elastase and myeloperoxidase regulate the formation of neutrophil extracellular traps. *J Cell Biol* 2010; 191: 677-691.

16. Selders GS, Fetz AE, Radic MZ, Bowlin GL. An overview of the role of neutrophils in innate immunity, inflammation and host-biomaterial integration. *Regen Biomater* 2017; 4: 55-68.

17. Saffarzadeh M, Juenemann C, Queisser MA, Lochnit G, Barreto G, Galuska SP, Lohmeyer J, Preissner KT. Neutrophil extracellular traps directly induce epithelial

AJRCCM Articles in Press. Published June 13, 2022 as 10.1164/rccm.202102-0446OC

and endothelial cell death: a predominant role of histones. *PLoS One* 2012; 7: e32366.

18. Genschmer KR, Russell DW, Lal C, Szul T, Bratcher PE, Noerager BD, Abdul Roda M, Xu X, Rezonzew G, Viera L, Dobosh BS, Margaroli C, Abdalla TH, King RW, McNicholas CM, Wells JM, Dransfield MT, Tirouvanziam R, Gaggar A, Blalock JE. Activated PMN Exosomes: Pathogenic Entities Causing Matrix Destruction and Disease in the Lung. *Cell* 2019; 176: 113-126 e115.

19. Drannik AG, Nag K, Sallenave JM, Rosenthal KL. Antiviral activity of trappin-2 and elafin in vitro and in vivo against genital herpes. *J Virol* 2013; 87: 7526-7538.

20. Taylor S, Moonen JR, Miyagawa K, Gu M, Sa S, Hennigs JK, Wang L, Rabinovitch M. Increased Migration of Neutrophils Across Endothelial Cells from Patients with Pulmonary Arterial Hypertension is Related to Reduced Platelet Endothelial Cell Adhesion Molecule -1 and is Prevented by the Neutrophil Elastase Inhibitor Elafin. *Arterioscler Thromb Vasc Biol* 2016; 36: A596.

21. Taylor S, Cao A, Wang L, Gu M, Miyagawa K, Rabinovitch M. Heightened Elastase Along With Propensity to Form Extracellular Traps and an Antiviral Signature. *Circ Res* 2017; 136: A16861.

22. Taylor S, Benayoun BA, Contrepois K, Cao A, Moonen JR, Wang L, Gu M, Miyagawa K, Thompson R, Snyder MP, Rabinovitch M. How the Antiviral Signature in Neutrophils from Patients with Pulmonary Arterial Hypertension Affects Function. *Am J Respir Crit Care Med* 2019; 199: A6750.

AJRCCM Articles in Press. Published June 13, 2022 as 10.1164/rccm.202102-0446OC

23. Simonneau G, Gatzoulis MA, Adatia I, Celermajer D, Denton C, Ghofrani A, Gomez Sanchez MA, Krishna Kumar R, Landzberg M, Machado RF, Olschewski H, Robbins IM, Souza R. Updated clinical classification of pulmonary hypertension. *J Am Coll Cardiol* 2013; 62: D34-41.

24. Martinod K, Witsch T, Farley K, Gallant M, Remold-O'Donnell E, Wagner DD. Neutrophil elastase-deficient mice form neutrophil extracellular traps in an experimental model of deep vein thrombosis. *J Thromb Haemost* 2016; 14: 551-558.

25. Carstanjen D, Yamauchi A, Koornneef A, Zang H, Filippi MD, Harris C, Towe J, Atkinson S, Zheng Y, Dinauer MC, Williams DA. Rac2 regulates neutrophil chemotaxis, superoxide production, and myeloid colony formation through multiple distinct effector pathways. *J Immunol* 2005; 174: 4613-4620.

26. Stadtmann A, Zarbock A. CXCR2: From Bench to Bedside. *Front Immunol* 2012; 3: 263.

27. Jones SA, Wolf M, Qin S, Mackay CR, Baggiolini M. Different functions for the interleukin 8 receptors (IL-8R) of human neutrophil leukocytes: NADPH oxidase and phospholipase D are activated through IL-8R1 but not IL-8R2. *Proc Natl Acad Sci U S A* 1996; 93: 6682-6686.

28. Morland CM, Morland BJ, Darbyshire PJ, Stockley RA. Migration of CD18-deficient neutrophils in vitro: evidence for a CD18-independent pathway induced by IL-8. *Biochim Biophys Acta* 2000; 1500: 70-76.

AJRCCM Articles in Press. Published June 13, 2022 as 10.1164/rccm.202102-0446OC

29. Wilson ZS, Witt H, Hazlett L, Harman M, Neumann BM, Whitman A, Patel M, Ross RS, Franck C, Reichner JS, Lefort CT. Context-Dependent Role of Vinculin in Neutrophil Adhesion, Motility and Trafficking. *Sci Rep* 2020; 10: 2142.

30. Singer, II. Association of fibronectin and vinculin with focal contacts and stress fibers in stationary hamster fibroblasts. *J Cell Biol* 1982; 92: 398-408.

31. Walzog B, Scharffetter-Kochanek K, Gaehtgens P. Impairment of neutrophil emigration in CD18-null mice. *Am J Physiol* 1999; 276: G1125-1130.

32. Grabowski P, Hesse S, Hollizeck S, Rohlfs M, Behrends U, Sherkat R, Tamary H, Unal E, Somech R, Patiroglu T, Canzar S, van der Werff Ten Bosch J, Klein C, Rappsilber J. Proteome Analysis of Human Neutrophil Granulocytes From Patients With Monogenic Disease Using Data-independent Acquisition. *Mol Cell Proteomics* 2019; 18: 760-772.

33. Munir M, Berg M. The multiple faces of proteinkinase R in antiviral defense. *Virulence* 2013; 4: 85-89.

34. Huttenhain R, Xu J, Burton LA, Gordon DE, Hultquist JF, Johnson JR, Satkamp L, Hiatt J, Rhee DY, Baek K, Crosby DC, Frankel AD, Marson A, Harper JW, Alpi AF, Schulman BA, Gross JD, Krogan NJ. ARIH2 Is a Vif-Dependent Regulator of CUL5-Mediated APOBEC3G Degradation in HIV Infection. *Cell Host Microbe* 2019; 26: 86-99 e87.

AJRCCM Articles in Press. Published June 13, 2022 as 10.1164/rccm.202102-0446OC

35. Brown C, Morham SG, Walsh D, Naghavi MH. Focal adhesion proteins talin-1 and vinculin negatively affect paxillin phosphorylation and limit retroviral infection. *J Mol Biol* 2011; 410: 761-777.

36. Pelchen-Matthews A, Giese S, Mlcochova P, Turner J, Marsh M. beta2 integrin adhesion complexes maintain the integrity of HIV-1 assembly compartments in primary macrophages. *Traffic* 2012; 13: 273-291.

37. Saito T, Miyagawa K, Chen SY, Tamosiuniene R, Wang L, Sharpe O, Samayoa E, Harada D, Moonen JAJ, Cao A, Chen PI, Hennigs JK, Gu M, Li CG, Leib RD, Li D, Adams CM, Del Rosario PA, Bill M, Haddad F, Montoya JG, Robinson WH, Fantl WJ, Nolan GP, Zamanian RT, Nicolls MR, Chiu CY, Ariza ME, Rabinovitch M. Upregulation of Human Endogenous Retrovirus-K Is Linked to Immunity and Inflammation in Pulmonary Arterial Hypertension. *Circulation* 2017; 136: 1920-1935.

38. Otsuki S, Saito T, Taylor S, Li D, Moonen JR, Marciano DP, Harper RL, Cao A, Wang L, Ariza ME, Rabinovitch M. Monocyte-released HERV-K dUTPase engages TLR4 and MCAM causing endothelial mesenchymal transition. *JCI Insight* 2021; 6.

39. Liu F, Vermesh O, Mani V, Ge TJ, Madsen SJ, Sabour A, Hsu EC, Gowrishankar G, Kanada M, Jokerst JV, Sierra RG, Chang E, Lau K, Sridhar K, Bermudez A, Pitteri SJ, Stoyanova T, Sinclair R, Nair VS, Gambhir SS, Demirci U. The Exosome Total Isolation Chip. *ACS Nano* 2017; 11: 10712-10723.

AJRCCM Articles in Press. Published June 13, 2022 as 10.1164/rccm.202102-0446OC

40. Taylor S, Dirir O, Zamanian RT, Rabinovitch M, Thompson AAR. The Role of Neutrophils and Neutrophil Elastase in Pulmonary Arterial Hypertension. *Front Med (Lausanne)* 2018; 5: 217.

41. Hahn J, Schauer C, Czegley C, Kling L, Petru L, Schmid B, Weidner D, Reinwald C, Biermann MHC, Blunder S, Ernst J, Lesner A, Bauerle T, Palmisano R, Christiansen S, Herrmann M, Bozec A, Gruber R, Schett G, Hoffmann MH. Aggregated neutrophil extracellular traps resolve inflammation by proteolysis of cytokines and chemokines and protection from antiproteases. *FASEB J* 2019; 33: 1401-1414.

42. Villanueva E, Yalavarthi S, Berthier CC, Hodgin JB, Khandpur R, Lin AM, Rubin CJ, Zhao W, Olsen SH, Klinker M, Shealy D, Denny MF, Plumas J, Chaperot L, Kretzler M, Bruce AT, Kaplan MJ. Netting neutrophils induce endothelial damage, infiltrate tissues, and expose immunostimulatory molecules in systemic lupus erythematosus. *J Immunol* 2011; 187: 538-552.

43. Smith CW, Rothlein R, Hughes BJ, Mariscalco MM, Rudloff HE, Schmalstieg FC, Anderson DC. Recognition of an endothelial determinant for CD 18-dependent human neutrophil adherence and transendothelial migration. *J Clin Invest* 1988; 82: 1746-1756.

44. Canadas I, Thummalapalli R, Kim JW, Kitajima S, Jenkins RW, Christensen CL, Campisi M, Kuang Y, Zhang Y, Gjini E, Zhang G, Tian T, Sen DR, Miao D, Imamura Y, Thai T, Piel B, Terai H, Aref AR, Hagan T, Koyama S, Watanabe M, Baba H, Adeni AE, Lydon CA, Tamayo P, Wei Z, Herlyn M, Barbie TU, Uppaluri

AJRCCM Articles in Press. Published June 13, 2022 as 10.1164/rccm.202102-0446OC

R, Sholl LM, Sicinska E, Sands J, Rodig S, Wong KK, Paweletz CP, Watanabe H, Barbie DA. Tumor innate immunity primed by specific interferon-stimulated endogenous retroviruses. *Nat Med* 2018; 24: 1143-1150.

45. Grow EJ, Flynn RA, Chavez SL, Bayless NL, Wossidlo M, Wesche DJ, Martin L, Ware CB, Blish CA, Chang HY, Pera RA, Wysocka J. Intrinsic retroviral reactivation in human preimplantation embryos and pluripotent cells. *Nature* 2015; 522: 221-225.

46. Chiappinelli KB, Strissel PL, Desrichard A, Li H, Henke C, Akman B, Hein A, Rote NS, Cope LM, Snyder A, Makarov V, Budhu S, Slamon DJ, Wolchok JD, Pardoll DM, Beckmann MW, Zahnow CA, Merghoub T, Chan TA, Baylin SB, Strick R. Inhibiting DNA Methylation Causes an Interferon Response in Cancer via dsRNA Including Endogenous Retroviruses. *Cell* 2015; 162: 974-986.

47. Chen J, Foroozesh M, Qin Z. Transactivation of human endogenous retroviruses by tumor viruses and their functions in virus-associated malignancies. *Oncogenesis* 2019; 8: 6.

48. Zhou F, Li M, Wei Y, Lin K, Lu Y, Shen J, Johanning GL, Wang-Johanning F. Activation of HERV-K Env protein is essential for tumorigenesis and metastasis of breast cancer cells. *Oncotarget* 2016; 7: 84093-84117.

49. Tie CH, Fernandes L, Conde L, Robbez-Masson L, Sumner RP, Peacock T, Rodriguez-Plata MT, Mickute G, Gifford R, Towers GJ, Herrero J, Rowe HM.

AJRCCM Articles in Press. Published June 13, 2022 as 10.1164/rccm.202102-0446OC

KAP1 regulates endogenous retroviruses in adult human cells and contributes to innate immune control. *EMBO Rep* 2018; 19.

50. Gooding AJ, Zhang B, Jahanbani FK, Gilmore HL, Chang JC, Valadkhan S, Schiemann WP. The lncRNA BORG Drives Breast Cancer Metastasis and Disease Recurrence. *Sci Rep* 2017; 7: 12698.

51. Ghosh S, Guimaraes JC, Lanzafame M, Schmidt A, Syed AP, Dimitriades B, Borsch A, Ghosh S, Mittal N, Montavon T, Correia AL, Danner J, Meister G, Terracciano LM, Pfeffer S, Piscuoglio S, Zavolan M. Prevention of dsRNA-induced interferon signaling by AGO1x is linked to breast cancer cell proliferation. *EMBO J* 2020; 39: e103922.

52. Savale L, Sattler C, Gunther S, Montani D, Chaumais MC, Perrin S, Jais X, Seferian A, Jovan R, Bulifon S, Parent F, Simonneau G, Humbert M, Sitbon O. Pulmonary arterial hypertension in patients treated with interferon. *Eur Respir J* 2014; 44: 1627-1634.

53. Nellaker C, Yao Y, Jones-Brando L, Mallet F, Yolken RH, Karlsson H. Transactivation of elements in the human endogenous retrovirus W family by viral infection. *Retrovirology* 2006; 3: 44.

54. Sellam J, Proulle V, Jungel A, Ittah M, Miceli Richard C, Gottenberg JE, Toti F, Benessiano J, Gay S, Freyssinet JM, Mariette X. Increased levels of circulating microparticles in primary Sjogren's syndrome, systemic lupus erythematosus and

AJRCCM Articles in Press. Published June 13, 2022 as 10.1164/rccm.202102-0446OC

rheumatoid arthritis and relation with disease activity. *Arthritis Res Ther* 2009; 11: R156.

55. Zhang M, Xin W, Ma C, Zhang H, Mao M, Liu Y, Zheng X, Zhang L, Yu X, Li H, Zhu D. Exosomal 15-LO2 mediates hypoxia-induced pulmonary artery hypertension in vivo and in vitro. *Cell Death Dis* 2018; 9: 1022.

56. Balaj L, Lessard R, Dai L, Cho YJ, Pomeroy SL, Breakefield XO, Skog J. Tumour microvesicles contain retrotransposon elements and amplified oncogene sequences. *Nat Commun* 2011; 2: 180.

57. Li K, Zhang F, Wei L, Han Z, Liu X, Pan Y, Guo C, Han W. Recombinant Human Elafin Ameliorates Chronic Hyperoxia-Induced Lung Injury by Inhibiting Nuclear Factor-Kappa B Signaling in Neonatal Mice. *J Interferon Cytokine Res* 2020; 40: 320-330.

AJRCCM Articles in Press. Published June 13, 2022 as 10.1164/rccm.202102-0446OC

FIGURE LEGENDS

Figure 1. Increased NE protein and NE-mediated NETosis in PAH neutrophils.

Neutrophils were isolated from peripheral blood of healthy donor controls (Con) and PAH patients (PAH) as described in the Methods. **(A)** Representative western immunoblot and quantification below, displaying NE relative to histone H3 (H3) in PAH vs. Con neutrophils (n=8 Con and n=12 PAH). **(B)** NE activity in neutrophil cell lysates as determined by production of BODIPY FL labeled fluorescent elastin fragments from self-quenching BODIPY FL-conjugated bovine neck ligament elastin (n=11 Con and n=10 PAH). **(C)** NE activity in the extracellular supernatant 2h after IL-8 stimulation of neutrophils (n=3). In a-e $5x10^6$ cells were used for each assay. **(D)** Number of neutrophils per mL blood in Con and PAH, determined using a Millipore scepter cell counter (n=11 Con and n=10 PAH). **(E)** Total NE activity calculated per 1mL blood. NE activity measured in 1b, relative to neutrophils counted per 1d, to yield NE per mL of blood. **(F)** Neutrophil extracellular traps (NET) were visualized via H3 citrullination (red) and SYTOX green, and quantified by SYTOX green fluorescence, 60 min following PMA stimulation and treatment with vehicle (Veh) or the NE inhibitor elafin (1 μg/mL). The nuclei were counterstained with DAPI (blue). Scale bar = 40 μm. Violin plots represents variable distribution of 4 representative biological replicates (n = 24-104 cells). In A-E: Bars represent mean ± SEM. *p<0.05, **p<0.01, ***p<0.001 by unpaired Student t-test (A, B, D, E). In F for the violin plots, ****p<0.0001 by one-way ANOVA followed by Dunnett's post hoc test.

AJRCCM Articles in Press. Published June 13, 2022 as 10.1164/rccm.202102-0446OC

Figure 2. PAH neutrophils exhibit increased adhesion and reduced migration.

(A) Neutrophils were incubated on fibronectin-coated coverslips for 5 min and the mean number of adherent cells was assessed from 3-5 randomly selected visual fields. Representative image of adherent neutrophils and quantification on the right (n=6 Con and n=9 PAH). Scale bar=40 μM. **(B)** Representative western immunoblot and quantification below of ITGB1 in PAH vs. Con neutrophils (n=3). **(C)** Neutrophils were allowed to adhere to fibronectin coated coverslips for 5 min and then stimulated with 100 ng/mL IL-8 in RPMI for 30 min. Migration of PAH vs. Con neutrophils is illustrated as spider plots and distance migrated quantified (on the right) using MtrackJ (Image J). Quantification was performed for at least 10 migratory cells per field (n=3 fields). **(D)** Calcein-AM labeled PAH vs. Con neutrophils were plated on fibronectin coated transwell chambers, and then stimulated with 100 ng/mL IL-8. Transmigration was assessed after 60 min of stimulation (n=4). **(E)** Calcein-AM labeled PAH vs. Con neutrophils were incubated on Con or PAH PAEC monolayers grown to confluence in transwell chambers. Trans-endothelial migration of PAH vs. Con neutrophils across Con or PAH PAEC 60 min following IL-8 (100 ng/mL) stimulation (n=8-12). In **A-D**: Bars represent mean ± SEM. *p<0.05, **p<0.01, ***p<0.001 by Mann-Whitney test (A, D). In **E**: Range represent mean ± SEM. *p<0.05, **p<0.01, ***p<0.001 by one-way ANOVA followed by Dunnett's post hoc test.

Figure 3. Proteomic analysis links increased vinculin to PAH neutrophil dysfunction.

(A) Unbiased proteomic analysis of isolated PAH vs. Con neutrophils by mass

AJRCCM Articles in Press. Published June 13, 2022 as 10.1164/rccm.202102-0446OC

spectroscopy. Heatmap depicts unsupervised hierarchical clustering of 483 differentially expressed proteins between the two groups (adjusted P value <0.10, n=6 Con and n=12 PAH. **(B)** Integrated Molecular Pathway-Level Analysis (IMPALA) reflecting significant differentially expressed proteins in PAH vs. Con neutrophils consistent with functional abnormalities identified in Figures 1 and 2. **(C)** Fold-change in NE, CTSG, RAC2, CXCR1, CXCR2 from proteomics analysis comparing PAH vs. Con neutrophils (n=6 Con and n=12 PAH). **(D)** STRING analysis of significant proteins in the Adhesion and TEM pathways, depicting protein up- or down-regulated in PAH vs. Con.
(E) Representative western immunoblot and quantification below, validating the upregulation of VCL in PAH vs. Con neutrophils (n=6). **(F)** Validation and quantification of ITGB2 expression in neutrophils from Con or PAH by FACS analysis. Representative scatter graphs on the left, with quantification on the right (n=7 Con and n=8 PAH. In C, E, F: Bars represent mean ± SEM. *p<0.05, **p<0.01, by Mann-Whitney test.

Figure 4. Transcriptomic analysis reveals an antiviral signature in PAH neutrophils.

(A) Unbiased transcriptomics analysis was performed on neutrophils isolated from PAH vs. Con patients. Heatmap depicts unsupervised hierarchical clustering of 1,565 differentially expressed genes between the two groups (adjusted P value <0.05). (n=6 Con and n=9 PAH). **(B)** IMPaLA pathway analysis of significant genes in PAH vs. Con neutrophils. **(C)** Heatmap of significant differentially regulated genes in the interferon pathway, derived from the IMPaLA pathway analysis. **(D)** STRING analysis of significantly changed genes in the interferon pathway, depicting genes that are up- or down-regulated with key central nodes in PAH vs. Con. **(E)** mRNA expression by PCR,

AJRCCM Articles in Press. Published June 13, 2022 as 10.1164/rccm.202102-0446OC

validating the changes in *PKR, RIG-I, IFNAR1, ARIH1,* and *IFNGR2 observed* in neutrophils isolated form Con or PAH patients. Bars represent mean ±SEM. *PKR* (n=8); *IFNR1* and *ARIH1* (n=6); *RIG-I* (n=6 Con and n=9 PAH); and *INFNGR*2 (n=3). *p<0.05, **p<0.01 by Mann-Whitney test.

Figure 5. An increase in HERV-K envelope protein in PAH neutrophils is related to the antiviral signature and heightened NE.

(A) Representative western immunoblot analysis and quantification of HERV-K envelope (HERV-K env) relative to histone H3 (H3) in PAH vs. Con neutrophils (n=6 Con and n=10 PAH). **(B)** Immunofluorescence microscopy visualization of HERV-K env protein (green) and nuclei by DAPI staining (blue) in Con and PAH neutrophils. Antibodies used for staining are described in the "Methods". A range of z-stack images was collected for image analysis. Mean fluorescence intensity (MFI) and cell area were quantified via image j from 3-5 randomly selected visual fields (n=3). Scale bar = 20μm. **(C-F)** HL-60 cells were cultured in RPMI complete media and transfected using HL-60 Cell Avalanche transfection reagent per manufacturer's protocol. **(C)** RT-qPCR analysis of *HERV-K envelope*, NE, *RIG-I*, and *PKR* mRNA in HL-60 cells overexpressing HERV-K env (n=3). Raw PCR data, including the $\Delta\Delta$Ct calculation, is included in **Table E7.** **(D)** Representative western immunoblot and quantification of NE relative to H3 in HL-60 cells overexpressing HERV-K env (n=3). **(E)** Western immunoblot analysis and quantification of HERV-K dUTPase (dUTPase) in plasma collected from Con or PAH patients. Plasma was depleted of albumin, measured by BCA, and run on a gradient gel (n=17). (**F**) Representative western immunoblot analysis and quantification of VCL relative to H3 in dHL-60 cells, treated with 10 μg/mL HERV-K dUTPase or Veh (HERV-

AJRCCM Articles in Press. Published June 13, 2022 as 10.1164/rccm.202102-0446OC

K dUTPase elution buffer) for 24 h (n=4). Bars represent mean ±SEM. In A, ***p<0.001 by Mann-Whitney test; in E, ***p<0.001 by by unpaired Student t-test; and in F, #p<0.05 by Mann-Whitney test.

Figure 6. CD66b PAH EVs display increased NE and elevated HERV-K envelope.

EVs were isolated from plasma of 17 healthy donor controls and 17 PAH patients, using the ExoTIC device described under 'Methods'**.** CD66b positive neutrophil EVs were pulled down using anti-CD66b beads, from pooled EVs of Con and PAH pooled plasma. **(A)** Size distribution of the pooled EVs, determined using Nanosight.
(B) Representative transmission electron microscopy (TEM) images of CD66b positive neutrophil EVs derived from pooled plasma of PAH vs. Con patients. Scale bar=100 nm. **(C)** Western immunoblot analysis and quantification of NE and HERV-K envelope from the same number of pooled PAH vs. Con neutrophil EVs, relative to the EV marker CD9. H3 from PAH neutrophil total lysate was used as a negative control and represented the lack of enrichment of NE and HERV-K with equivalent protein loading. **(D)** NE activity in the same number of PAH vs. Con EVs after 120 min incubation. NE was assessed by the production of BODIPY FL labeled fluorescent elastin fragments from self-quenching BODIPY FL-conjugated bovine neck ligament elastin. Bars represent mean ± SEM; n=3 technical replicates of the pooled EVs.

Figure 7. CD66b EVs cause pulmonary hypertension in a mouse model.

CD66b EVs were isolated from plasma of PAH patients or healthy controls. Adult male mice (8 weeks) were injected with PAH vs. Con plasma EVs ($1.63x10^7$) at a volume of 100 µL. The PAH plasma EVs were preincubated for 30 min with either elafin (0.02

AJRCCM Articles in Press. Published June 13, 2022 as 10.1164/rccm.202102-0446OC

mg/kg mouse weight in a volume of 4-6 µL from a 100 µg/mL stock solution), and or an equivalent volume of vehicle (PBS). In a separate experiment we confirmed that the addition of Elafin did not change the number of EVs (PAH EVs: 2.72 x 10^8 particles/mL and PAH Elafin EVs: 2.75 x 10^8 particles/mL). The EV suspensions were then injected twice a week, for 5 weeks. Hemodynamic function was evaluated 2 days after the last injection.

(A) Illustration of murine study protocol. **(B)** Pulmonary artery acceleration time (PAAT). **(C)** Right ventricular systolic pressure (RVSP). **(D)** Right ventricular hypertrophy (RVH). **(E)** Microscopy images of lung sections of the mice, labeled for αSMA (brown, smooth muscle cell marker) showing examples of nonmuscular, partially muscular and fully musularized vessels. Scale bar=40 µm. In B-E bars represent mean ± SEM. *p<0.05 **p<0.01, ***p<0.001 by one-way ANOVA followed by Dunnett's post test comparing each group mean with the control group.

Figure 8. Schematic representation of PAH neutrophil.

The secretion of HERV-K dUTPase from monocytes results in the upregulation of vinculin thereby increasing neutrophil adhesion and reducing migration. An increase in HERV-K envelope (env) in the neutrophil is likely via double strated (ds) RNA required for the interferon response and heightened neutrophil elastase. The increase in neutrophil elastase promotes neutrophil extracellular traps NETs. Elastase released from granules associates with HERV-K env in EVs causing pathologic features of pulmonary arterial hypertension.

AJRCCM Articles in Press. Published June 13, 2022 as 10.1164/rccm.202102-0446OC

Figure 1

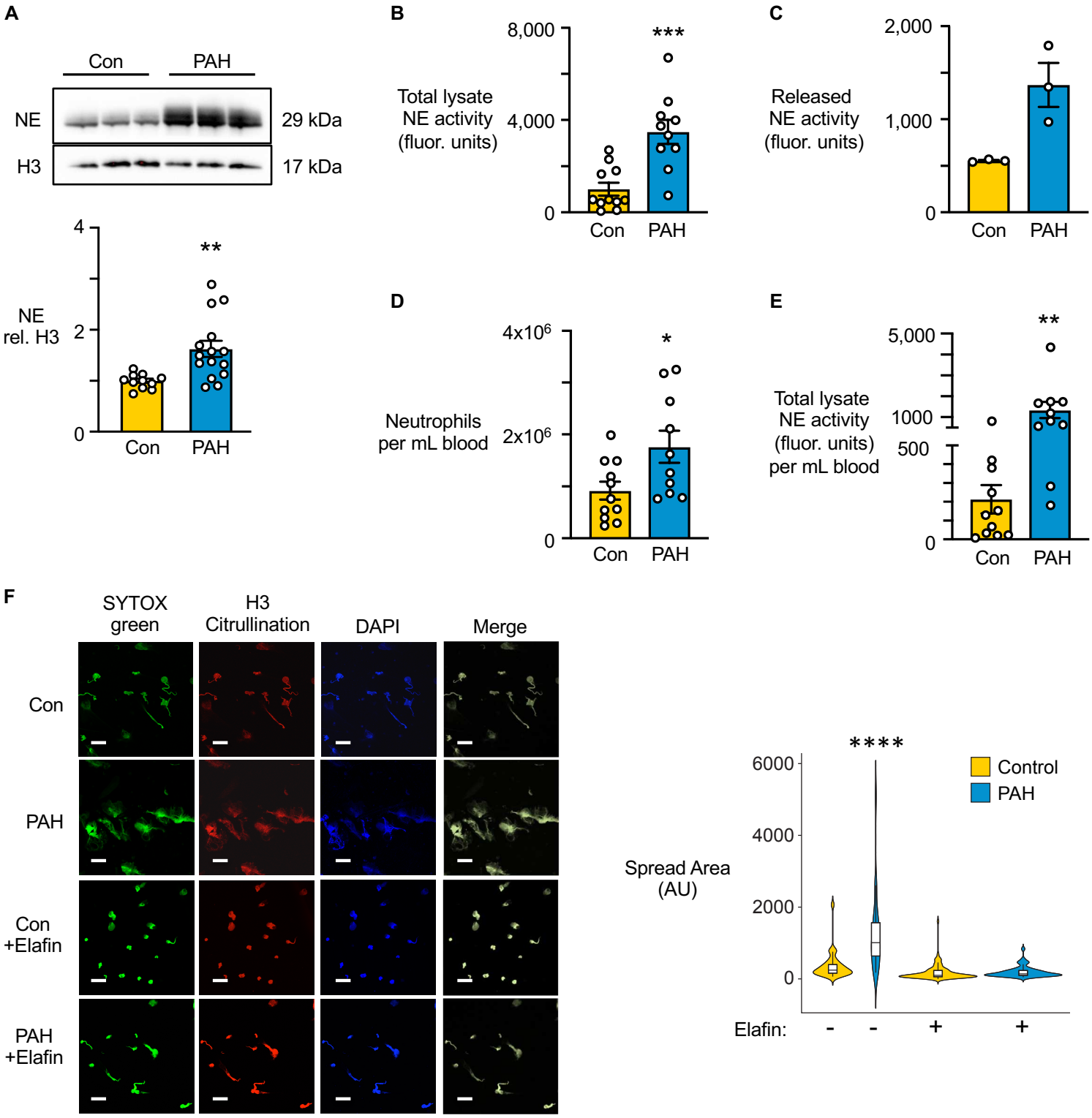

AJRCCM Articles in Press. Published June 13, 2022 as 10.1164/rccm.202102-0446OC

Figure 2

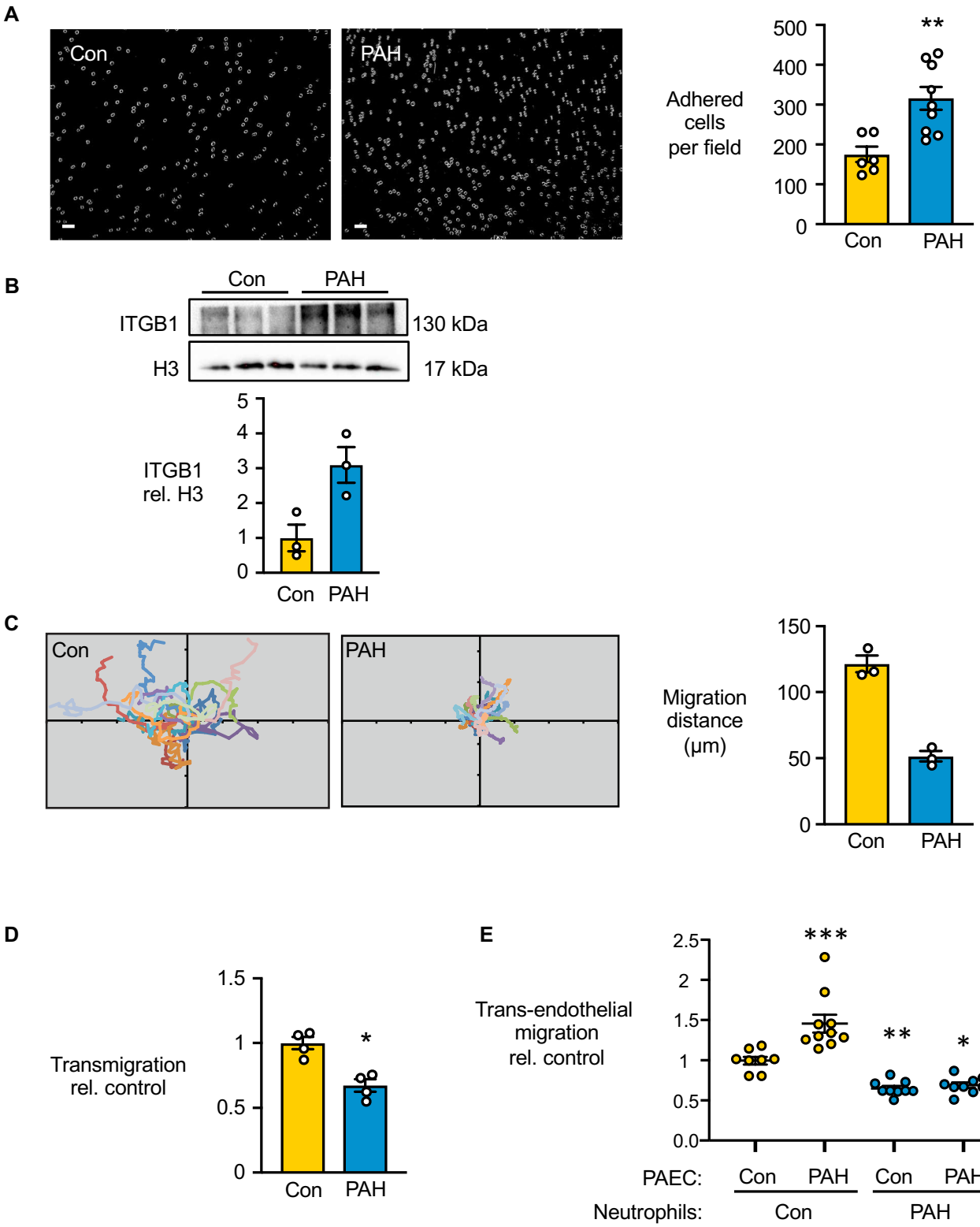

AJRCCM Articles in Press. Published June 13, 2022 as 10.1164/rccm.202102-0446OC

Figure 3

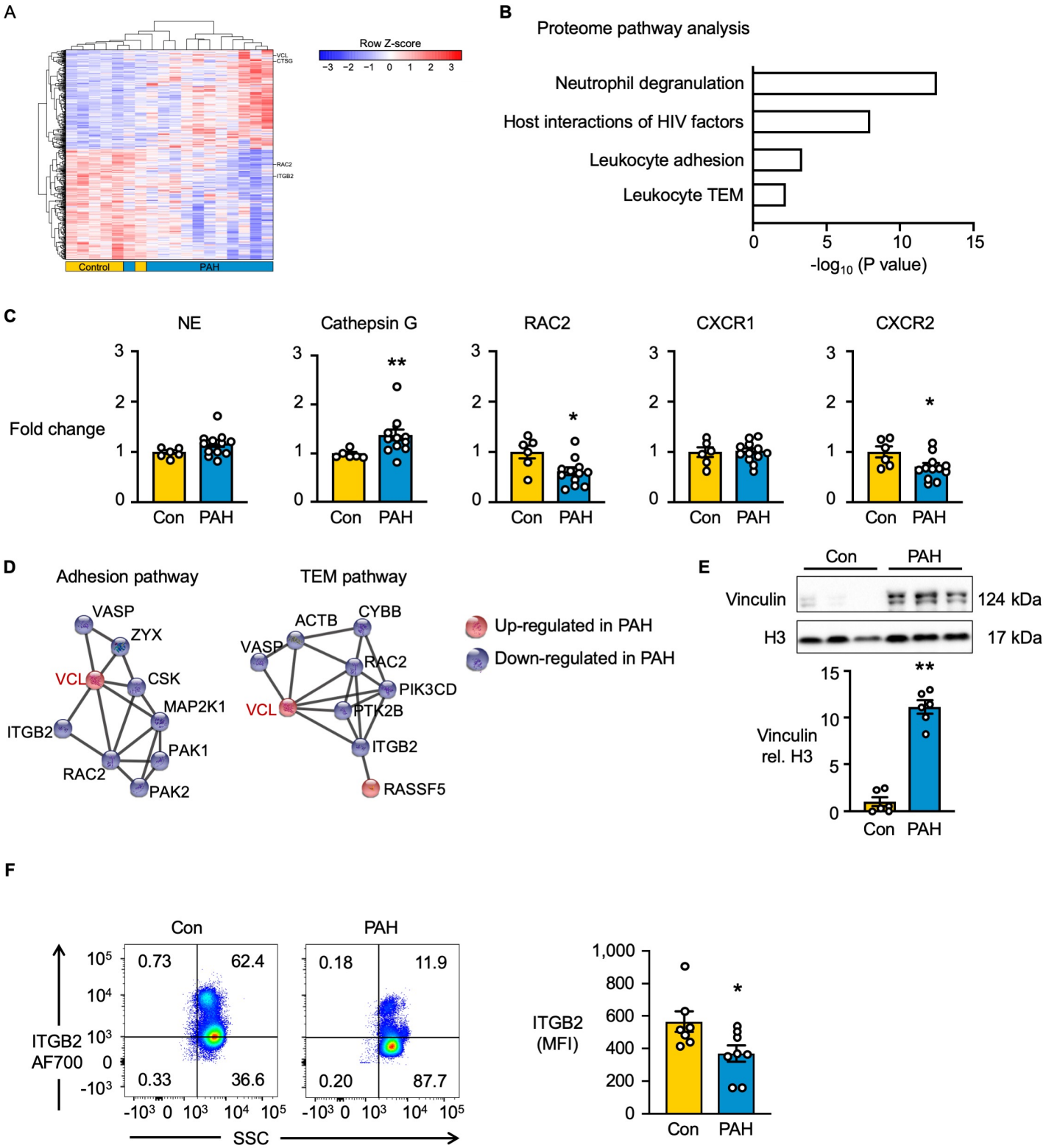

AJRCCM Articles in Press. Published June 13, 2022 as 10.1164/rccm.202102-0446OC

Figure 4

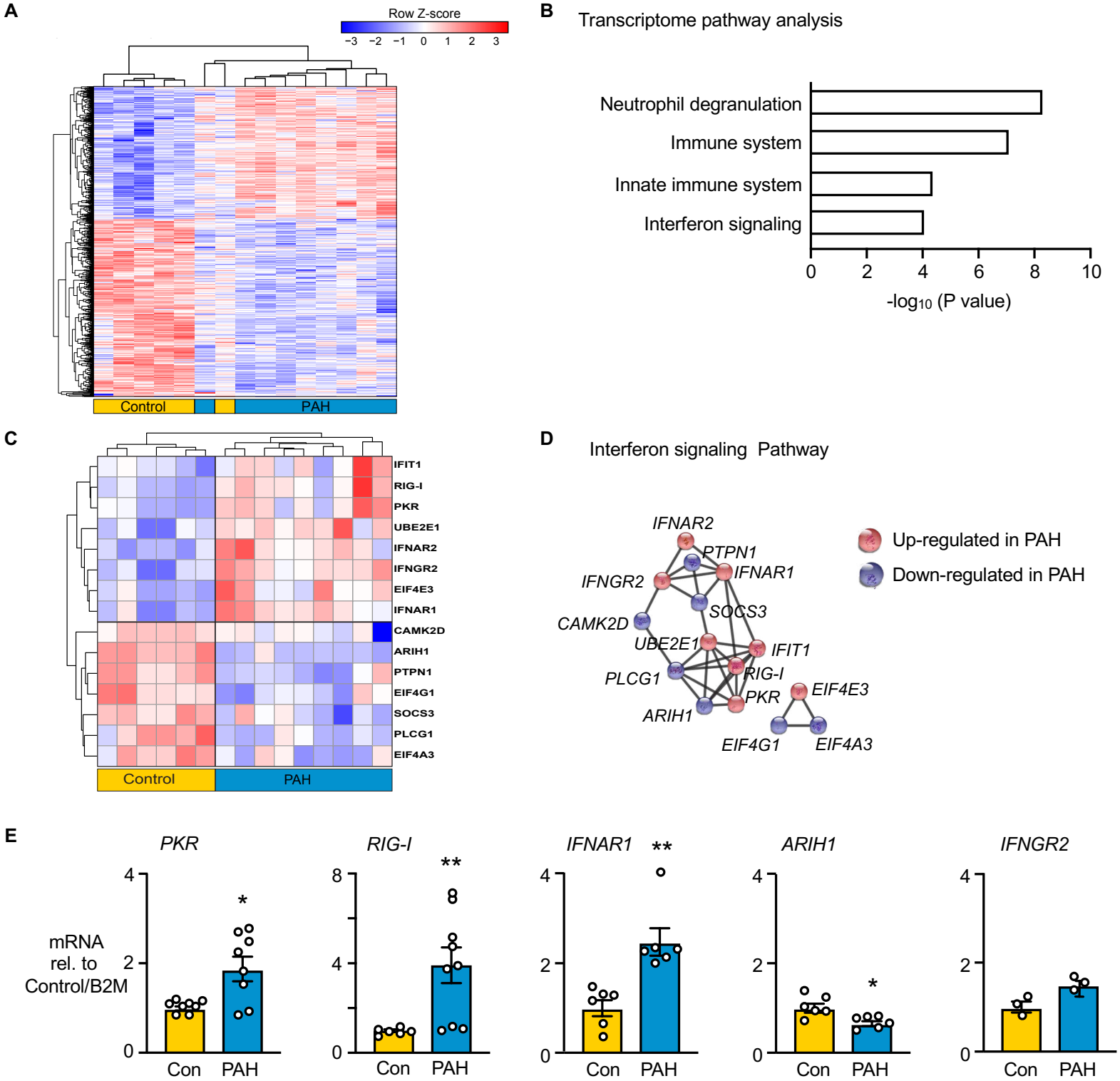

AJRCCM Articles in Press. Published June 13, 2022 as 10.1164/rccm.202102-0446OC

Figure 5

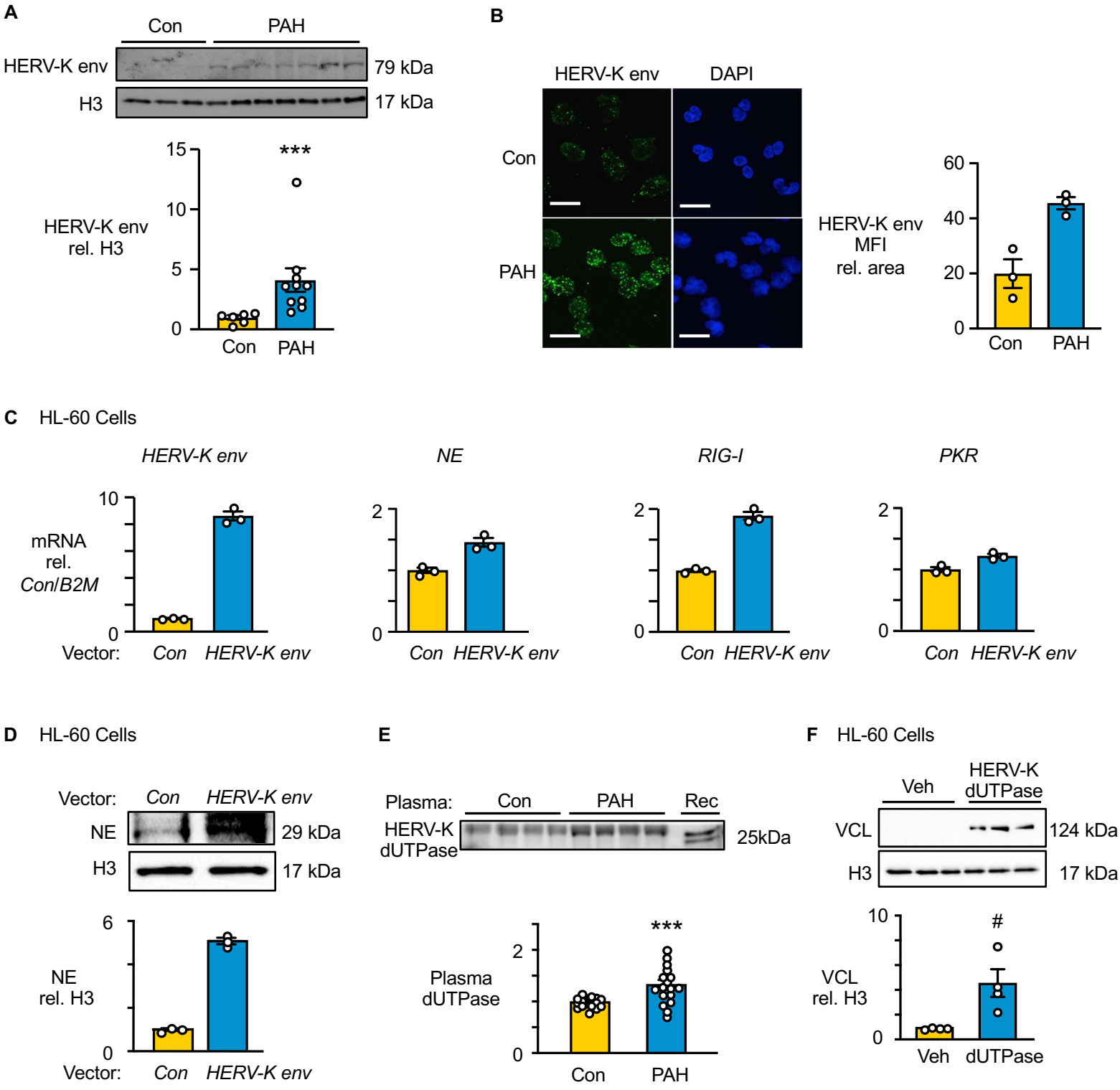

AJRCCM Articles in Press. Published June 13, 2022 as 10.1164/rccm.202102-0446OC

Figure 6

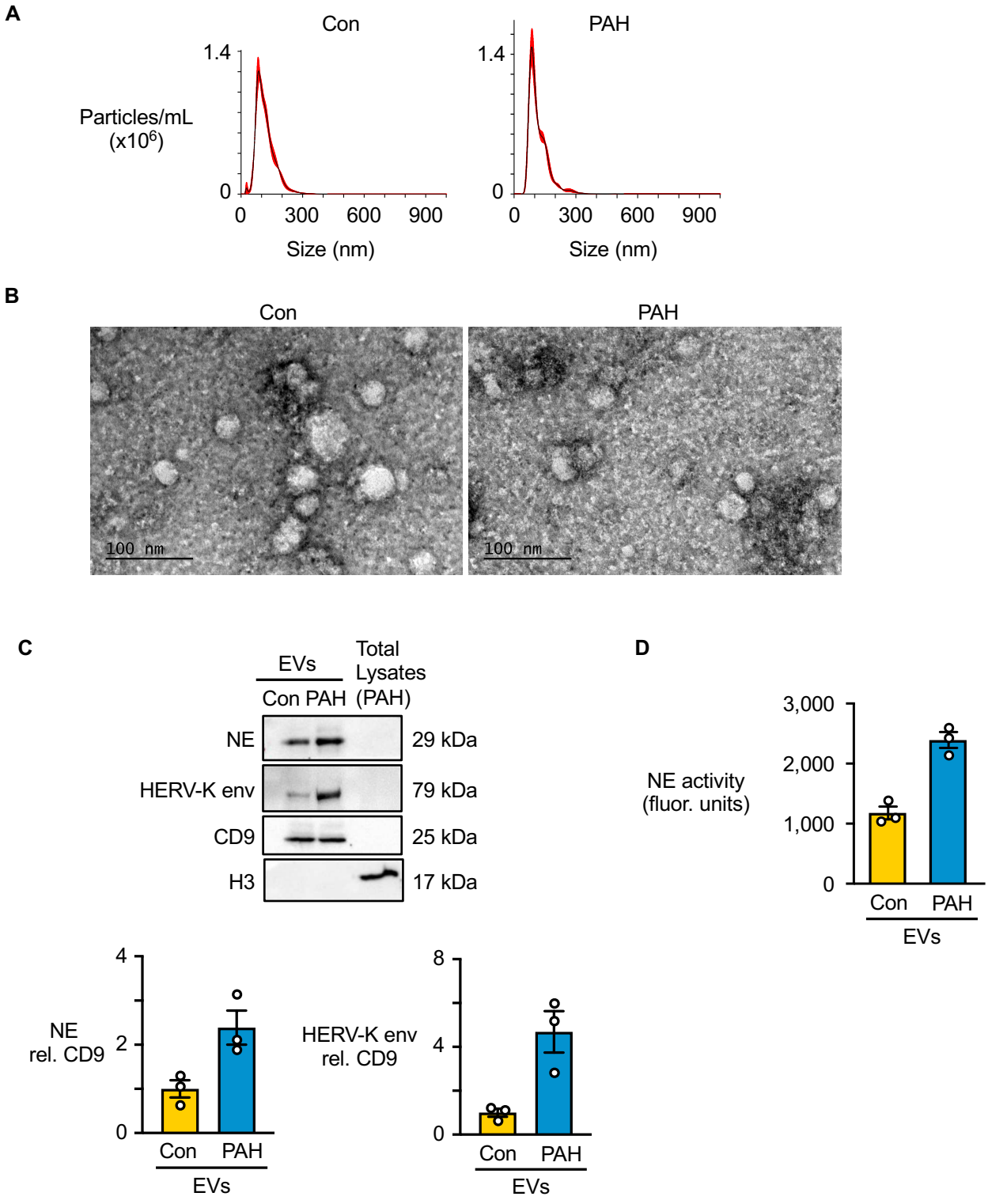

AJRCCM Articles in Press. Published June 13, 2022 as 10.1164/rccm.202102-0446OC

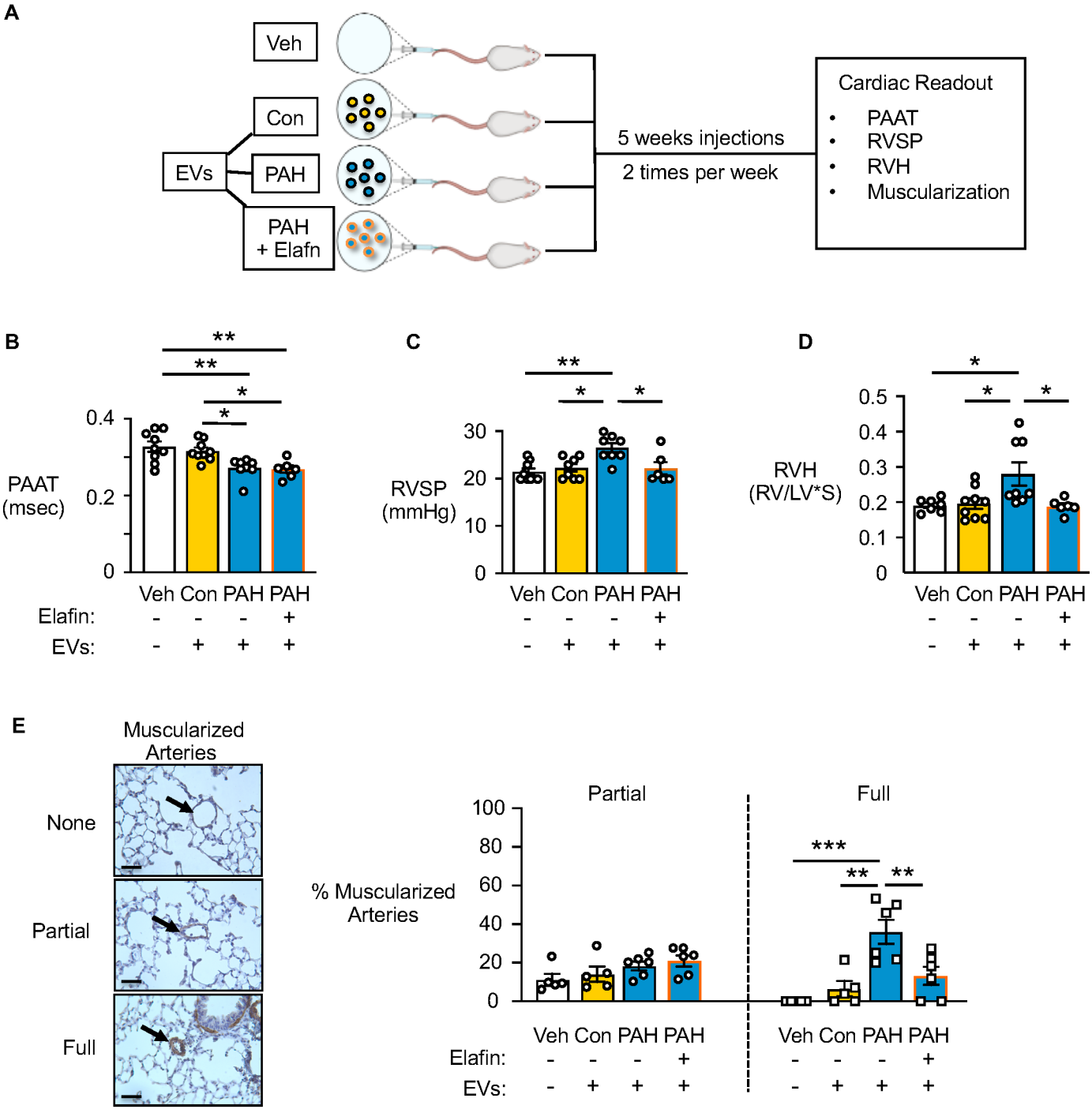

AJRCCM Articles in Press. Published June 13, 2022 as 10.1164/rccm.202102-0446OC

Figure 8

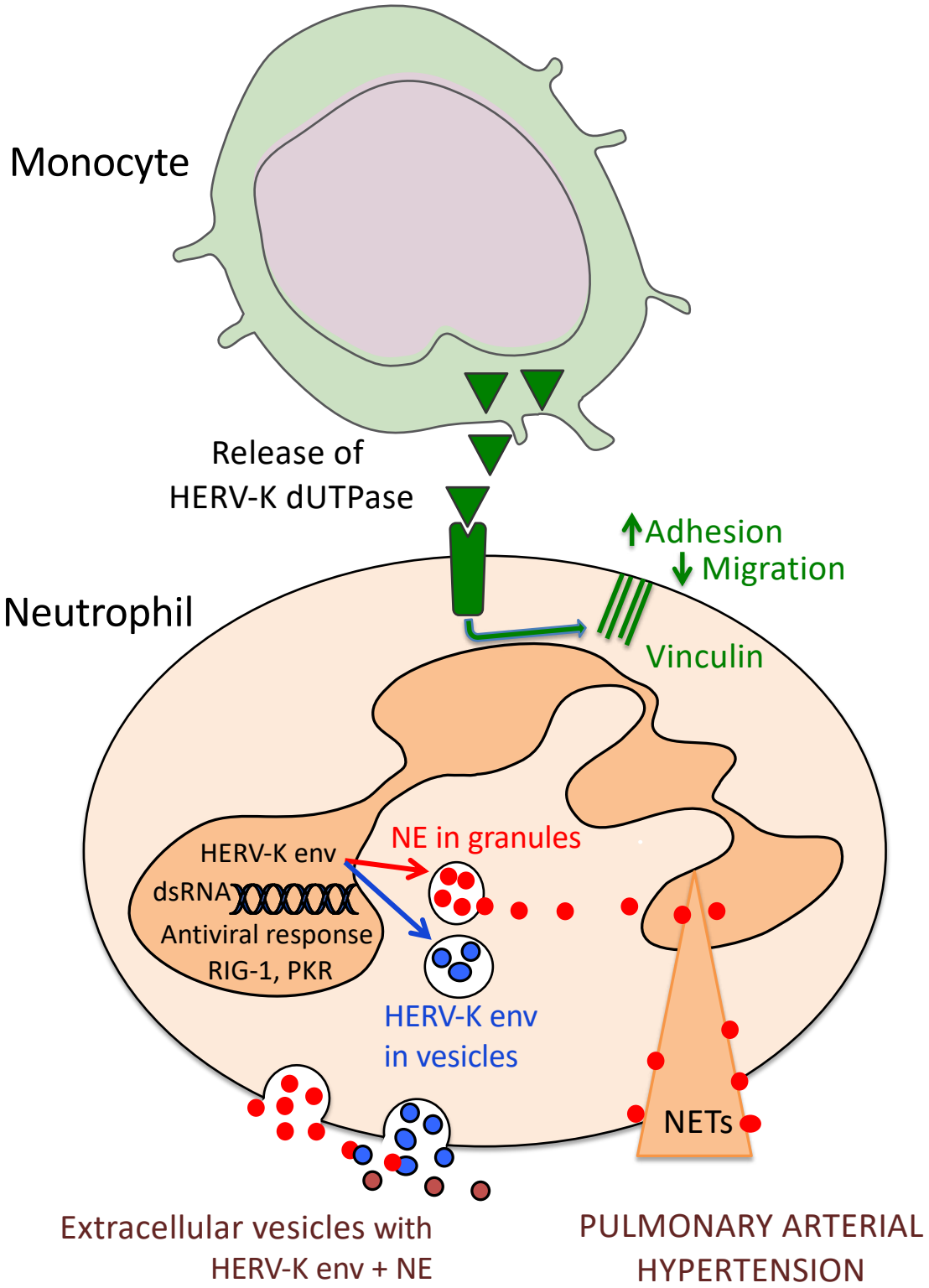

AJRCCM Articles in Press. Published June 13, 2022 as 10.1164/rccm.202102-0446OC

Online Data Supplement

Endogenous Retroviral Elements Generate Pathologic Neutrophils in Pulmonary Arterial Hypertension

Shalina Taylor*, Sarasa Isobe*, Aiqin Cao, Kévin Contrepois, Bérénice A. Benayoun, Lihua Jiang, Lingli Wang, Stavros Melemenidis, Mehmet O. Ozen, Shoichiro Otsuki, Tsutomu Shinohara, Andrew J. Sweatt, Jordan Kaplan, Jan-Renier Moonen, David P. Marciano, Mingxia Gu, Kazuya Miyagawa, Brandon Hayes, Raymond G. Sierra, Christopher J. Kupitz, Patricia A. Del Rosario, Andrew Hsi, A. A. Roger Thompson, Maria E. Ariza, Utkan Demirci, Roham T. Zamanian, Francois Haddad, Mark R. Nicolls, Michael P. Snyder, Marlene Rabinovitch‡

*These authors contributed equally to this work

‡Corresponding Author: marlener@stanford.edu

AJRCCM Articles in Press. Published June 13, 2022 as 10.1164/rccm.202102-0446OC

EXPANDED METHODS

PAH patient and control samples. All human samples used were coded and all patients and controls signed an informed consent under protocols approved by the Institutional Review Board on Human Subjects in Medical Research at Stanford University. We included PAH patients between the ages of 23 and 80 and healthy controls between the ages of 27 and 60. Although patients were initially screened as having IPAH, 3/68 were re-classified as having drug and toxin (WHO Group 1 PAH) and 5/68 had comorbidities not responsible for PAH (**Table E1**). Whole blood from PAH patients was obtained from the Stanford Pulmonary Arterial Hypertension biobank (Stanford IRB #14083), and blood from healthy volunteers was obtained from the Stanford Biobank under the University sponsored precision health initiative (Stanford IRB #40869). There were 71 samples collected from a total of 560 over that time period. Some experiments were carried out using de-identified blood from healthy individuals, obtained from the Stanford Blood Center (listed in T**able E3**; demographic information was not collected). PAEC used in the neutrophil trans-endothelial migration studies were from the Pulmonary Hypertension Breakthrough Initiative supported by NIH R24 HL123767 and the Cardiovascular Medical Research and Education Fund (CMREF). Patients characteristics, demographics, and hemodynamics are shown in **Tables E1 and E4** and a list of the medications for each patient is described in **Table E2**. Stanford biobank control samples used for the RNAseq and the untargeted proteomic LC/MS assay had echocardiographic studies performed to exclude cardiovascular disease (**Table E3**).

Reagents. See **Table E6**.

Neutrophil isolation. Human neutrophils were purified from peripheral blood using Miltenyi Biotec Macsxpress Neutrophil isolation kit, per manufacturer's instructions.

AJRCCM Articles in Press. Published June 13, 2022 as 10.1164/rccm.202102-0446OC

Purity of neutrophils after isolation was >95%, determined by Cytospin preparation (Cytospin 4; Thermo Scientific, Waltham, MA) and Diff-Quick staining. The neutrophil population was further confirmed by flow activated cell sorting (FACS) analysis with the neutrophil markers FITC anti-human CD66b and APC anti-human CD16. Isolated Neutrophils were counted using a Scepter™ 2.0 Cell Counter (MilliporeSigma, Burlington, MA).

HL-60 and dHL-60 cell culture. HL-60 cells were purchased from Sigma Aldrich and grown in complete media (RPMI 1640 medium supplemented with 5% FBS, 100 U/mL penicillin, and 100 µg/mL streptomycin) at 37°C in a 5% CO_2 humidified environment. The cells used in the assays were between passages 10-30. To differentiate HL-60 cells into a neutrophil-like phenotype, 1.3% DMSO was added to the cell growth medium in which the cells were cultured for 6-7 days. On the final day, differentiated HL-60 cells (dHL-60) were centrifuged at 1,300 RPM for 5 min and resuspended in complete media. Viable cells were counted on a hemocytometer using trypan blue exclusion.

HERV-K dUTPase protein purification. Recombinant HERV-K dUTPase protein was provided by Dr. Maria Ariza (Ohio State University). In some studies cells were incubated with recombinant HERV-K dUTPase at a concentration of 10 µg/mL for 24 h prior to assay. The HERV-K gene encoding the dUTPase was cloned into the pTrcHis Topo TA expression vector and the sequence was verified by DNA sequencing analysis as previously described (E1). The purity of the expressed protein was assessed by SDS-PAGE and capillary-liquid chromatography nanospray tandem mass spectrometry performed at the Ohio State University Mass Spectrometry and Proteomics Facility. High-purity dUTPase preparations, free of contaminating DNA, RNA, lipopolysaccharide, and peptidoglycan, were used.

AJRCCM Articles in Press. Published June 13, 2022 as 10.1164/rccm.202102-0446OC

PAEC cell culture. Primary small PAEC were harvested from the lungs of PAH patients undergoing lung transplantation, or from unused donor lungs (controls), obtained from the Pulmonary Hypertension Breakthrough Initiative (PHBI). Cells were cultured in EC medium supplemented with 5% FBS, 1% antibiotic/antimycotic, and 1% ECGS, and used between passages 4 and 7.

NE activity. NE activity was measured using EnzChek Elastase Assay Kit (Thermofisher Scientific, Waltham, MA) according to the manufacturer's instructions. All assays were carried out the same amount (25 μg /mL) of substrate. For determination of intracellular NE activity, neutrophils were lysed with RIPA buffer followed by sonication. The solution was then centrifuged, and lysates were collected for NE activity analysis. For measurement of extracellular NE activity, neutrophils were stimulated with IL-8 (100 ng/mL) for 30 min at 37°C, and the supernatant collected for NE activity analysis. All samples assayed contained the same number of neutrophils.

Myeloperoxidase (MPO) activity. MPO activity was measured using the Neutrophil Myeloperoxidase Activity Assay kit (Item No. 600620, Cayman Chemical, Ann Arbor, MI), according to the manufacturer's instructions. The kit utilizes 3,3',5,5'-tetramethyl-benzidine (TMB) as a chromogenic substrate, which upon reacting with MPO, yields a blue color detectable by its absorbance at 650 nm. For determination of MPO activity, neutrophils were lysed with RIPA buffer followed by sonication. The solution was then centrifuged, and lysates were collected for MPO activity analysis.

Neutrophil extracellular trap (NET) formation assay. Coverslips were pretreated with 100 μg/ml poly-d-lysine at 4°C overnight in phosphate buffered saline without calcium and magnesium (PBS-/-). Neutrophils were added to the coverslips for 5 min, and non-adherent cells washed away with PBS-/-. Phorbol myristate acetate (PMA) was added to

AJRCCM Articles in Press. Published June 13, 2022 as 10.1164/rccm.202102-0446OC

the media at a final concentration of 100 nM for 60 min, with vehicle (PBS) or elafin (1 µg/mL) (Proteo-Biotech-AG, a kind gift of Dr. Oliver Wiedow, Kiel Germany). Cells were washed with PBS then stained with cell impermeable SYTOX green nucleic acid stain (3 µM, ThermoFisher Scientific) for 30 min. Cells were then washed and fixed with 4% PFA for 15 min at room temperature and stained for H3 citrullination and neutrophil elastase **(Table E6)**. The antibodies were visualized with Alexa Fluor 488 (Neutrophil elastase) and Alexa Fluor 647 (H3 citrullination). Quantification of NETs was assessed by measuring the spread area of SYTOX green positive DNA by capturing 3 images randomly from 4 biological replicates. Images were acquired using a Leica Sp8 (Leica, Wetzlar, Germany) confocal laser-scanning microscope with a 40X objective, and Leica Application Suite X software.

Migration (Chemokinesis). The migration assay was used to determine real-time migration of neutrophils using time-lapse tracking. Coverslips were pretreated with 50 µg/mL fibronectin at 4°C overnight in PBS. Neutrophils were added to fibronectin pretreated coverslips for 5 min, non-adherent cells washed with PBS, and IL-8 added to the media at a concentration of 100 ng/mL. Cell migration was observed using a confocal laser-scanning microscope (FV1000, Olympus, Center Valley, PA) with a 40X objective, using the phase contrast mode. Frames were taken every 10 sec for 30 min and analyzed using ImageJ software.

Transmigration assays. Transmigration assays were performed in a modified Boyden chamber using the Corning FluoroBlok 24-well, 3 µm pore size inserts. The inserts were coated with fibronectin (Sigma Aldrich; 50 µg/mL) at 4°C overnight in PBS. The lower chamber was filled with DMEM supplemented with 1% BSA, 100 nM fMLP, or 100 ng/mL IL-8. Neutrophils ($5x10^5$ cells/ml) were labeled with Calcein AM (3 µM) and plated on the fibronectin substratum. Neutrophils were allowed to migrate for 30 min in the presence

AJRCCM Articles in Press. Published June 13, 2022 as 10.1164/rccm.202102-0446OC

of chemoattractant, and quantified via fluorescence plate reader at excitation and emission maxima of 494 nm and 517 nm, respectively.

Transendothelial migration assay (TEM). TEM was determined using the Corning FluoroBlok 24-well, 3 μm pore size inserts. PAECs were plated and grown to confluency on the inserts and washed with PBS. Neutrophils ($5x10^5$ cells/mL) were labeled with Calcein AM (3 μM) and plated onto a pre-washed endothelial monolayer. IL-8 (100 ng/mL) was dispensed into the lower chamber, and neutrophils were allowed to transmigrate through the endothelial monolayer towards the IL-8 chemoattractant. Neutrophil migration through the endothelial cell layer into the lower chambers was measured using a fluorescence plate reader at excitation and emission maxima of 494 nm and 517 nm, respectively.

Adhesion assay. Fibronectin (Sigma Aldrich, St. Louis, MO; 50 μg/mL) in PBS was applied onto 4 well chamber slides at 4°C, overnight. Purified neutrophils ($1x10^5$) were added to a fibronectin substratum or a monolayer of PAEC and incubated at 37°C for 5 min. The chamber slides were washed and at least 3 different fields of adherent cells in each chamber were imaged under light microscopy using a 10x objective (for adhesion on fibronectin), or using the green light channel on a Keyence BZ-X fluorescence microscope (Osaka, Japan), under 20X objective (for adhesion to PAEC).

and quantified.

Flow cytometry. Neutrophils were incubated in blocking buffer (3% BSA in PBS) for 30 min at 4°C, then stained for surface expression using Alexa Fluor® 700 conjugated ITGB2 antibody for 1h at 4°C. Neutrophils were washed with PBS supplemented with 1% BSA and fixed in a final concentration of 4% paraformaldehyde for 15 min at room temperature. The stained and fixed neutrophils were then suspended in PBS for data acquisition. Data

AJRCCM Articles in Press. Published June 13, 2022 as 10.1164/rccm.202102-0446OC

was acquired using a Beckton Dickenson LSR II flow cytometer and analyzed using FlowJo version 10.4.2 software for mean fluorescent intensity (MFI). To ensure maximal purity, neutrophils were selected by using side scatter vs. forward scatter plots. Forward and side scatter gating strategy was used to determine cell size, granularity, and to exclude dead cells and debris from the neutrophil population. Unstained cells were used as a gating control for ITGB2 AF700.

Immunofluorescence staining. Cells adherent to fibronectin were fixed with 4% paraformaldehyde for 15 min, permeabilized with 0.5% Triton X-100 for 1 min, and blocked in 5% FBS and 2% HSA in PBS-T (0.1%Tween 20) for 30 min. Cells were washed and then stained with HERV-K envelope primary antibodies (1:1000) (Ango San Ramon, CA) overnight at 4°C and Alexa Fluor 488 secondary antibodies (1:500) (Invitrogen) for 1 h at room temperature, washed, then mounted with DAPI Fluoromount-G (SouthernBiotech, Birmingham, AL). Confocal analysis was performed using a Leica Sp8 (Leica, Buffalo Grove, IL) confocal laser-scanning microscope with a 40X objective and Leica Application Suite X software.

Transmission Electron Microscopy. Pooled EV samples were prepared for electron microscopy in PBS. Grids were glow discharged for 20 sec in a Denton Desktop Turbo III vacuum system and then covered with 5 µL of sample and allowed to adsorb to a 300 mesh copper grid with formvar and carbon coating (Cat# FCF300-CU, Electron Microscopy Sciences, Hatfield, PA) for 3 min. The sample was washed by touching the grid sample side down with two drops of water. Uranyl Acetate (1% in water) was then dripped through a 0.2 µm mesh syringe filter over the grid, allowing the third drop to remain on the grid for 1 min, and most of the stain to wash away. Grids were observed using a JEOL JEM-1400 120kV electron microscope, and images acquired using a Gatan Orius 2k x 4k digital camera.

AJRCCM Articles in Press. Published June 13, 2022 as 10.1164/rccm.202102-0446OC

Western Immunoblot. Neutrophils were isolated and washed three times with ice-cold PBS, and neutrophil lysates prepared by adding lysis buffer (10 mM Tris-HCl and 1% SDS), then boiled for 10 min before centrifugation. Protein concentration was determined by the BCA assay (Thermo). Equal amounts of protein were separated by SDS-PAGE and transferred onto nitrocellulose membranes. Membranes were incubated overnight at 4°C with antibodies against vinculin (1:1000), NE (1:500), HERV-K envelope (1:1000), H3 (1:3000), HERV-K dUTPase (1:500) or CD9 (1:1000), in 5% BSA-PBS containing 0.1% Tween-20. Secondary antibodies were added according to manufacturer's protocol and membranes were imaged using chemiluminescence reagent Clarity Western ECL Substrate (BioRad laboratories, Hercules, CA) and a BioRad ChemiDoc XRS system. Densitometric quantifications were performed using Image Lab software version 5.2.1.

Reverse-Transcriptase qPCR (RT-qPCR). Total neutrophil RNA was extracted using the Direct-zol RNA Kits (Zymo Research, Irvine, CA). The quantity and quality of RNA was determined using a BioTek Synergy H1 Hybrid Reader (Winooski, VT). qPCR was performed using 5 µL Powerup SYBR green PCR Master Mix (Applied Biosystems, Foster City, CA), 2 µL of dH_2O and 2 µL of cDNA sample in a 10 µL reaction. Each measurement was carried out in duplicate using a CFX384 Real-Time System (Bio-Rad, Hercules, CA). The PCR conditions were: 50°C for 2 min, 95°C for 10 min, followed by 44 cycles of 95°C for 15 sec, and 60°C for 60 sec. The raw PCR data for **Figure 5C** including the $\Delta\Delta$Ct calculation, is included in **Table E7.**

Primers. Primer sequences used are listed in **Table E8** in the Online Data Supplement. Gene expression levels were normalized to beta-2-microglobulin (B2M).

Plasmid transfection. HL-60 cells were transfected with HERV-K envelope vector (VectorBuilder, Chicago, IL) or EGFP control vector (VectorBuilder) using HL-60 Cell

AJRCCM Articles in Press. Published June 13, 2022 as 10.1164/rccm.202102-0446OC

Avalanche™ Transfection Reagent per manufactures instructions (EZ biosystems, College Park, MD).

EV isolation from plasma and CD66b pulldown. Human plasma (500µL) was prepared from 17 blood draws from separate healthy donor controls and 17 blood draws from 16 PAH patients, as one blood draw was obtained from the same patient one year later. EVs were isolated from the plasma using the EV Total Isolation Chip (ExoTIC) as described in (E2). ExoTIC-harvested EVs were further purified using CD66b/CEACAM 8 antibody (Sigma), a specific human neutrophil marker, which was conjugated to beads using the Dynabeads Antibody Coupling Kit per manufacturer's instructions (ThermoFisher). EVs were co-incubated with magnetic beads conjugated with a CD66b/CEACAM 8 antibody in a shaker for 18 h at 4°C. Using a magnet, unbound EV supernatant was removed and captured beads were washed. To dissociate the beads from the CD66b/CEACAM 8 positive EVs, an acid wash was performed by adding 200 µL of 50 mM pH 2.5 glycine solution to tube containing beads for 10 min, followed by addition of 70 µL 1M pH 7.5 Tris buffer to neutralize the solution. For the experiments related to Figure E7, total EVs were first enriched by differential centrifugation (10 min x 300 g, 10 min x 2000 g, 30 min x 10,000 g, 70min x 100,000 g all at 4°C) (Sorvall WX+ Ultracentrifuge, Thermo Fisher Scientific), washed and resuspended in PBS, and stored at -80°C as described previously (E3).

The purity, size, and concentration of the eluted EVs were evaluated by nanotracking analysis on a Nanosight NS300 (Malvern, United Kingdom). EVs from the 17 healthy donor controls were pooled, and the EVs from the 17 PAH patients were pooled, and equal concentrations of the pooled EVs were aliquoted and stored in -80°C for further experiments.

AJRCCM Articles in Press. Published June 13, 2022 as 10.1164/rccm.202102-0446OC

Untargeted Proteomics from Neutrophils by LC-MS.

Sample preparation. Proteomic analysis was carried out using neutrophils isolated from 6 healthy control subjects and 12 PAH patients. Unstimulated neutrophils ($5x10^6$) were lysed in 10 mM Tris-HCI and 1% SDS, and 40 µg of protein per lane run on SDS-PAGE at 100 volts for 10 min. After Coomassie blue staining, the protein bands from each sample were excised with a clean razor blade. Proteins were reduced, alkylated and digested overnight using Trypsin/Lys-C and peptides were extracted from the gel. Peptide extracts were then dried in a speed vac, reconstituted in 100 mM TEAB and protein concentrations were measured using the BCA method. Peptides were labeled with TMT 10plex reagent (Thermo Fisher) as instructed by the vendor and subsequently combined at equal amount. Each pool contained 9 samples and one reference pool sample, which is an equimolar mixture of all the study samples.

***Data acquisition*.** Tryptic peptides were separated in 2 two dimensions on a MClass 2DnLC (Waters, city, state). First dimension consisted of a reverse phase chromatography at high pH, followed by an orthogonal separation at low pH in the second dimension. In the first dimension, the mobile phases were 20 mM ammonium formate at pH 10 (Solvent A) and 100% acetonitrile (Solvent B). Peptides were separated on a Xbridge 300 µm x 5 cm C18 5.0 µm column (Waters) using 15 discontinuous step gradients at 2 µL/min. In the second dimension, peptides were loaded to an in-house packed 100 µm ID/15 µm tip ID x 28 cm C18-AQ 1.8 µm resin column with buffer A (0.1% formic acid in water). Peptides were eluted using a 180-min gradient from 5% to 40% buffer B (0.1% formic acid in acetonitrile) at a flow rate of 600 nL/min. The LC system was directly coupled in-line with an Orbitrap Fusion Lumos Mass Spectrometer. The source was operated at 1.8-2.2 kV to optimize the nanospray with the ion transfer tube at 275°C. The mass spectrometer was run in a data dependent mode. Full MS scan was

AJRCCM Articles in Press. Published June 13, 2022 as 10.1164/rccm.202102-0446OC

acquired in the Orbitrap mass analyzer from 400-1500 m/z with resolution of 120,000. Precursors were isolated with an isolation window of 0.7 m/z and fragmented using CID at 35% energy in ion trap in rapid mode. AGC target was 10^4 and the maximum injection time was 100 ms. Subsequently, 8 fragment ions were selected for MS3 analysis, isolated with an m/z window of 1.6, and fragmented with HCD at 65% energy. Resulting fragments were detected in the Orbitrap at 60,000 resolutions, with a maximum injection time of 150 ms or until the AGC target value of 10^5 was reached.

***Data processing*.** Raw data were processed using Proteome Discoverer software PD2.1 (Thermo) with precursor and fragment ion mass tolerance of 10 ppm and 0.6 Dalton, respectively, for database search. The search included cysteine carbamidomethylation as a fixed modification. Acetylation at protein N-terminus, methionine oxidation and Tandem Mass Tag (TMT) at peptide N-terminus and lysine were used as variable modifications. Up to two missed cleavages were allowed for trypsin digestion. Only unique peptides with a minimum of six amino acids were considered for protein identification. The peptide false discovery rate (FDR) was set at 1%. Data were searched against the uniprot human proteome database. Quantitative results at the protein level were reported relative to the reference pool sample. Batch effect was corrected by applying median-normalization and proteins detected in less than 2/3 of the samples were discarded. Differential analysis was performed on $\log_2$-transformed data using a two-sided Welsh t test. Proteins were considered significant with a q-value below 0.10. Functional correlation networks were plotted using the webtool STRING (http://string-db.org).

AJRCCM Articles in Press. Published June 13, 2022 as 10.1164/rccm.202102-0446OC

RNA-seq analysis pipeline.

Sample Preparation. RNA sequencing (RNA-seq) was evaluated using unstimulated neutrophils from 6 healthy control subjects and 9 PAH patients. Total RNA was prepared for sequencing using the Takara Bio SMARTer: SMARTer Stranded Total RNA-Seq Kit v2 - Pico Input Mammalian kit according to the manufacturer's instructions.

Data acquisition and processing. Pooled libraries were sequenced using the HiSeq 2500 sequencer (Illumina, San Diego, CA, SA) at the Stanford Center for Genomics and Personalized Medicine facility. Healthy donor controls and PAH samples were sequenced in each pooled lane to correct for potential batch effect. Sequencing data were demultiplexed and converted into fastq files using Illumina's bcl2fastq conversion software (v2.20). Quality and adapter trimming along with filtering of rRNA reads was performed using BBDuk (v37.22). cDNA sequences of protein coding and lncRNA genes were obtained from human genome assembly GRCh38 (ens85). Paired-end 100bp reads were mapped to the indexed reference transcript using kallisto 0.43.0 and the –fr-stranded option (E4). DEseq2 normalized fold-changes were used to estimate differential gene expression between control and PAH neutrophils using the 'DESeq2' R package (DESeq2 v1.16.1) (E5). We identified 1565 significantly differentially expressed genes at FDR <5% (896 downregulated, 669 upregulated). The heatmap of expression across samples for significant genes was plotted using the R package 'pheatmap' v1.0.8.

Mouse model for the induction of pulmonary hypertension by neutrophil EVs. The Animal Care Committee at Stanford University approved all experimental protocols used in this study, following the published guidelines of the National Institutes of Health and the American Physiological Society. Isoflurane anesthesia (1.5%, 1 L/min oxygen) was used during these procedures. Adult male mice (8 weeks of age) were given tail-vein

AJRCCM Articles in Press. Published June 13, 2022 as 10.1164/rccm.202102-0446OC

injections twice weekly for five weeks of previously aliquoted and frozen EVs ($1.63x10^7$) from pooled healthy donor control or PAH plasma brought to room temperature. Prior to injection, the PAH EVs were incubated for 30 min with either elafin in PBS (0.02 mg/kg mouse weight in a volume of 4-6 µL from a 100 µg/mL stock solution) or an equivalent volume of PBS. Male mice were used for comparison with previous studies from our group using monocyte EVs (E6) or recombinant HERV-K dUTPase, where only males were used (E7). Four groups were studied (i) PBS-Vehicle, (ii) pooled EVs of healthy donor controls, (iii) pooled PAH EVs, or (iv) pooled elafin treated PAH EVs. The first cohort consisted of n=3 in groups (i-iii), and the second cohort consisted of n=6 in all groups, and group (iv) was added. Cardiac function, right ventricular systolic pressure, and right ventricular hypertrophy and pulmonary vascular morphometry were assessed as previously described (E6-E8). Cardiac function, including pulmonary artery acceleration time (PAAT) and left ventricular (LV) ejection and cardiac output were assessed as described by Stypmann et al (E8), using a Vivid 7 ultrasound machine (GE Healthcare, Pittsburgh, PA) and 13-MHz linear array transducer under Isoflurane anesthesia (1.5%, 1 L/min oxygen).

Right ventricular systolic pressure (RVSP) was also measured under Isoflurane anesthesia (1.5%, 2L/min oxygen) by inserting a 1.4F Millar catheter (Millar Instruments, Houston, TX) via the right jugular vein. Data were collected by Power Lab Data Acquisition system (AD Instruments, Colorado Springs, CO) and analyzed by LabChart software (AD Instruments, Colorado Springs, CO). After hemodynamic measurements, the lungs were flushed with saline. Right ventricular hypertrophy was assessed by the weight ratio of the right ventricle (RV) to that of the left ventricle (LV) plus septum. Right lungs were snap-frozen in liquid nitrogen and stored at -80° C. Left lungs were fixed with 10% formalin for histology. Paraffin embedded and formaldehyde fixed lung sections

AJRCCM Articles in Press. Published June 13, 2022 as 10.1164/rccm.202102-0446OC

were stained for alpha-SMA (Sigma-Aldrich) using the Dako Animal Research Kit (Dako, Denmark) per manufactures instructions as previously described. Light microscopic images were acquired for quantification of percent partially and fully muscularized peripheral alveolar duct and alveolar wall arteries. Three fields (200x magnification) were assessed (one in each of three lung sections/mouse) as previously described (E6). Quantification of muscularization was conducted in a manner blinded as to the cohort to which the mouse tissue section belonged.

Statistical Analysis. Individual data points are shown, with bars representing mean ± standard error of the mean (SEM). We were limited by the number of experiments that could be done using freshly isolated neutrophils, so in general the n in these studies is lower than in those where we could use frozen neutrophils. The Statistical significance was determined by one-way ANOVA followed by Dunnett's multiple comparison test, or two-sided unpaired t-test analysis as indicated in the figure legends. Data with a sample size $n<8$ was analyzed using the Mann-Whitney non-parametric test. Samples with n of 3 are confirmatory of other assays or represent technical replicates from cell lines or pooled samples. In some of the figures, the average of the control values is set as one and the fold change of each individual control value is shown to reflect variance, and for the test samples, the fold change is shown for each determination, relative to the average of the control cohort. Statistical analysis was performed using GraphPad Prism (v8.4.1) or R package 'impute' (v1.52.0). Pathway enrichment analysis was conducted using the webtool IMPaLA (https://impala.molgen.mpg.de/).

AJRCCM Articles in Press. Published June 13, 2022 as 10.1164/rccm.202102-0446OC

Online References:

E1. Ariza ME, Williams MV. A human endogenous retrovirus K dUTPase triggers a TH1, TH17 cytokine response: does it have a role in psoriasis? The Journal of investigative dermatology 2011; 131: 2419-2427.

E2. Liu F, Vermesh O, Mani V, Ge TJ, Madsen SJ, Sabour A, Hsu EC, Gowrishankar G, Kanada M, Jokerst JV, Sierra RG, Chang E, Lau K, Sridhar K, Bermudez A, Pitteri SJ, Stoyanova T, Sinclair R, Nair VS, Gambhir SS, Demirci U. The Exosome Total Isolation Chip. ACS Nano 2017; 11: 10712-10723.

E3. Li P, Kaslan M, Lee SH, Yao J, Gao Z. Progress in Exosome Isolation Techniques. Theranostics 2017; 7: 789-804.

E4. Bray NL, Pimentel H, Melsted P, Pachter L. Near-optimal probabilistic RNA-seq quantification. Nat Biotechnol 2016; 34: 525-527.

E5. Love MI, Huber W, Anders S. Moderated estimation of fold change and dispersion for RNA-seq data with DESeq2. Genome Biol 2014; 15: 550.

E6. Otsuki S, Saito T, Taylor S, Li D, Moonen JR, Marciano DP, Harper RL, Cao A, Wang L, Ariza ME, Rabinovitch M. Monocyte-released HERV-K dUTPase engages TLR4 and MCAM causing endothelial mesenchymal transition. *JCI Insight* 2021; 6.

E7. Saito T, Miyagawa K, Chen SY, Tamosiuniene R, Wang L, Sharpe O, Samayoa E, Harada D, Moonen JAJ, Cao A, Chen PI, Hennigs JK, Gu M, Li CG, Leib RD, Li D, Adams CM, Del Rosario PA, Bill M, Haddad F, Montoya JG, Robinson WH, Fantl WJ, Nolan GP, Zamanian RT, Nicolls MR, Chiu CY, Ariza ME, Rabinovitch M. Upregulation of Human Endogenous Retrovirus-K Is Linked to Immunity and Inflammation in Pulmonary Arterial Hypertension. Circulation 2017; 136: 1920-1935.

AJRCCM Articles in Press. Published June 13, 2022 as 10.1164/rccm.202102-0446OC

E8. Stypmann J, Engelen MA, Troatz C, Rothenburger M, Eckardt L, Tiemann K. Echocardiographic assessment of global left ventricular function in mice. *Lab. Anim.* 2009;43:127-137

AJRCCM Articles in Press. Published June 13, 2022 as 10.1164/rccm.202102-0446OC

SUPPLEMENTARY TABLES

Table E1: Demographics and assays used for PAH patients

Sample[1]	Gender	Age (Yr)	Race	Ethnicity	Diagnosis[2]	PAP[3]	PVR[4]	6MWD[5]	NYHA[6]	Assays
PAH-1	F	30	Other	Hispanic or Latino	IPAH	43	4.8	525.79	II	Transmigration Figure 2C (Figure E2A), TEM Figure 2E, MPO activity Figure E1E
PAH-2A	F	37	Other	Hispanic or Latino	IPAH	20	2.7	502.93	I	NE WB Figure 1A, NE Activity Extracellular Figure 1C (Figure E1D), Transmigration Figure 2D (Figure E2A)
PAH-2B	F	37	Other	Hispanic or Latino	IPAH	20	2.7	608.08	I	NE activity Total lysate Figure 1B (Figure E1B, E1C), Neutrophil/mL Figure 1D, NE activity/mL blood Figure 1E, NETosis Figure 1F, Proteomics Figure 3A-D (Figure E3A-C), RNAseq Figure 4A-D (Figure E4A-B)
PAH-3	F	59	White	Unknown	IPAH	44	11.2	571.51	I/II	Adhesion Figure 2A, TEM Figure 2E, dUTPase WB Figure 5E, EV Figure 6A-D (Figure E7B, E7C), Animal Figure 7B-E
PAH-4A	F	42	Other	Hispanic or Latino	IPAH	68	12.2	457.21	II	dUTPase WB Figure 5E, EV Figure 6A-D (Figure E7B, E7C), Animal Figure 7B-E
PAH-4B	F	44	Other	Hispanic or Latino	IPAH	53	5.7	480.07	II	HERV-K WB Figure 5A, MPO activity Figure E1E
PAH-5	F	31	White	Unknown	IPAH	48	11.4	557.79	I	ITGB2 FACS Figure 3F, HERV-K WB Figure 5A, HERV-K Confocal Figure 5B, dUTPase WB Figure 5E, EV Figure 6A-D (Figure E7B, E7C), Animal Figure 7B-E
PAH-6A	F	47	White	Not Hispanic or Latino	IPAH	43	8.3	574.55	I	PCR Figure 4E, dUTPase WB Figure 5E, EV Figure 6A-D (Figure E7B, E7C), Animal Figure 7B-E
PAH-6B	F	48	White	Not Hispanic or Latino	IPAH	43	8.3	594.37	I	ITGB2 FACS Figure 3F, EV Figure 6B-E, Animal Figure 7B-E
PAH-7A	F	65	White	Not Hispanic or Latino	IPAH	35	5.6	406.91	II	NE WB Figure 1A, dUTPase WB Figure 5E, EV Figure 6A-D (Figure E7B, E7C), Animal Figure 7B-E
PAH-7B	F	66	White	Not Hispanic or Latino	IPAH	35	5.6	405.39	II	VCL WB Figure 3E, ITGB2 FACS Figure 3F, HERV-K WB Figure 5A
PAH-8A	F	38	Asian	Not Hispanic or Latino	IPAH	57	13.7	495.31	II/III	Adhesion Figure 2A
PAH-8B	F	48	Asian	Not Hispanic or Latino	IPAH	57	13.7	405.39	III	NE WB Figure 1A, Chemokinesis Figure 2B, Proteomics Figure 3A-D (Figure E3A-C), RNAseq Figure 4A-D (Figure E4A-B)
PAH-8C	F	49	Asian	Not Hispanic or Latino	IPAH	57	13.7	585.22	II	NE activity Total lysate Figure 1B (Figure E1B, E1C), Neutrophil/mL Figure 1D, NE activity/mL blood Figure 1E, Transmigration Figure 2D (Figure E2A)
PAH-8D	F	49	Asian	Not Hispanic or Latino	IPAH	58	12	548.65	II/III	NETosis Figure 1F (Figure E1F), HERV-K WB Figure 5A
PAH-8E	F	50	Asian	Not Hispanic or Latino	IPAH	58	12	571.51	II	VCL WB Figure 3E, dUTPase WB Figure 5E, EV Figure 6A-D (Figure E7B, E7C), Animal Figure 7B-E

AJRCCM Articles in Press. Published June 13, 2022 as 10.1164/rccm.202102-0446OC

Sample[1]	Gender	Age (Yr)	Race	Ethnicity	Diagnosis[2]	PAP[3]	PVR[4]	6MWD[5]	NYHA[6]	Assays
PAH-9A	F	39	Other	Hispanic or Latino	IPAH	54	11.3	548.65	II	NE WB Figure 1A, Adhesion Figure 2A, Transmigration Figure 2D (Figure E2A), Proteomics Figure 3A-D (Figure E3A-C), RNAseq Figure 4A-D (Figure E4A-B)
PAH-9B	F	40	Other	Hispanic or Latino	IPAH	66	13.8	548.65	III	NE activity Total lysate Figure 1B (Figure E1B, E1C), NE Activity Extracellular Figure 1C (Figure E1D), Neutrophil/mL Figure 1D, NE activity/mL blood Figure 1E, Chemokinesis Figure 2C, dUTPase WB Figure 5E, EV Figure 6A-D, Animal Figure 7B-E
PAH-10A	F	35	White	Not Hispanic or Latino	D&T associated PAH (anorexigen) Comorbidity: Mild Intermittent Asthma	49	7.0	466.35	II	NE WB Figure 1A, MPO activity Figure E1E
PAH-10B	F	36	White	Not Hispanic or Latino	D&T associated PAH (see PAH-10A)	49	7.0	466.35	III	NE WB Figure 1A, TEM Figure 2E
PAH-11	F	80	White	Not Hispanic or Latino	IPAH	52	17.7	292.61	II	NE Activity Extracellular Figure 1C (Figure E1D)
PAH-12	F	73	White	Not Hispanic or Latino	IPAH	39	5.8	449.59	II	NE activity Total lysate Figure 1B (Figure E1C), Neutrophil/mL Figure 1D, NE activity/mL blood Figure 1E, TEM Figure 2E, Proteomics Figure 3A-D (Figure E3A-C), RNAseq Figure 4A-D (Figure E4A-B)
PAH-13	F	52	White	Hispanic or Latino	IPAH	35	6.7	521.21	II	NE WB Figure 1A, Proteomics Figure 3A-D (Figure E3A-C), RNAseq Figure 4A-D (Figure E4A-B)
PAH-14A	F	57	White	Not Hispanic or Latino	IPAH	62	16.5	384.05	II/III	Adhesion Figure 2A
PAH-14B	F	57	White	Not Hispanic or Latino	IPAH	62	16.5	411.49	III	NE WB Figure 1A, Proteomics Figure 3A-D (Figure E3A-C), RNAseq Figure 4A-D (Figure E4A-B)
PAH-14C	F	58	White	Not Hispanic or Latino	IPAH	62	16.5	411.49	II	NE activity Total lysate Figure 1B (Figure E1C), Neutrophil/mL Figure 1D, NE activity/mL blood Figure 1E, NETosis Figure 1F
PAH-14D	F	58	White	Not Hispanic or Latino	IPAH	62	16.5	429.77	II	VCL WB Figure 3E, dUTPase WB Figure 5E, EV Figure 6A-D, Animal Figure 7B-E
PAH-14E	F	59	White	Not Hispanic or Latino	IPAH	50	9.2	420.63	II	ITGB2 FACS Figure 3F, HERV-K Confocal Figure 5B
PAH-14F	F	60	White	Not Hispanic or Latino	IPAH	50	9.2	426.73	II	HERV-K WB Figure 5A
PAH-15A	F	50	Black	Not Hispanic or Latino	IPAH	52	7.6	361.19	I/II	Adhesion Figure 2A, Chemokinesis Figure 2C, dUTPase WB Figure 5E
PAH-15B	F	50	Black	Not Hispanic or Latino	IPAH	52	7.6	388.62	I/II	NETosis Figure 1F

AJRCCM Articles in Press. Published June 13, 2022 as 10.1164/rccm.202102-0446OC

Sample[1]	Gender	Age (Yr)	Race	Ethnicity	Diagnosis[2]	PAP[3]	PVR[4]	6MWD[5]	NYHA[6]	Assays
PAH-15C	F	51	Black	Not Hispanic or Latino	IPAH	52	7.6	365.76	II	Proteomics Figure 3A-D (Figure E3A-C), NE WB Figure 1A
PAH-16	F	53	White	Not Hispanic or Latino	IPAH Comorbidity: COPD	39	8	403.86	II/III	NE WB Figure 1A, VCL WB Figure 3E, HERV-K WB Figure 5A, dUTPase WB Figure 5E, EV Figure 6A-D, Animal Figure 7B-E
PAH-17A	F	61	White	Not Hispanic or Latino	IPAH	44	13.8	524.26	III	NE activity Total lysate Figure 1B (Figure E1C), Neutrophil/mL Figure 1D, NE activity/mL blood Figure 1E
PAH-17B	F	62	White	Not Hispanic or Latino	IPAH	44	13.8	451.11	III	TEM Figure 2E, MPO activity Figure E1E
PAH-17C	F	63	White	Not Hispanic or Latino	IPAH	44	13.8	521.21	III	PCR Figure 4E
PAH-18	F	32	White	Not Hispanic or Latino	IPAH	45	10.6	734.58	I	PCR Figure 4E, dUTPase WB Figure 5E, EV Figure 6A-D, Animal Figure 7B-E
PAH-19A	F	65	Other	Hispanic or Latino	IPAH	60	11.1	365.76	II	Adhesion Figure 2A
PAH-19B	F	66	Other	Hispanic or Latino	IPAH	48	11	319.43	III	Proteomics Figure 3A-D (Figure E3A-C), RNAseq Figure 4A-D (Figure E4A-B)
PAH-19C	F	66	Other	Hispanic or Latino	IPAH	48	11	374.91	II	PCR Figure 4E
PAH-20	F	59	Black	Not Hispanic or Latino	IPAH Comorbidity: Mild COPD	61	17.1	315.47	III	VCL WB Figure 3E, HERV-K WB Figure 5A
PAH-21	F	54	Other	Not Hispanic or Latino	IPAH Comorbidity: End Stage Renal Disease	41	6.1	274.32	II/III	TEM Figure 2E, Proteomics Figure 3A-D (Figure E3A-C), RNAseq Figure 4A-D (Figure E4A-B)
PAH-22A	F	38	Asian	Not Hispanic or Latino	IPAH	33	3.8	624.85	I	Proteomics Figure 3A-D (Figure E3A-C)
PAH-22B	F	39	Asian	Not Hispanic or Latino	IPAH	33	3.8	617.23	I	PCR Figure 4E
PAH-22C	F	39	Asian	Not Hispanic or Latino	IPAH	33	3.8	594.37	I	(Cytospin Figure E1A), Adhesion Figure 2A, Migration Figure 2C
PAH-23A	F	66	Black	Not Hispanic or Latino	IPAH Comorbidity: Mild COPD, Sleep Disordered Breathing	56	14.5	39.62	III	(Cytospin Figure E1A), Adhesion Figure 2A
PAH-23B	F	68	Black	Not Hispanic or Latino	IPAH Comorbidity: See PAH-23A	69	15.6	73.15	III	TEM Figure 2E, ITGB2 FACS Figure 3F

AJRCCM Articles in Press. Published June 13, 2022 as 10.1164/rccm.202102-0446OC

Sample[1]	Gender	Age (Yr)	Race	Ethnicity	Diagnosis[2]	PAP[3]	PVR[4]	6MWD[5]	NYHA[6]	Assays
PAH-24	F	23	White	Hispanic or Latino	IPAH	33	6.8	551.09	II	NE WB Figure 1A, NE activity Total lysate Figure 1B (Figure E1C), Neutrophil/mL Figure 1D, NE activity/mL blood Figure 1E
PAH-25	F	29	White	Not Hispanic or Latino	IPAH	58	11.1	67.06	IV	NE activity Total lysate Figure 1B (Figure E1C), Neutrophil/mL Figure 1D, NE activity/mL blood Figure 1E
PAH-26	F	33	Asian	Not Hispanic or Latino	IPAH	51	8.1	525.79	I/II	Migration Figure 2C, TEM Figure 2D
PAH-27A	F	40	White	Not Hispanic or Latino	IPAH	25	5.4	585.22	III	NE WB Figure 1A (dUTPase WB Figure E5A)
PAH-27B	F	40	White	Not Hispanic or Latino	IPAH	25	5.4	594.37	II	NE activity Total lysate Figure 1B (Figure E1C) Neutrophil/mL Figure 1D, NE activity/mL blood Figure 1E
PAH-27C	F	40	White	Not Hispanic or Latino	IPAH	25	5.4	594.37	II	ITGB2 FACS Figure 3F
PAH-27D	F	42	White	Not Hispanic or Latino	IPAH	34	8.2	571.51	II/III	dUTPase WB Figure 5E, EV Figure 6A-D, Animal Figure 7B-E
PAH-27E	F	42	White	Not Hispanic or Latino	IPAH	34	8.2	594.37	II/III	Migration Figure 2C, PCR Figure 4E, HERV-K WB Figure 5A, HERV-K Confocal Figure 5B
PAH-27F	F	42	White	Not Hispanic or Latino	IPAH	34	8.24	594.36	I	EC Adhesion Figure E2B, Released NE Activity Figure E7A, ITGB1 WB Figure 2B
PAH-28	F	45	White	Unknown	D&T associated PAH (Methamph-etamine)	52	20	658.38	I/II	dUTPase WB Figure 5E, EV Figure 6A-D, Animal Figure 7B-E
PAH-29	F	51	Asian	Not Hispanic or Latino	IPAH	35	7.8		II	VCL WB Figure 3E, HERV-K WB Figure 5A, dUTPase WB Figure 5E, EV Figure 6A-D, Animal Figure 7B-E
PAH-30A	F	54	Unknown	Unknown	IPAH	48	12.2	556.27	II	dUTPase WB Figure 5E, EV Figure 6A-D, Animal Figure 7B-E
PAH-30B	F	54	Unknown	Unknown	IPAH	48	12.2	502.93	II	PCR Figure 4E, HERV-K WB Figure 5A, MPO activity Figure E1E
PAH-31	F	49	White	Not Hispanic or Latino	IPAH	47	8	416.06	III	PCR Figure 4E, (dUTPase WB Figure E5A), MPO activity Figure E1E
PAH-32	F	51	White	Not Hispanic or Latino	IPAH	53	11.4	457.21	II	ITGB2 FACS Figure 3F
PAH-33A	F	33	Other	Hispanic or Latino	IPAH	58	14.7	441.97	II	NE WB Figure 1A, (dUTPase WB Figure E5A), MPO activity Figure E1E
PAH-33B	F	33	Other	Hispanic or Latino	IPAH	58	14.7	310.90	III	PCR Figure 4E
PAH-34A	F	53	White	Not Hispanic or Latino	IPAH	33	5.8	566.93	II	TEM Figure 2E
PAH-34B	F	54	White	Not Hispanic or Latino	IPAH	33	5.8	603.51	II	ITGB2 FACS Figure 3F, dUTPase WB Figure 5E, EV Figure 6A-D, Animal Figure 7B-E

AJRCCM Articles in Press. Published June 13, 2022 as 10.1164/rccm.202102-0446OC

Sample[1]	Gender	Age (Yr)	Race	Ethnicity	Diagnosis[2]	PAP[3]	PVR[4]	6MWD[5]	NYHA[6]	Assays
PAH-35A	F	45	Black	Not Hispanic or Latino	IPAH	38	6.1		II	NE activity Total lysate Figure 1B (Figure E1C), Neutrophil/mL Figure 1D, NE activity/mL blood Figure 1E, dUTPase WB Figure 5E, EV Figure 6B-E, Mouse Figure 7B-E
PAH-35B	F	45	Black	Not Hispanic or Latino	IPAH	38	6.1		II	Proteomics Figure 3A-D (Figure E3A-C), RNAseq Figure 4A-D (Figure E4A-B)
PAH-36	F	29	White	Unknown	IPAH	51	12.5	501.40	I/II	(Cytospin Figure E1A), Adhesion Figure 2A, Proteomics Figure 3A-D (Figure E3A-C)
PAH-37	F	47	Other	Hispanic or Latino	IPAH	48	7.07	469.39	I/II	CD66b CD16 FACS Figure E1A, Released NE Activity Figure E7A, ITGB1 WB Figure 2B
PAH-38	F	63	Other	Hispanic or Latino	IPAH	42	8.27	338.32	II	Released NE Activity Figure E7A, ITGB1 WB Figure 2B

[1] A, B, etc., following the number indicate a separate draw from the same patient

[2] Diagnosis: IPAH, Idiopathic PAH; D&T Drug and toxin associated PAH, COPD, Chronic obstructive pulmonary disease

[3] PAP: Mean Pulmonary Arterial Pressure, test closest to the time of blood draw

[4] PVR: Pulmonary vascular resistance in Woods Units, test closest to the time of blood draw

[5] 6MWD: Distance (in meters) walked in six minutes, test closest to the time of blood draw

[6] NYHA: New York Heart Association functional classification

AJRCCM Articles in Press. Published June 13, 2022 as 10.1164/rccm.202102-0446OC

Table E2: Medication prescribed for PAH patients

Patient	PAH Medications
PAH-1	sildenafil
PAH-2A	none
PAH-2B	none
PAH-3	ambrisentan
PAH-4A	ambrisentan, sildenafil, treprostinil
PAH-4B	ambrisentan, sildenafil, treprostinil
PAH-5	bosentan, sildenafil, treprostinil
PAH-6A	flolan
PAH-6B	epoprostenol
PAH-7A	macitentan, sildenafil
PAH-7B	macitentan, sildenafil
PAH-8A	tadalafil, flolan
PAH-8B	tadalafil, flolan
PAH-8C	tadalafil, flolan
PAH-8D	epoprostenol, tadalafil
PAH-8E	epoprostenol, tadalafil
PAH-9A	flolan, macitentan, sildenafil
PAH-9B	flolan, macitentan, sildenafil
PAH-10A	ambrisentan, tadalafil, treprostinil
PAH-10B	ambrisentan, tadalafil, remodulin
PAH-11	macitentan
PAH-12	macitentan, tadalafil
PAH-13	ambrisentan, sildenafil, tyvaso
PAH-14A	ambrisentan, sildenafil, flolan
PAH-14B	ambrisentan, sildenafil, flolan
PAH-14C	ambrisentan, epoprostenol, sildenafil
PAH-14D	ambrisentan, epoprostenol, sildenafil
PAH-14E	ambrisentan, epoprostenol, sildenafil
PAH-14F	ambrisentan, epoprostenol, sildenafil
PAH-15A	tadalafil, treprostinil
PAH-15B	tadalafil, treprostinil
PAH-15C	tadalafil, treprostinil
PAH-16	tadalafil
PAH-17A	bosentan, sildenafil
PAH-17B	bosentan, selexipag, sildenafil
PAH-17C	bosentan, sildenafil

AJRCCM Articles in Press. Published June 13, 2022 as 10.1164/rccm.202102-0446OC

Patient	PAH Medications
PAH-18	macitentan, tadalafil
PAH-19A	ambrisentan, flolan
PAH-19B	ambrisentan, flolan
PAH-19C	ambrisentan, flolan
PAH-20	sildenafil, treprostinil
PAH-21	remodulin
PAH-22A	tadalafil, treprostinil
PAH-22B	tadalafil, treprostinil
PAH-22C	tadalafil, treprostinil
PAH-23A	sildenafil, treprostinil
PAH-23B	macitentan, sildenafil, remodulin
PAH-24	ambrisentan, tadalafil, treprostinil
PAH-25	ambrisentan, sildenafil, treprostinil
PAH-26	remodulin, sildenafil
PAH-27A	sildenafil
PAH-27B	macitentan, sildenafil
PAH-27C	macitentan, sildenafil
PAH-27D	macitentan, sildenafil
PAH-27E	macitentan, sildenafil
PAH-27F	sildenafil, ambrisentan
PAH-28	ambrisentan, tadalafil, treprostinil
PAH-29	ambrisentan, sildenafil
PAH-30A	ambrisentan
PAH-30B	ambrisentan, tadalafil, treprostinil
PAH-31	ambrisentan, selexipag, sildenafil
PAH-32	macitentan, sildenafil
PAH-33A	ambrisentan, sildenafil, remodulin
PAH-33B	ambrisentan, sildenafil, remodulin
PAH-34A	bosentan, epoprostenol
PAH-34B	bosentan, epoprostenol
PAH-35A	iloprost, sildenafil
PAH-35B	iloprost, sildenafil
PAH-36	tadalafil, flolan
PAH-37	epoprostenol, sildenafil, macitentan
PAH-38	sildenafil, macitentan

AJRCCM Articles in Press. Published June 13, 2022 as 10.1164/rccm.202102-0446OC

Table E3: Demographics of Donor Controls, and Assays

Sample	Age (Yr)	Gender	Race	Ethnicity	Echo done (Yes/No)	IVS	PW	LVID	LVEF	E/e'	Estimated RAP	Assays
CON-1	30	M	White	Hispanic	No							NE activity Total lysate Figure 1B (Figure E1B), NETosis Figure 1D, RNAseq Figure 4A-D (Figure E4A-B)
CON-2	29	F	White	Non-Hispanic	Yes	0.78	0.76	4.3	64.5	5.3	5	(Cytospin Figure E1A), Adhesion Figure 2A, EV Figure 6A-D (Figure E7B, E7C), Animal Figure 7B-E
CON-3	41	F	Asian	Non-Hispanic	Yes	0.7	0.71	4.4	61	6.9	5	NE WB Figure 1A, NETosis Figure 1D, Adhesion Figure 2A, Proteomics Figure 3A-D (Figure E3A-C), VCL WB Figure 3E, RNAseq Figure 4A-D (Figure E4A-B), HERV-K WB Figure 5A, HERV-K Confocal Figure 5B, dUTPase WB Figure 5E, EV Figure 6A-D (Figure E7B, E7C), Animal Figure 7B-E
CON-4	29	F	Caucasian	Non-Hispanic	Yes							NE WB Figure 1A, NETosis Figure 1D (Figure E1F), Proteomics Figure 3A-D (Figure E3A-C), RNAseq Figure 4A-D (Figure E4A-B), EV Figure 6A-D (Figure E7B, E7C), Animal Figure 7B-E
CON-5	34	F	Asian	Non-Hispanic	No							NETosis Figure 1D, VCL WB Figure 3E, ITGB2 FACS Figure 3F, PCR Figure 4E, HERV-K WB Figure 5A, HERV-K Confocal Figure 5B, dUTPase WB Figure 5E, EV Figure 6A-D (Figure E7B, E7C), Animal Figure 7B-E
CON-6	49	F	White	Hispanic	Yes	0.86	0.86	4.9	63.3	10.1	5	NE activity Total lysate Figure 1B (Figure E1B), NETosis Figure 1D, Proteomics Figure 3A-D (Figure E3A-C), EV Figure 6A-D (Figure E7B, E7C), Animal Figure 7B-E
CON-7	32	F	American Indian/Alaska Native	Hispanic	Yes	0.94	0.87	4.4	65.6	8.2	5	(Cytospin Figure E1A), Adhesion Figure 2A, Proteomics Figure 3A-D (Figure E3A-C), RNAseq Figure 4A-D (Figure E4A-B), EV Figure 6A-D (Figure E7B, E7C), Animal Figure 7B-E
CON-8	41	F	Black	Non-Hispanic	Yes	0.75	0.69	4.1	69.9	8.6	5	Proteomics Figure 3A-D (Figure E3A-C), RNAseq Figure 4A-D (Figure E4A-B), EV Figure 6A-D, Animal Figure 7B-E
CON-9	50	F	Black	Non-Hispanic	Yes	1.3	1.3	5.3	64.8	11.2	5	NE activity Total lysate Figure 1B (Figure E1B), Proteomics Figure 3A-D (Figure E3A-C), RNAseq Figure 4A-D (Figure E4A-B), EV Figure 6A-D, Animal Figure 7B-E
CON-10	33	F	Black	Non-Hispanic	Yes	0.69	0.77	4.6	68.4	8.3	5	VCL WB Figure 3E, ITGB2 FACS Figure 3F, dUTPase WB Figure 5E, EV Figure 6A-D, Animal Figure 7B-E, EC Adhesion Figure E2B
CON-11	40	F	White	Non-Hispanic	No							VCL WB Figure 3E, PCR Figure 4E, HERV-K WB Figure 5A, HERV-K Confocal Figure 5B, dUTPase WB Figure 5E, EV Figure 6A-D, Animal Figure 7B-E
CON-12	40	M	White	Non-Hispanic	No							NE WB Figure 1A, VCL WB Figure 3E, ITGB2 FACS Figure 3F, HERV-K WB Figure 5A, dUTPase WB Figure 5E, EV Figure 6A-D, Animal Figure 7B-E
CON-13	35	F	White	Non-Hispanic	No							NETosis Figure 1D, dUTPase WB Figure 5E, EV Figure 6A-D, Animal Figure 7B-E

AJRCCM Articles in Press. Published June 13, 2022 as 10.1164/rccm.202102-0446OC

Sample	Age (Yr)	Gender	Race	Ethnicity	Echo done (Yes/No)	IVS	PW	LVID	LVEF	E/e'	Estimated RAP	Assays
CON-14	24	F	White	Non-Hispanic	No							ITGB2 FACS Figure 3F, dUTPase WB Figure 5E, EV Figure 6A-D, Animal Figure 7B-E
CON-15	36	F	Asian	Non-Hispanic	No							dUTPase WB Figure 5E, EV Figure 6A-D, Animal Figure 7B-E
CON-16	31	F	Not reported	Not reported	No							dUTPase WB Figure 5E, EV Figure 6A-D, Animal Figure 7B-E
CON-17	31	F	White	Non-Hispanic	No							PCR Figure 4E, dUTPase WB Figure 5E, EV Figure 6A-D, Animal Figure 7B-E
CON-18	60	F	Black	Non-Hispanic	No							PCR Figure 4E, dUTPase WB Figure 5E, EV Figure 6A-D, Animal Figure 7B-E

Age (years); IVS: interventricular septum (cm); LVEF: left ventricular ejection fraction (%); LVID: left ventricular internal dimension (cm); PW: posterior wall (cm); RAP: right atrial pressure (mmHg); E/e': ratio between early mitral inflow velocity and mitral annular early diastolic velocity.

Blood Bank Controls and Assays*

Sample	Assays
BBD 1, 2, 3, 12, 18, 26, 31, 47	NE WB Figure 1A (n=8)
BBD 1, 2, 3, 12, 18, 26, 32, 36	NE activity Total lysate Figure 1B (Figure E1C) (n=8)
BBD 6, 8, 16, 22	NETosis Figure 1D (n=4)
BBD 59, 60	Cytospin Figure E1A (n=2)
BBD 1, 2, 3	NE activity Total lysate Figure E1B and E1D(n=3)
BBD 24, 25, 28, 29, 43, 45, 48	MPO Activity Figure E1E (n=7)
BBD 4, 6, 8	Adhesion Figure 2A (n=3)
BBD 5, 10, 14	Migration Figure 2B (n=3)
BBD 7, 9, 11	Transmigration Figure 2C (Figure E2A) (n=3)
BBD 6	Transmigration Figure E2A
BBD 13, 15, 17, 20, 21, 23, 30, 33	TEM Figure 2D (n=8)
BBD 61	Endothelial Adhesion Figure E2A (n=1)
BBD 19	VCL WB Figure 3E (n=1)
BBD 27, 57, 58	ITGB2 FACS Figure 3F (n=3)

AJRCCM Articles in Press. Published June 13, 2022 as 10.1164/rccm.202102-0446OC

Sample	Assays
BBD 34, 39, 49, 50	PCR Figure 4E (n=3-4)
BBD 35, 40	HERV-K WB Figure 5A (n=2)
BBD 41, 42, 44, 46, 52, 55	dUTPase WB Figure 5E (n=6)
BBD 51, 53, 54	dUTPase WB Figure E5A (n=3)
BBD 37, 38, 56	Released NE Activity Figure E7A (n=3)

*BBD designate Blood Bank Donor. Demographic information was not collected for the Blood Bank Donors

AJRCCM Articles in Press. Published June 13, 2022 as 10.1164/rccm.202102-0446OC

Table E4: PAEC Demographics

a. Donor controls					
Patient	**Age (yr)**	**Gender**	**Race**	**Ethnicity**	**Cause of Death**
EC CON1	33	F	White	Non-Hispanic	Head trauma. Blunt injury.
EC CON2	57	F	White	Non-Hispanic	Acute Myocardial Infarction
EC CON3	1	M	White	Non-Hispanic	Anoxia/Drowning

b. PAH Patients									
Patient	**Age (yr)**	**Gender**	**Race**	**Ethnicity**	**Diagnosis[1]**	**PAP[2]**	**PVR[3]**	**6MWD[4]**	**PAH Meds**
EC PAH1	22	F	White	Non-Hispanic	FPAH	82	16.04	375.82	sildenafil, ambrisentan, tadalafil, inhaled treprostinil, treprostinil (orenitram)
EC PAH2	27	F	White	Non-Hispanic	IPAH	69	12.11	359.66	sildenafil, SC treprostinil, IV treprostinil, bosentan, inhaled iloprost
EC PAH3	53	M	White	Non-Hispanic	IPAH	33	3.86	77.72	sildenafil, tadalafil, macitentan, IV epoprostenol

[1] Diagnosis: FPAH, Familial PAH; IPAH, Idiopathic PAH

[2] PAP: Mean Pulmonary Arterial Pressure, test closest to the time of blood draw

[3] PVR: Pulmonary vascular resistance in Woods Units, test closest to the time of blood draw

[4] 6MWD: Distance (in meters) walked in six minutes, test closest to the time of blood draw

AJRCCM Articles in Press. Published June 13, 2022 as 10.1164/rccm.202102-0446OC

Table E5: Correlative Genes and Proteins from the Omics Analysis

Gene/Protein	Correlation	Protein p-value	mRNA p-value
EIF3J	Decreased	0.003299398	0.000164377
TUBB4B	Decreased	0.019693895	0.0000112
TCP1	Decreased	0.001135572	0.0000459
SUN2	Decreased	0.005046265	0.0000971
TPD52L2	Decreased	0.000716389	0.00000437
PCYT2	Decreased	0.008718198	0.000219796
STOML2	Decreased	0.016078615	0.000000427
PSMC4	Decreased	0.013149119	0.00000294
EEF1D	Decreased	0.006689322	0.000320571
MECP2	Decreased	0.009342118	0.0000423
POLR2A	Decreased	0.018024105	0.002416794
RALY	Decreased	0.009951085	0.003563528
SF1	Decreased	0.014691391	0.000407631
AMPD2	Decreased	0.000421312	0.000422481
CHD4	Decreased	0.023893101	4.52E-09
SRRT	Decreased	0.01383299	0.0000182
ARIH1	Decreased	0.032208307	0.00001
COPS5	Increased	0.013280254	0.004345779
VBP1	Increased	0.032490686	0.00188536
VPS36	Increased	0.021535145	0.002750826
PFN1	Increased	0.014676215	0.002221079
CSTA	Increased	0.003669109	0.000904283
TM9SF2	Increased	0.005699783	0.0000727
PGGT1B	Increased	0.027796704	0.000186515
PGAM1	Increased	0.030360717	0.001498589
BROX	Increased	0.010059018	0.001607269
ARCN1	Increased	0.000267714	0.001629735
MYCBP	Increased	0.029877858	0.001891447
SH3BGRL	Increased	0.001591546	0.001628348
UQCR10	Increased	0.006935534	0.000919845
CTSS	Increased	0.006901583	0.002102924
MTARC1	Increased	0.001422351	0.000791293
SELL	Increased	0.012844352	0.00010617

AJRCCM Articles in Press. Published June 13, 2022 as 10.1164/rccm.202102-0446OC

Table E6: Reagents and Resources

REAGENT or RESOURCE	SOURCE	IDENTIFIER/SEQUENCE
Antibodies		
Anti-human CD66b/CEACAM 8	Sigma	Cat#: SAB4301144-100
Anti-Neutrophil Elastase	Abcam	Cat#: ab68672
Anti-Histone H3	Abcam	Cat#: ab24834
Anti-Vinculin	Abcam	Cat#: ab18058
Anti-HERV-K Envelope	Ango	Cat#: Herm 1811-5
Anti-dUTPase	Dr. Ariza	Cat#: ab265
CD9 Monoclonal Antibody (Ts9)	ThermoFisher	Cat #: 10626D
Anti-ITGB2 Flor antibody	Novus	Cat#: NB500-480AF700
GAPDH Antibody (G-9)	Santa Cruz	Cat#: sc-365062
Alexa Fluor488 donkey anti mouse IgG (H +L)	ThermoFisher	Cat#: A21202
Alexa Fluor594 donkey anti rabbit IgG (H +L)	ThermoFisher	Cat#: A21207
α-smooth muscle actin antibody	Sigma-Aldrich	Cat#: A2547
CD9 Antibody	ThermoFisher	Cat#: 10626D
Anti-Histone H3 (Citrulline R2+R8+R17) antibody	Abcam	Cat#: 5103
Anti-PADI4	Abcam	Cat#: ab128086
Recombinant Anti-CD66b antibody	Abcam	Cat#: ab170875
Anti-Integrin beta 1 antibody [12G10]	Abcam	Cat#: ab30394
FITC anti-human CD66b	Biolegend	Cat#: 50-166-209
APC anti-human CD16	Biolegend	Cat#: 50-165-788
Vectors		
EGFP control vector	VectorBuilder	ID: VB180814-1915cef
HERV-K Env vector	VectorBuilder	ID: VB180814-1914ntz

AJRCCM Articles in Press. Published June 13, 2022 as 10.1164/rccm.202102-0446OC

REAGENT or RESOURCE	SOURCE	IDENTIFIER/SEQUENCE
Reagents, Cells, Chemicals, Peptides, and Recombinant Proteins		
HL-60 Cell Avalanche™ Transfection Reagent	EZ biosystems	Cat#: EZT-HL60-1
RPMI 1640	Life Technologies	Cat#: 11875119
GIBCO	Life Technologies	Cat#: 10438026
P/S	Life Technologies	Cat#: 15140122
DMSO	Sigma Aldrich	Cat#: D2650-100ML
SYTOX green nucleic acid	ThermoFisher	Cat# S7020
DAPI Fluoromount-G	SouthernBiotech	Cat#: 0100-20
Fibronectin from human plasma	Sigma Aldrich	Cat#: F0895-2MG
Recombinant Human CXCL8/IL-8	R&D Systems	Cat#: 208-IL-050
Elafin	Proteo-Biotech-AG	Gift
Calcein AM, Cell Permeant Dye	ThermoScientific	Cat#: C3100MP
DPBS	ThermoFisher	Cat#: 10010023
Poly D lysine Solution	EMD Millipore	Cat#: A-003-E
N-Formyl-Met-Leu-Phe	Sigma Aldrich	Cat#: F3506-10MG
1M Tris-HCL	Life Technologies	Cat#: 15567-027
UltraPure 10%SDS	Life Technologies	Cat#: 24730-020
HL-60	Sigma Aldrich	Cat#: 98070106-1VL
Bovine Serum Albumin	Sigma Aldrich	Cat#: A3059-500G
Glycine 1 M solution	Millipore	Cat#: 67419-1ML-F
Formvar/Carbon Film	Electron Microscopy Science	Cat#: FCF300-CU
Commercial Assays and Kits		
Dynabeads Antibody Coupling Kit 14311D	ThermoFisher (Invitrogen)	Cat#: 14311D
EnzChek™ Elastase Assay Kit	Thermofisher Scientific	Cat#: E12056
Neutrophil Myeloperoxidase assay kit	Cayman Chemical	Cat#: 600620
MACSxpress Neutrophil Isolation Kit	MACS Miltenyi Biotec	Cat#: 130-104-434

AJRCCM Articles in Press. Published June 13, 2022 as 10.1164/rccm.202102-0446OC

REAGENT or RESOURCE	SOURCE	IDENTIFIER/SEQUENCE
SMARTer® Stranded Total RNA-Seq Kit - Pico Input Mammalian - 12 Rxns	TAKARA	Cat#: 635005
Albumin depletion kit	Thermofisher Scientific	Cat#: 85160
Corning® FluoroBlok™ Inserts, 24 well	Corning Incorporated Life Sciences	Cat#: 351151
Direct-zol RNA Kits	Zymoresearch	Cat#: R2062
DakoArk	Dako	Cat#: K3954
ON-TARGETplus Human VCL siRNA	Dharmacon	Cat#: L-009288-00-0010 10 nmol
Dako Liquid DAB + Substrate Chromogen System	Dako	Cat#: K3468

AJRCCM Articles in Press. Published June 13, 2022 as 10.1164/rccm.202102-0446OC

Table E7: Raw Data with ΔΔCT Values for the Data Presented in Figure 5C

	B2M	B2M	B2M	Average			
CON 1	18.95509027	18.23330861	18.13612245	18.44150711			
CON 2	18.44941696	18.28379093	18.30630476	18.34650422			
CON 3	18.13034355	18.13698037	18.98170797	18.41634397			
HERV-K env 1	18.1022563	18.12194516	18.90856583	18.3775891			
HERV-K env 2	17.99945868	18.03710609	18.8791331	18.30523263			
HERV-K env 3	18.28112537	18.48361531	18.52437395	18.42970488			
	HERV	**HERV**	**HERV**	**Average**	**ΔCt**	**ΔΔCt**	**2^-(ΔΔCt)**
CON 1	21.72532986	21.68805022	21.89798157	21.77045389	3.328946775	0.03915605	0.973224099
CON 2	21.48088238	21.52133954	21.67902795	21.56041662	3.213912407	-0.075878318	1.054002521
CON 3	21.90598635	21.61584665	21.70673787	21.74285696	3.326512994	0.036722268	0.974867284
HERV-K env 1	18.69834436	18.59904479	18.61872535	18.63870483	0.261115737	-3.028674988	8.160598639
HERV-K env 2	18.4160477	18.67993526	18.47720384	18.5243956	0.219162971	-3.070627754	8.401388338
HERV-K env 3	18.52979708	18.48134206	18.51716774	18.50943563	0.079730752	-3.210059973	9.253890149
	NE	**NE**	**NE**	**Average**	**ΔCt**	**ΔΔCt**	**2^-(ΔΔCt)**
CON 1	22.90968041	22.19019152	22.92841702	22.67609631	4.234589204	-0.10930618	1.07870934
CON 2	22.88977369	22.95571605	22.31974914	22.72174629	4.375242078	0.031346694	0.978506477
CON 3	22.99810261	22.5874535	22.92904039	22.83819884	4.42185487	0.077959486	0.947396675
HERV-K env 1	22.26570836	22.14382794	22.29127822	22.23360484	3.856015744	-0.48787964	1.402382249
HERV-K env 2	22.16489225	22.41036516	22.0463318	22.2071964	3.901963775	-0.441931609	1.358421887
HERV-K env 3	21.92333184	22.10113992	22.28696074	22.10381084	3.67410596	-0.669789423	1.59084075
	RIG-I	**RIG-I**	**RIG-I**	**Average**	**ΔCt**	**ΔΔCt**	**2^-(ΔΔCt)**
CON 1	28.41554763	28.27406054	28.35778038	28.34912952	9.907622406	-0.05419233	1.038277677
CON 2	28.32629483	28.35794638	28.24209777	28.30877966	9.962275445	0.000460708	0.999680713
CON 3	28.52866843	28.48089201	28.28611053	28.43189032	10.01554636	0.053731622	0.963441102
HERV-K env 1	27.25905128	27.31681263	27.40990711	27.32859034	8.951001245	-1.010813491	2.015047003
HERV-K env 2	27.32215779	27.54250239	27.28393306	27.38286442	9.077631789	-0.884182947	1.845719025
HERV-K env 3	27.57986292	27.57437602	27.47415505	27.542798	9.113093123	-0.848721613	1.800904418
	PKR	**PKR**	**PKR**	**Average**	**ΔCt**	**ΔΔCt**	**2^-(ΔΔCt)**
CON 1	24.44973266	24.22010163	24.39738757	24.35574062	5.914233509	0.053313691	0.963720239
CON 2	24.06346331	24.15555915	24.09463261	24.10455169	5.758047475	-0.102872343	1.073909443
CON 3	24.25980284	24.48567751	24.23498696	24.32682244	5.91047847	0.049558652	0.966231872
HERV-K env 1	23.84033939	24.07332858	23.98157011	23.96507936	5.587490265	-0.273429554	1.208677666
HERV-K env 2	23.59464541	23.92324954	23.87959098	23.79916198	5.493929351	-0.366990467	1.289659729
HERV-K env 3	24.00952365	24.15886961	23.99864654	24.05567993	5.625975057	-0.234944761	1.176861676

ΔCt = Ct (gene of interest) – Ct (B2M)
ΔΔCt = ΔCt (HERV-K env) – ΔCt Control average
Fold gene expression = 2^-(ΔΔCt)

AJRCCM Articles in Press. Published June 13, 2022 as 10.1164/rccm.202102-0446OC

Table E8: Primers used for qPCR

GENE	SOURCE	FORWARD	REVERSE
PKR	Stanford PAN facility	tggaaagcgaacaaggagtaag	ccaaagcgtagaggtccactt
RIG-I	Stanford PAN facility	tgtgggcaatgtcatcaaaa	gaagcacttgctacctcttgc
IFNAR2	Stanford PAN facility	ccttaaaatgcaccctccttc	ttcctcctattttggcagattc
IFNAR1	Stanford PAN facility	aagggcgaggacgaagag	tcgacctctacttttgaggaga
IFNGR2	Stanford PAN facility	gctgctgctcggagtctt	ggtctccaaagttagctgtgct
ARIH1	Stanford PAN facility	tgggataaagagaagctaatgga	attaattacatgacactcagcaaagag
HERV-K env	Applied Biosystems	gctgccctgccaaacctgag	cctgagtgacatcccgcttacc
NE	Stanford PAN facility	gactcgcgtgtcttttcctc	gcagggacaccatgaagg
VCL	Stanford PAN facility	gatgaagctcgcaaatggtc	tctgcctcagctacaacacct
B2M	Stanford PAN facility	ttctggcctggaggctatc	tcaggaaatttgactttccattc

AJRCCM Articles in Press. Published June 13, 2022 as 10.1164/rccm.202102-0446OC

SUPPLEMENTARY FIGURES AND LEGENDS

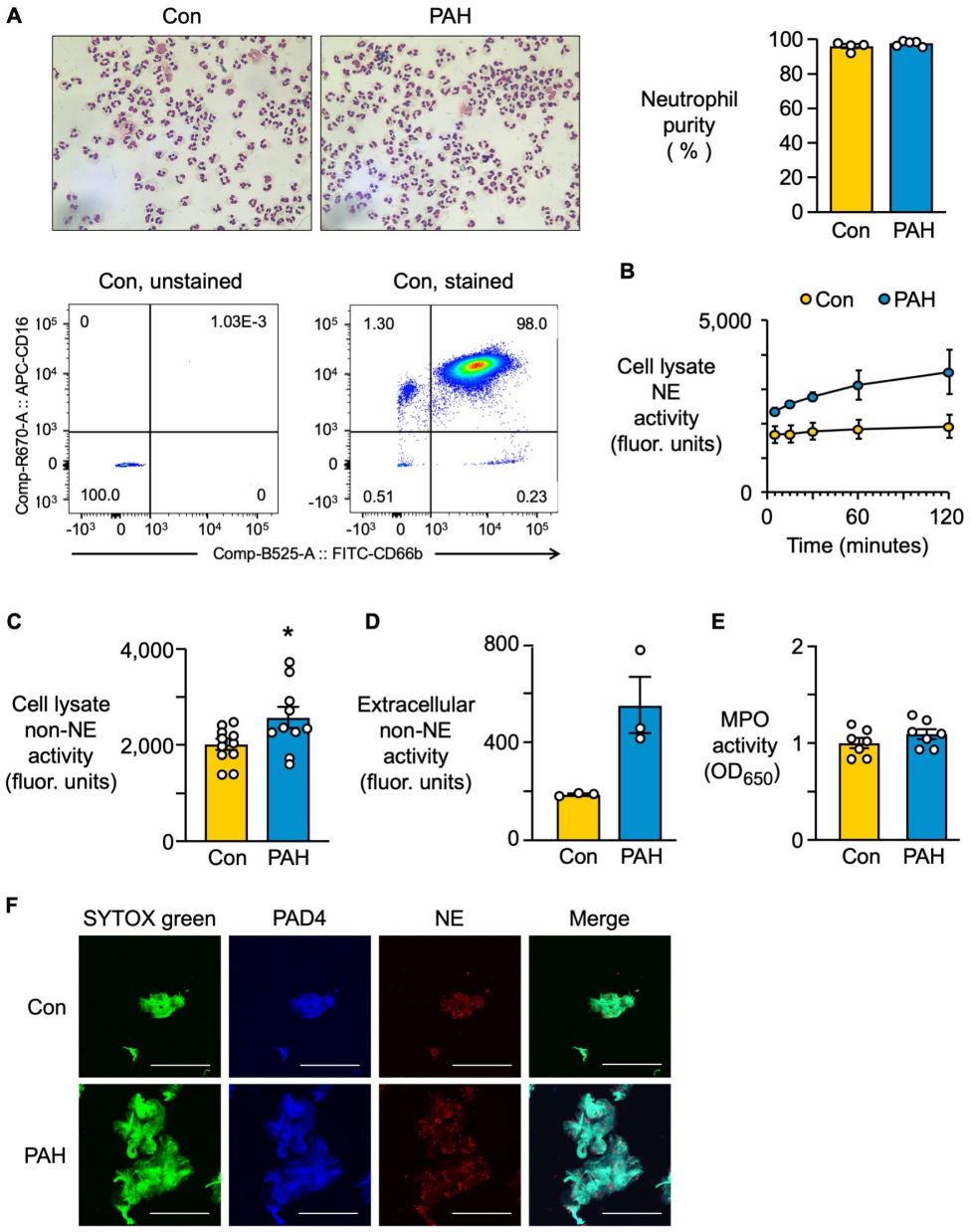

Figure E1. Purity of neutrophils, assessment of NE activity with time, elastase activity in neutrophils not attributed to neutrophil elastase and myeloperoxidase activity.

(A) Neutrophils were isolated from circulating human blood of PAH Patients or healthy donors, and the purity of the preparation was determined by microscopy following Diff-Quick staining after neutrophil isolation and Cytospin preparation (Cytospin 4; Thermo Scientific) (shown on right; n=4 Con or 5 PAH). Purity was further validated via FACs (shown for Control neutrophils). **(B)** NE activity in neutrophil cell lysates was determined

AJRCCM Articles in Press. Published June 13, 2022 as 10.1164/rccm.202102-0446OC

by production of BODIPY FL labeled fluorescent elastin fragments from self-quenching BODIPY FL-conjugated bovine neck ligament elastin in the extracellular supernatant after IL-8 stimulation of neutrophils. n=3 Con or PAH; $5x10^6$ cells were used for each assay. **(C)** Elastase activity that is not due to neutrophil elastase (NE) in neutrophil cellular lysates after 2 hours. Non-NE activity was assessed by the level of BODIPY FL labeled fluorescent elastin fragments produced from self-quenching BODIPY FL-conjugated bovine neck ligament elastin in the presence of the specific NE inhibitor N-Methoxysuccinyl-Ala-Ala-Pro-Val-chloromethyl ketone (n=11 Con or n=10 PAH). **(D)** Non-NE activity was measured in extracellular supernatant of PAH and control neutrophils 2 h after IL-8 stimulation in the presence of the specific NE inhibitor N-Methoxysuccinyl-Ala-Ala-Pro-Val-chloromethyl ketone (n=3). **(E)** Neutrophil Myeloperoxidase (MPO) activity was measured in total lysates utilizing 3,3',5,5'-tetramethyl-benzidine (TMB) as a chromogenic substrate, as described in “Methods” (n=7). **(F)** Following PMA stimulation, neutrophil extracellular traps (NET) were visualized by SYTOX green fluorescence, with NE (red), and PAD4 (blue). Scale bar=40 μm. Bars represent mean ± SEM. *p<0.05, **P<0.01 by unpaired Student t-test (C).

AJRCCM Articles in Press. Published June 13, 2022 as 10.1164/rccm.202102-0446OC

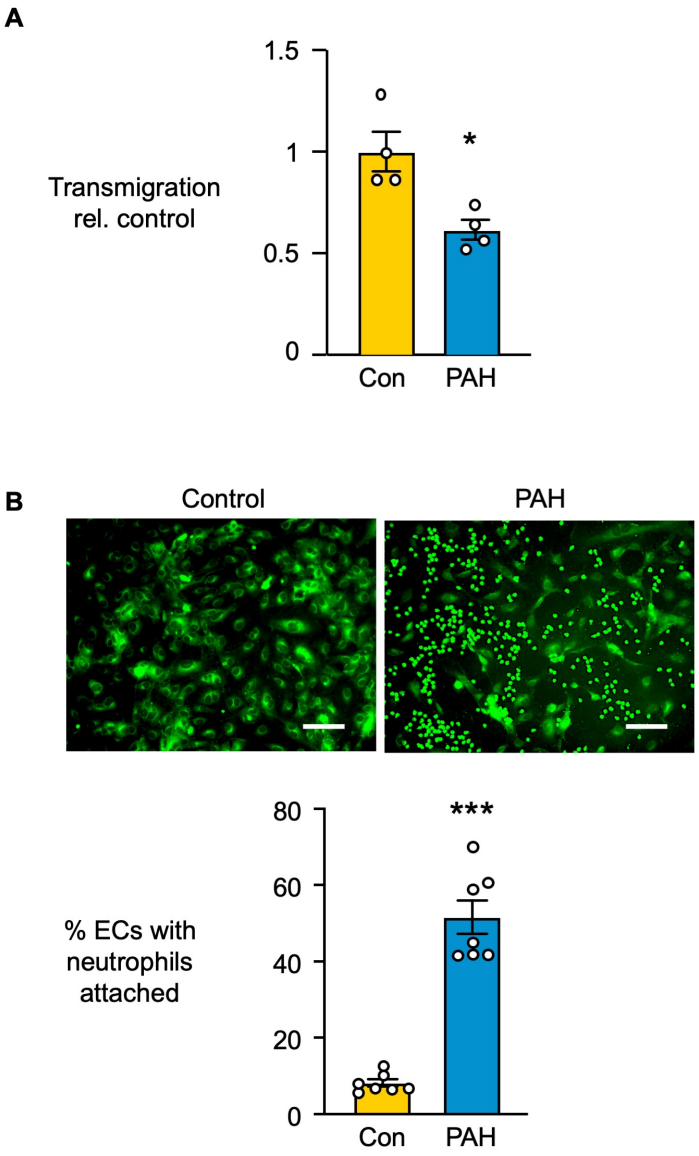

Figure E2. PAH neutrophils exhibit reduced transmigration, and increased adhesion to PAEC.

Neutrophils were isolated from circulating human blood of PAH Patients or healthy donor controls (Con). **(A)** Neutrophils were labeled with Calcein-AM, plated on fibronectin coated trans-well chambers, and stimulated with 100 nM fMLP. Transmigration was assessed after 60 min of stimulation (n=4 PAH or Controls). **(B)** PAH vs. Con neutrophils were incubated on Con PAEC monolayers grown to confluence, and adhesion of PAH and Con neutrophils on Con PAEC was assessed following 5 min of IL-8 (100 ng/mL) stimulation (n=7 fields each, using neutrophils from one PAH patient and one Control). Bars represent mean ± SEM. *$p<0.05$ and ***$p<0.001$ by Mann-Whitney test.

AJRCCM Articles in Press. Published June 13, 2022 as 10.1164/rccm.202102-0446OC

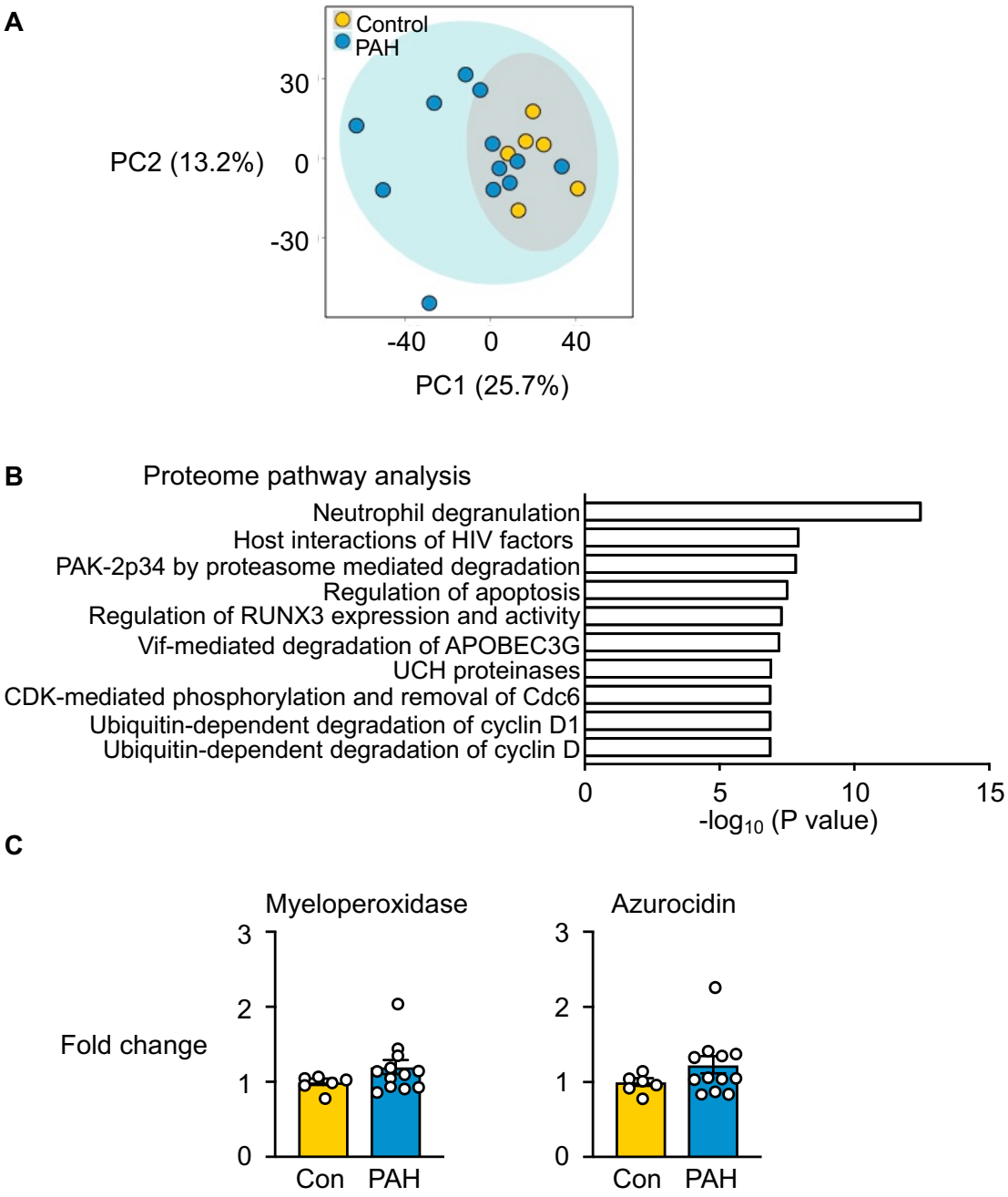

Figure E3. Identification of protein expression and pathways.

(A) Principal component analysis (PCA) plot of proteomics data that characterize the trends exhibited by the expression profiles of isolated PAH vs. Con neutrophils. Each dot represents a Con or PAH patient. **(B)** The top 10 pathways identified by Integrated Molecular Pathway-Level Analysis (IMPALA) of differentially expressed proteins in PAH vs. Con neutrophils. **(C)** Proteomic analysis of the fold-change in myeloperoxidase and Azurocidin in PAH vs. Con neutrophils (n=6 Con and n=12 PAH).

AJRCCM Articles in Press. Published June 13, 2022 as 10.1164/rccm.202102-0446OC

A

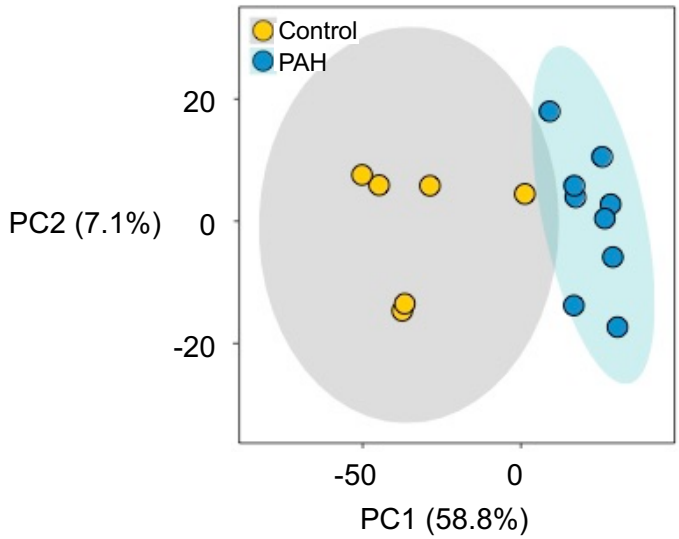

B

Transcription pathway analysis

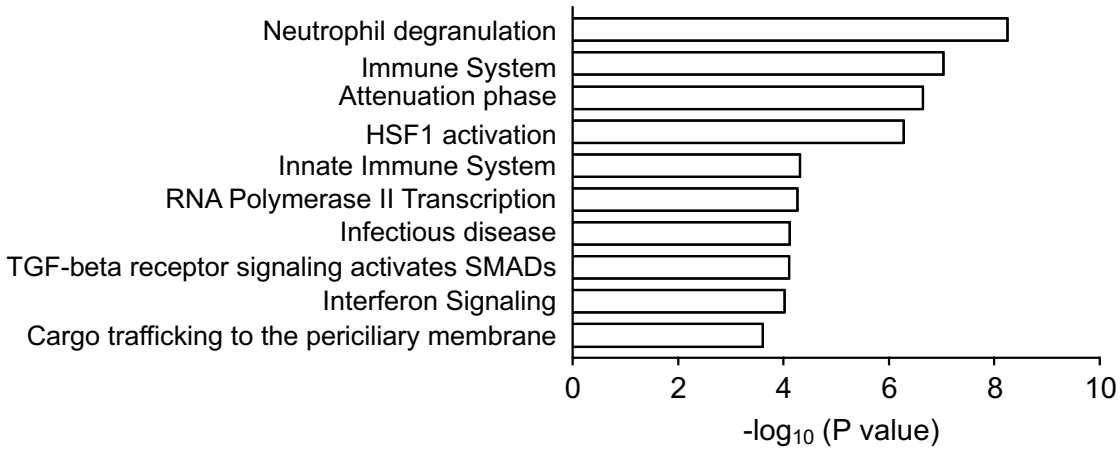

Figure E4. Identification of gene expression and pathways.

(A) Principal component analysis (PCA) plot of RNAseq data that characterizes the trends exhibited by the expression profiles of isolated PAH vs. Con neutrophils. Each dot represents a Con or PAH patient. **(B)** The top 10 pathways identified by Integrated Molecular Pathway-Level Analysis (IMPALA) of significant differentially expressed genes in PAH vs. Con neutrophils (n=6 Con and n=9 PAH patients).

AJRCCM Articles in Press. Published June 13, 2022 as 10.1164/rccm.202102-0446OC

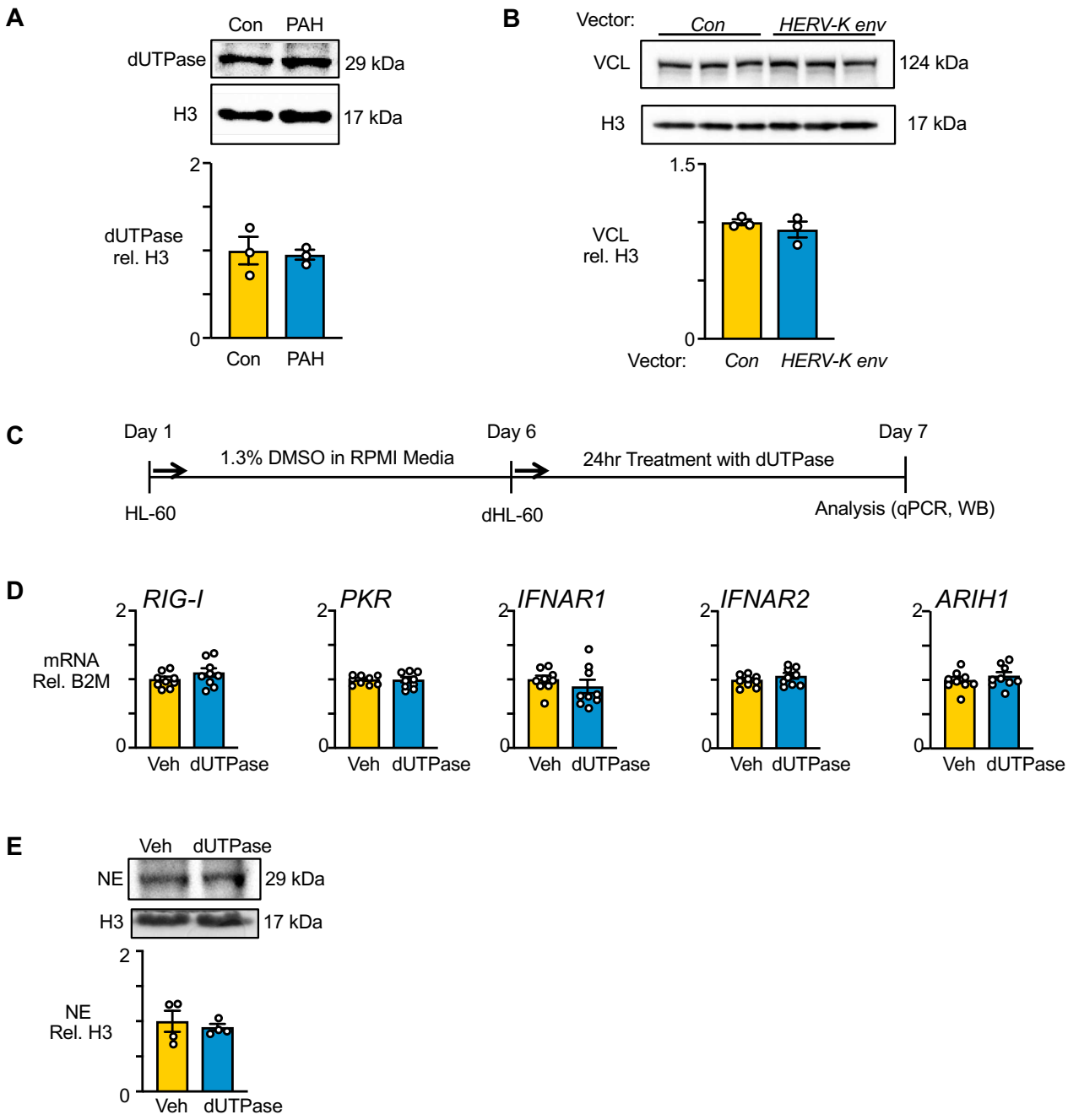

Figure E5. HERV dUTPase in neutrophils, and VCL and interferon following transfection of HL-60 cells with HERV-K envelope.

(A) Representative western immunoblot and quantification of HERV-K dUTPase relative to histone H3 (H3) in PAH vs. Con neutrophils (n=3). **(B)** Representative western immunoblot and quantification of VCL relative to H3 in HL-60 cells overexpressing HERV-K envelope (n=3). **(C)** Illustration of the timeline of HL-60 cell differentiation and stimulation with recombinant HERV-K dUTPase. **(D)** PCR analysis of *RIG-I*, *PKR, IFNAR1, IFNAR2, and ARIH1* in dHL-60 cells treated with HERV-K dUTPase (dUTPase) or Vehicle (Veh; HERV-K dUTPase elution buffer) for 24 h (n=9). **(E)** Representative western immunoblot and quantification of NE relative to H3 in dHL-60 cells treated with HERV-K dUTPase or Veh for 24 h (n=4). Bars represent mean ± SEM.

AJRCCM Articles in Press. Published June 13, 2022 as 10.1164/rccm.202102-0446OC

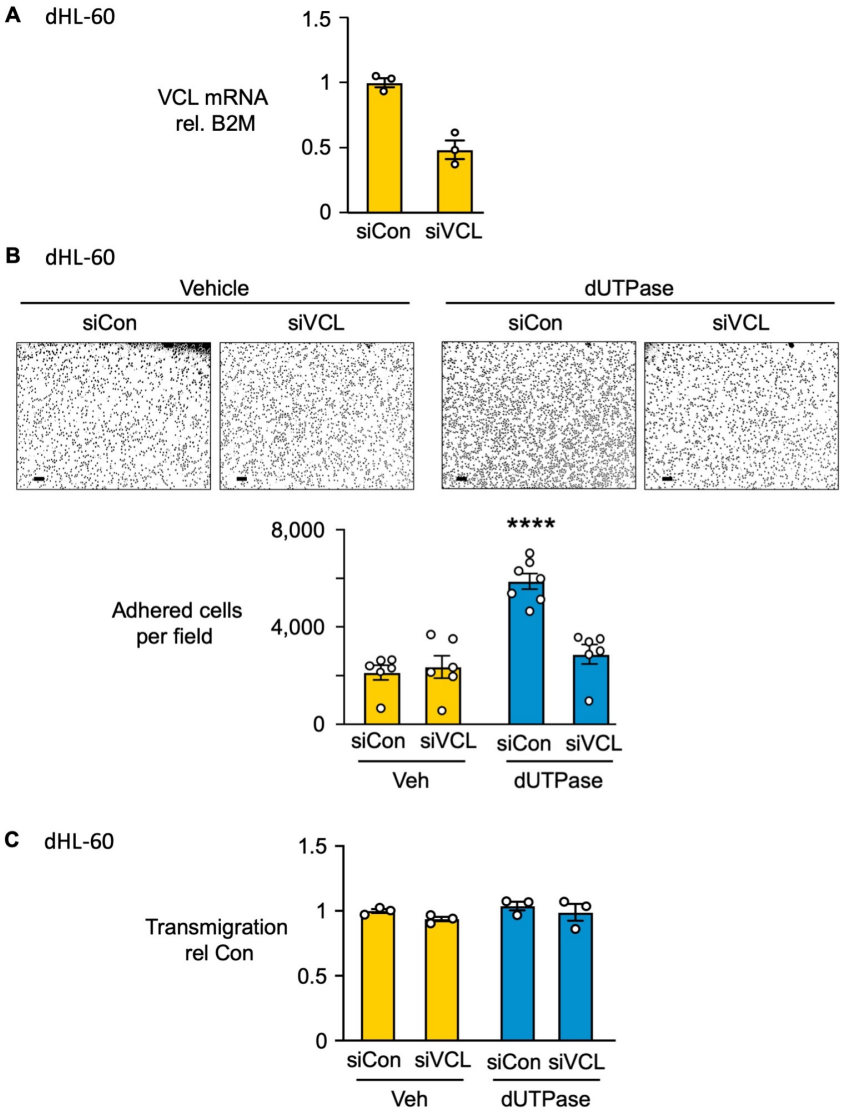

Figure E6. Reduction of VCL in dHL-60 cells causes reduced adhesion, but not migration, following HERV-K dUTPase treatment.

(A) RT-qPCR analysis of VCL mRNA in dHL-60 cells (n=3). Bars represent mean ± SEM. **(B)** dHL-60 cells were treated with HERV-K dUTPase or Vehicle (Veh; HERV-K dUTPase elution buffer) for 24 h. Thereafter, cells were incubated on fibronectin-coated coverslips for 5 min, then stimulated with 100 ng/mL IL-8 for 5 min. The mean number of adherent cells was assessed from 6 randomly selected visual fields. Representative image of adherent neutrophils and quantification on the right (n=6 fields). Bars represent mean ± SEM. ****p<0.0001 vs. siCon+Veh, by one-way ANOVA followed by Dunnett's multiple comparison test. Scale bar=40 μM. **(C)** dHL-60 cells were treated with HERV-K dUTPase or Vehicle (Veh; HERV-K dUTPase elution buffer) for 24 h. Thereafter cells were labeled with calcein-AM then plated on fibronectin coated transwell chambers, and stimulated with 100 ng/mL IL-8. Transmigration was assessed after 60 min of stimulation (n=3).

AJRCCM Articles in Press. Published June 13, 2022 as 10.1164/rccm.202102-0446OC

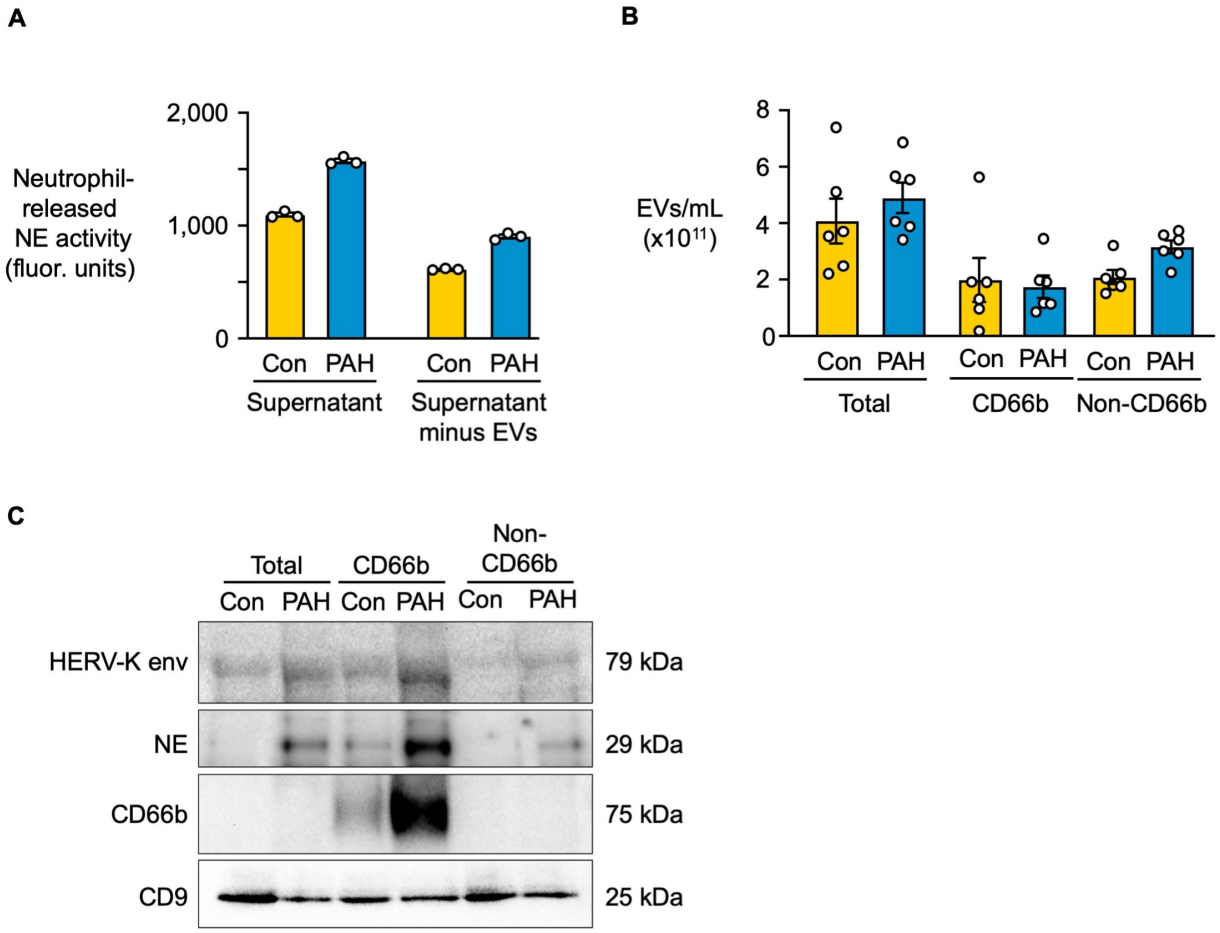

Figure E7. Neutrophils release EV-bound and free elastase; PAH EVs have elevated NE and HERV-K envelope.

(A) Neutrophils were isolated from whole blood of PAH patients or Controls (Con) and stimulated with IL-8 (100 ng/mL) for 2 hours. NE activity of supernatant and EV-depleted supernatant was determined by production of BODIPY FL labeled fluorescent elastin fragments from self-quenching BODIPY FL-conjugated bovine neck ligament elastin (n=3). Bars represent mean ± SEM. **(B-C)** EVs were isolated from plasma of 6 healthy donor controls (Con) and 6 PAH patients (PAH), using ultracentrifugation as described in "Methods". CD66b positive neutrophil EVs were pulled down using anti-CD66b beads. **(B)** The number of EVs, determined using Nanosight. **(C)** Western immunoblot analysis of CD66b, NE, and HERV-K envelope from pooled total EVs, CD66b pulldown (neutrophil EVs), and non CD66b EVs, relative to the EV marker CD9.

AJRCCM Articles in Press. Published June 13, 2022 as 10.1164/rccm.202102-0446OC

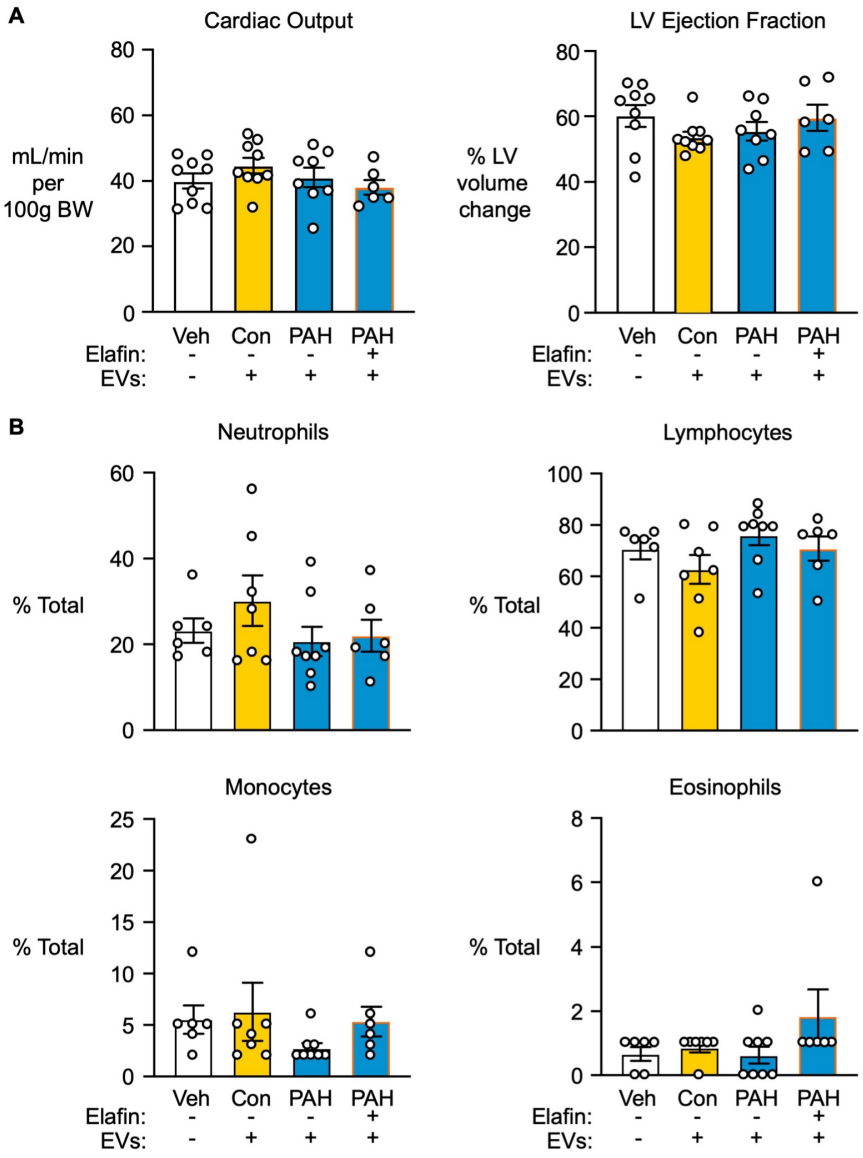

Figure E8. Cardiac function and complete blood count from the murine EV study. **(A)** Left ventricular (LV) function was assessed by 2D-echocardiagraphy prior to obtaining the RVSP data. Cardiac output shown on the left, and LV ejection fraction on the right. **(B)** Complete blood counts were determined in the experimental groups prior to sacrifice. The percentages of neutrophils, monocytes, lymphocytes, and eosinophils are shown. Basophils were not detectable.

AJRCCM Articles in Press. Published June 13, 2022 as 10.1164/rccm.202102-0446OC

SUPPLEMENTARY VIDEO

Video E1: Time Lapse imaging demonstration reduced migration (chemokinesis) in PAH vs. Control neutrophils in response to IL-8 (ng/mL).

Migration was observed using a confocal laser-scanning microscope (FV1000, Olympus, Center Valley, PA) with a 40X objective, using the phase contras mode. Frames were taken every 10 sec for 30 min and analyzed using ImageJ software. Graphic analysis of several experiments is presented in **Figure 2C**.

AJRCCM Articles in Press. Published June 13, 2022 as 10.1164/rccm.202102-0446OC

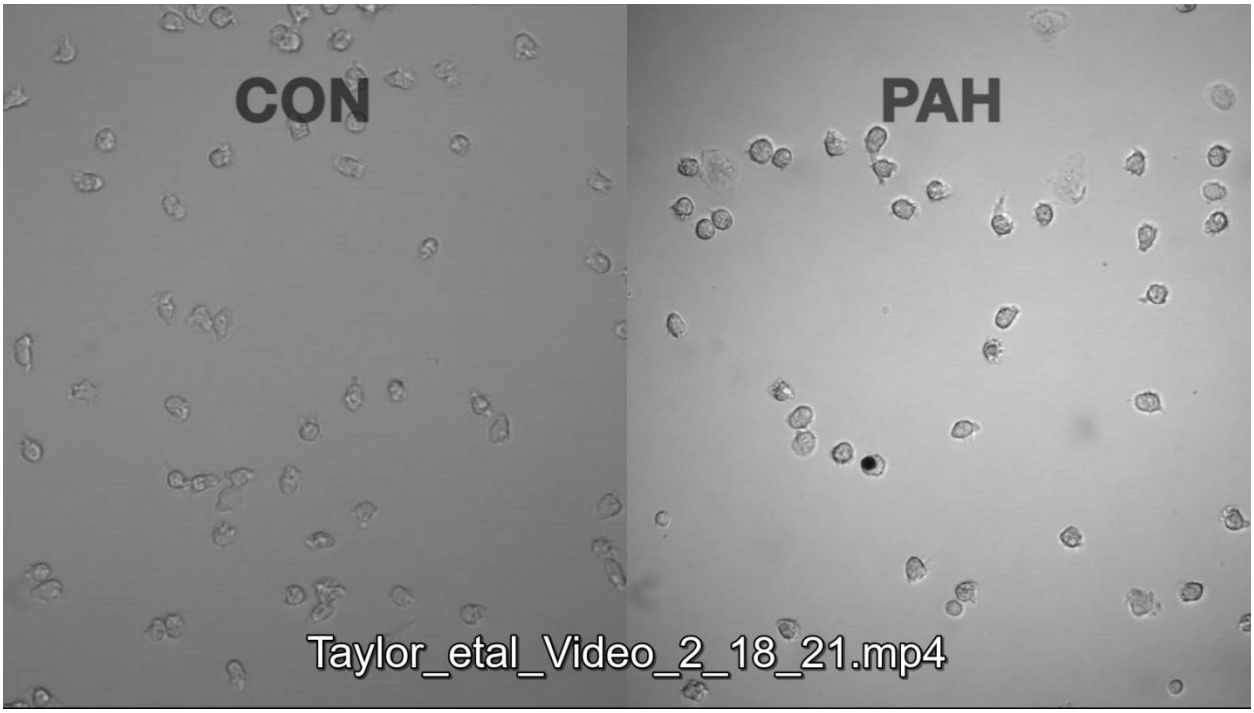

Still of Video E1

AJRCCM Articles in Press. Published June 13, 2022 as 10.1164/rccm.202102-0446OC